nagra.

Arbeitsbericht NAB 22-01

TBO Stadel-3-1: Data Report

Dossier IX Rock-mechanical and Geomechanical Laboratory Testing

June 2022

E. Crisci, L. Laloui & S. Giger

National Cooperative
for the Disposal of
Radioactive Waste

Hardstrasse 73
P.O. Box
5430 Wettingen
Switzerland
Tel. +41 56 437 11 11

www.nagra.ch

nagra.

Arbeitsbericht NAB 22-01

TBO Stadel-3-1: Data Report

Dossier IX Rock-mechanical and Geomechanical Laboratory Testing

June 2022

E. Crisci[1], L. Laloui[2] & S. Giger[3]

[1] Nesol - Numerical Engineering Solutions
EPFL Innovation Park Building D
[2] Laloui Consulting, Vevey
[3] Nagra

Keywords:
STA3-1, Nördlich Lägern, TBO, deep drilling campaign, geomechanics, geomechanical laboratory testing, triaxial tests, oedometric tests

National Cooperative for the Disposal of Radioactive Waste

Hardstrasse 73
P.O. Box
5430 Wettingen
Switzerland
Tel. +41 56 437 11 11

www.nagra.ch

Nagra Arbeitsberichte ("Working Reports") present the results of work in progress that have not necessarily been subject to a comprehensive review. They are intended to provide rapid dissemination of current information.

This NAB aims at reporting drilling results at an early stage. Additional borehole-specific data will be published elsewhere.

In the event of inconsistencies between dossiers of this NAB, the dossier addressing the specific topic takes priority. In the event of discrepancies between Nagra reports, the chronologically later report is generally considered to be correct. Data sets and interpretations laid out in this NAB may be revised in subsequent reports. The reasoning leading to these revisions will be detailed there.

This report was finalised in March 2023.

This Dossier was prepared by a project team consisting of:
E. Crisci (test coordination, formal analysis, QC and writing)
S. Giger (project administration, conceptualisation and writing)
L. Laloui (review and supervision)

The present report was prepared based on numerous contractor reports, to which many people from different laboratories contributed, namely B. Bohloli, T.S. Faleide, J. Stenebråten, R. Stankovic, V. Vajdova, R. Ewy, A. Ferrari, M. Rosone, H. Baumgartner, S. Louis and J. Menningen.

Editorial work: P. Blaser and M. Unger

The Dossier has greatly benefitted from technical discussions with external and internal experts. Their input and work are very much appreciated.

Copyright © 2022 by Nagra, Wettingen (Switzerland) / All rights reserved.
All parts of this work are protected by copyright. Any utilisation outwith the remit of the copyright law is unlawful and liable to prosecution. This applies in particular to translations, storage and processing in electronic systems and programs, microfilms, reproductions, etc.

Table of Contents

List of Tables

List of Figures

1 Introduction

1.1 Context

To provide input for site selection and the safety case for deep geological repositories for radioactive waste, Nagra has drilled a series of deep boreholes ("Tiefbohrungen", TBO) in Northern Switzerland. The aim of the drilling campaign is to characterise the deep underground of the three remaining siting regions located at the edge of the Northern Alpine Molasse Basin (Fig. 1-1).

In this report, we present the results from the Stadel-3-1 borehole.

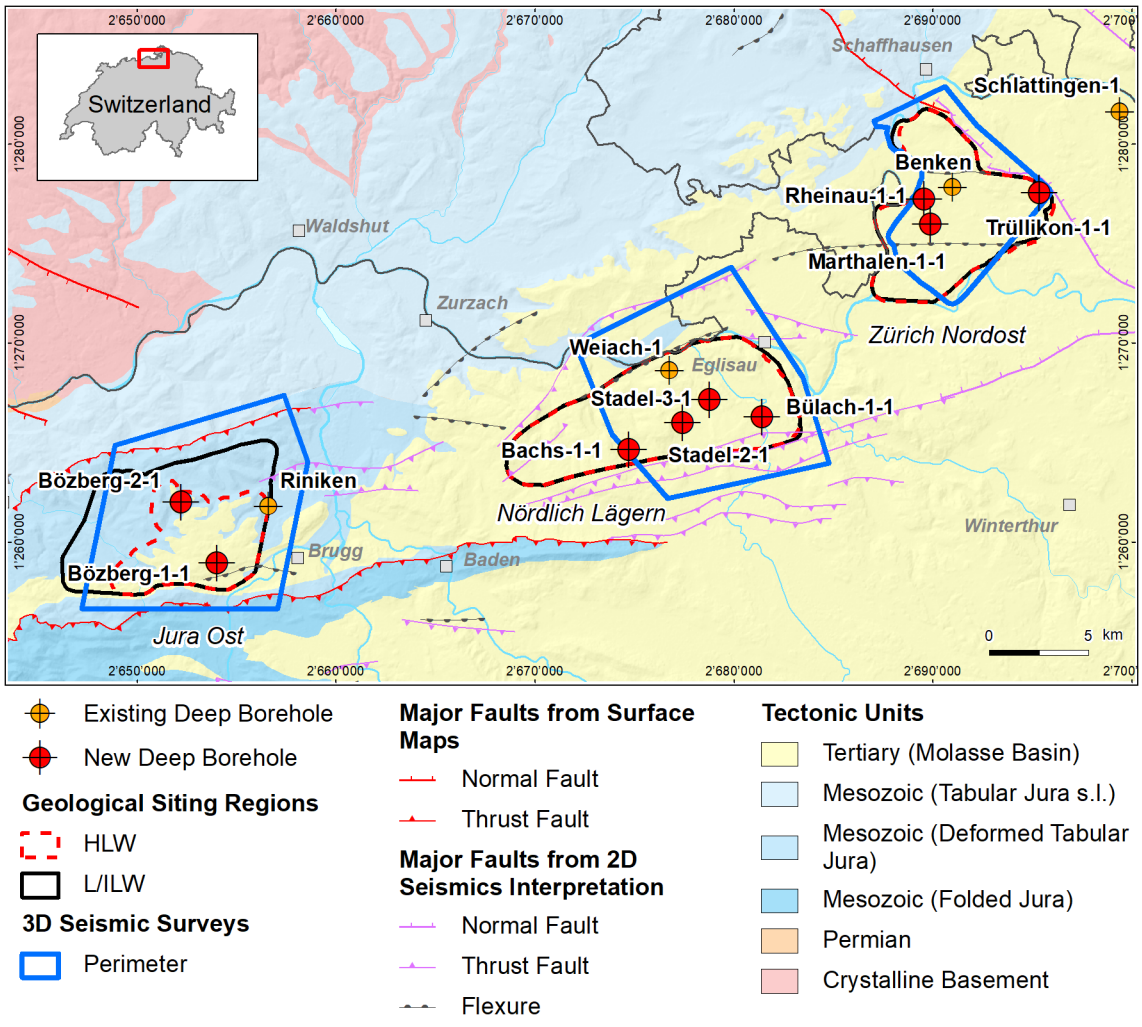

Fig. 1-1: Tectonic overview map with the three siting regions under investigation

1.2 Location and specifications of the borehole

The Stadel-3-1 (STA3-1) exploratory borehole is the sixth borehole drilled within the framework of the TBO project. The drill site is located in the central part of the Nördlich Lägern siting region (Fig. 1-2). The vertical borehole reached a final depth of 1'280.88 m (MD)[1]. The borehole specifications are provided in Tab. 1-1.

Tab. 1-1: General information about the STA3-1 borehole

Siting region	Nördlich Lägern
Municipality	Stadel (Canton Zürich / ZH), Switzerland
Drill site	Stadel-3 (STA3)
Borehole	Stadel-3-1 (STA3-1)
Coordinates	LV95: 2'678'792.885 / 1'267'161.988
Elevation	Ground level = top of rig cellar: 408.74 m above sea level (asl)
Borehole depth	1'280.88 m measured depth (MD) below ground level (bgl)
Drilling period	17th December 2020 – 25th June 2021 (spud date to end of rig release)
Drilling company	PR Marriott Drilling Ltd
Drilling rig	Rig-16 Drillmec HH102
Drilling fluid	Water-based mud with various amounts of different components such as[2]: 0.0 – 439.0 m: Polymers 439.0 – 640.0[3] m: Sodium chloride & polymers 640.0 – 1'035.0 m: Potassium silicate & polymers 1'035.0 – 1'101.0 m: Polymers 1'101.0 – 1'280.9 m: Sodium chloride & polymers

The lithostratigraphic profile and the casing scheme are shown in Fig. 1-3. The comparison of the core versus log depth[4] of the main lithostratigraphic boundaries in the STA3-1 borehole is shown in Tab. 1-2.

[1] Measured depth (MD) refers to the position along the borehole trajectory, starting at ground level, which for this borehole is the top of the rig cellar. For a perfectly vertical borehole, MD below ground level (bgl) and true vertical depth (TVD) are the same. In all Dossiers depth refers to MD unless stated otherwise.

[2] For detailed information see Dossier I.

[3] Borehole uncased below casing shoe at 437.4 m after drilling fluid exchange.

[4] Core depth refers to the depth marked on the drill cores. Log depth results from the depth observed during geophysical wireline logging. Note that the petrophysical logs have not been shifted to core depth, hence log depth differs from core depth.

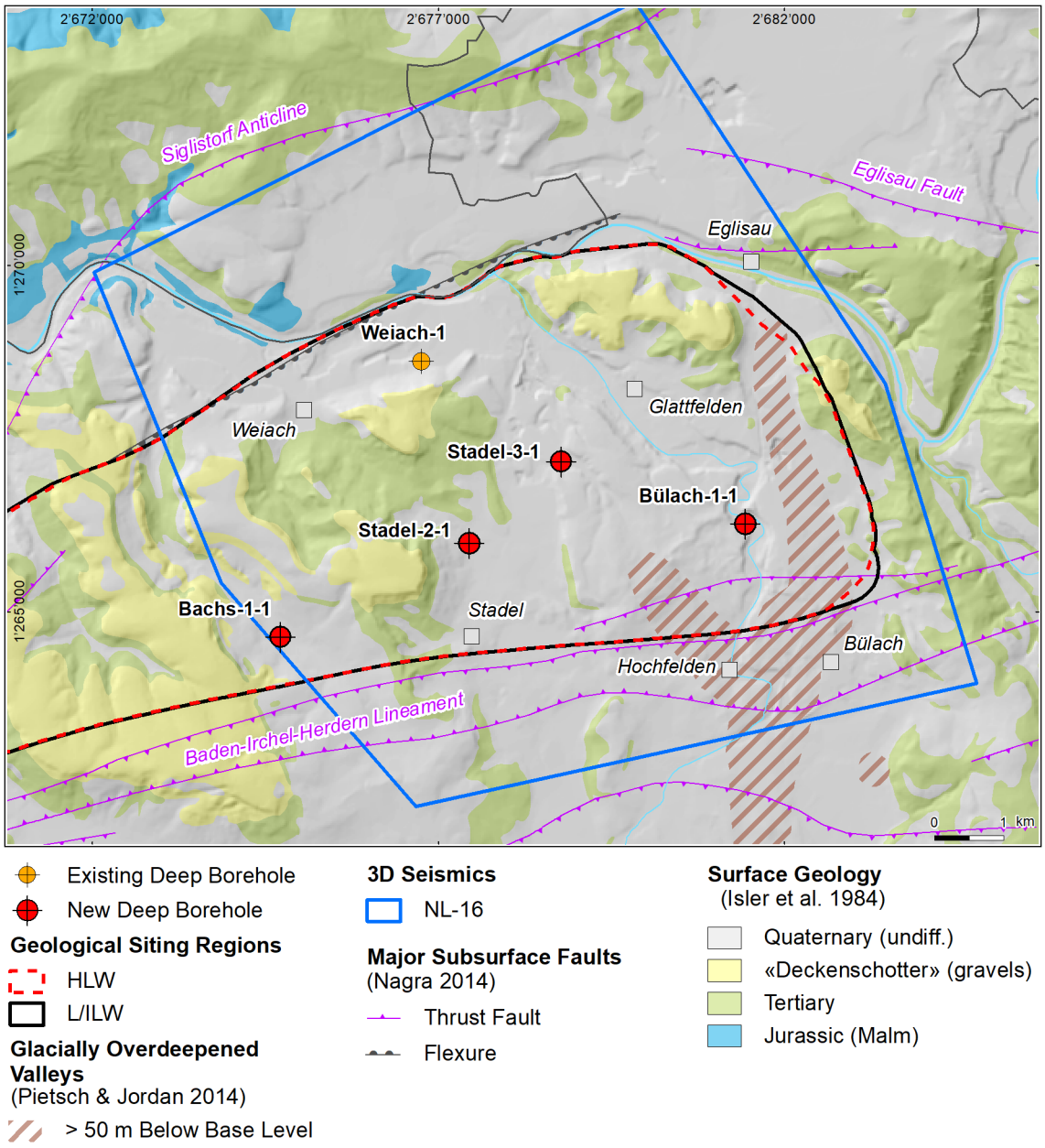

Fig. 1-2: Overview map of the investigation area in the Nördlich Lägern siting region with the location of the STA3-1 borehole in relation to the boreholes Weiach-1, BUL1-1, STA2-1 and BAC1-1

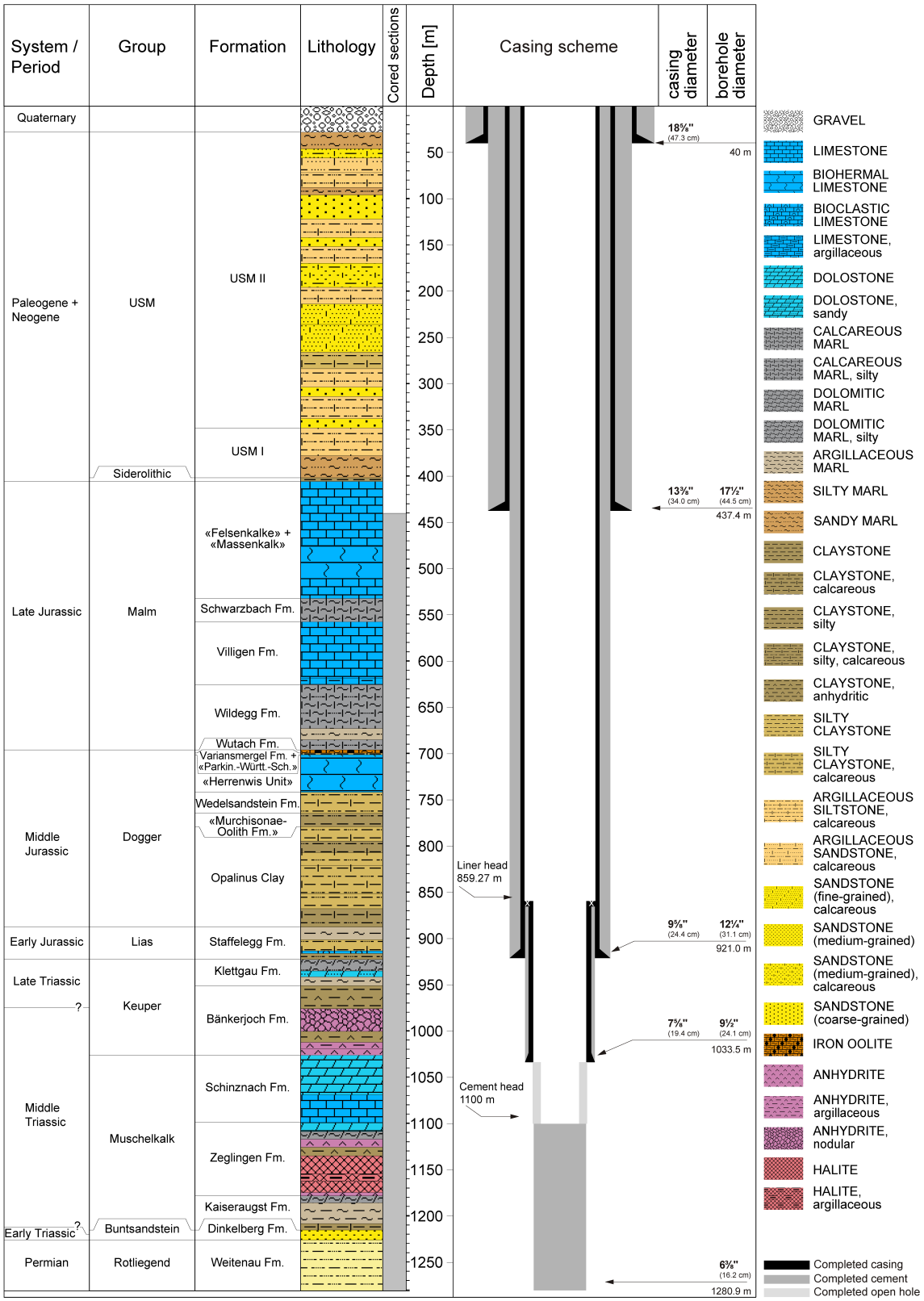

Fig. 1-3: Lithostratigraphic profile and casing scheme for the STA3-1 borehole[5]

[5] For detailed information see Dossier I and III.

Tab. 1-2: Core and log depth for the main lithostratigraphic boundaries in the STA3-1 borehole[6]

System / Period	Group	Formation		Core depth in m (MD)	Log depth in m (MD)	
Quaternary					**28.0**	—
Paleogene + Neogene	USM				402.0	—
	Siderolithic				**406.0**	—
Jurassic	Malm	«Felsenkalke» + «Massenkalk»		532.55	532.65	—
		Schwarzbach Formation		557.93	558.11	—
		Villigen Formation		625.58	625.64	—
		Wildegg Formation		696.03	696.15	—
	Dogger	Wutach Formation		699.47	699.59	—
		Variansmergel Formation + «Parkinsoni-Württembergica-Schichten»		701.65	701.77	—
		«Herrenwis Unit»		742.00	742.03	—
		Wedelsandstein Formation		764.97	764.94	—
		«Murchisonae-Oolith Formation»		779.26	779.16	—
		Opalinus Clay		887.94	887.72	—
	Lias	Staffelegg Formation		**922.71**	**922.44**	—
Triassic	Keuper	Klettgau Formation		951.13	951.57	—
		Bänkerjoch Formation		1026.62	1026.96	—
	Muschelkalk	Schinznach Formation		1099.03	1099.64	—
		Zeglingen Formation		1178.43	1178.73	—
		Kaiseraugst Formation		1215.50	1215.74	—
	Buntsandstein	Dinkelberg Formation		**1226.38**	**1226.68**	—
Permian	Rotliegend	Weitenau Formation	final depth	1280.88	1281.08	

[6] For details regarding lithostratigraphic boundaries see Dossier III and IV; for details about depth shifts (core goniometry) see Dossier V.

1.3 Documentation structure for the STA3-1 borehole

NAB 22-01 documents the majority of the investigations carried out in the STA3-1 borehole, including laboratory investigations on core material. The NAB comprises a series of stand-alone dossiers addressing individual topics and a final dossier with a summary composite plot (Tab. 1-3).

This documentation aims at early publication of the data collected in the STA3-1 borehole. It includes most of the data available approximately one year after completion of the borehole. Some analyses are still ongoing (e.g. diffusion experiments, analysis of veins, hydrochemical interpretation of water samples) and results will be published in separate reports.

The current borehole report will provide an important basis for the integration of datasets from different boreholes. The integration and interpretation of the results in the wider geological context will be documented later in separate geoscientific reports.

Tab. 1-3: List of dossiers included in NAB 22-01

Black indicates the dossier at hand.

Dossier	Title	Authors
I	TBO Stadel-3-1: Drilling	M. Ammen & P.-J. Palten
II	TBO Stadel-3-1: Core Photography	D. Kaehr & M. Gysi
III	TBO Stadel-3-1: Lithostratigraphy	P. Schürch, P. Jordan, M. Schwarz, H. Naef, R. Felber, T. Ibele & M. Gysi
IV	TBO Stadel-3-1: Microfacies, Bio- and Chemostratigraphic Analyses	S. Wohlwend, H.R. Bläsi, S. Feist-Burkhardt, B. Hostettler, U. Menkveld-Gfeller, V. Dietze & G. Deplazes
V	TBO Stadel-3-1: Structural Geology	A. Ebert, S. Cioldi, E. Hägerstedt & M. Gysi
VI	TBO Stadel-3-1: Wireline Logging, Micro-hydraulic Fracturing and Pressure-meter Testing	J. Gonus, E. Bailey, J. Desroches & R. Garrard
VII	TBO Stadel-3-1: Hydraulic Packer Testing	R. Schwarz, M. Willmann, H. Fisch L. Schlickenrieder, M. Voß & A. Pechstein
VIII	TBO Stadel-3-1: Rock Properties, Porewater Characterisation and Natural Tracer Profiles	L. Aschwanden, L. Camesi, E. Gaucher, T. Gimmi, A. Jenni, M. Kiczka, U. Mäder, M. Mazurek, D. Rufer, H.N. Waber, P. Wersin, C. Zwahlen & D. Traber
IX	TBO Stadel-3-1: Rock-mechanical and Geomechanical Laboratory Testing	E. Crisci, L. Laloui & S. Giger
X	TBO Stadel-3-1: Petrophysical Log Analysis	S. Marnat & J.K. Becker
	TBO Stadel-3-1: Summary Plot	Nagra

1.4 Scope and objectives of this dossier

The dossier at hand is organised as follows:

- Chapter 2 presents the aims of the laboratory testing programmes and introduces the laboratories involved.
- Chapter 3 provides an overview of core sampling, conditioning and storage methods, and also explains the non-destructive method used to evaluate core integrity prior to shipping to the laboratories.
- Chapter 4 introduces the testing methods used in the testing programmes and provides an overview of the executed tests per formation.
- Chapter 5 documents the results of the rock-mechanical testing programme.
- Chapter 6 documents the triaxial and the oedometric test results of the geomechanical testing programme. Given the greater complexity of the testing procedure and the relevance of the test results for site evaluation, these test results are more rigorously documented than the rock-mechanical test results.
- A short discussion on the representativeness of the results is provided in Chapter 7.

Furthermore, large documentation of the performed tests is reported in the appendix, and includes:

A – Photo documentation of the rock-mechanical testing programme

B – XCT (medical X-ray tomography) cross-sections, with indication of the section used for geomechanical testing

C – Diagnostic plots of the triaxial tests (geomechanical testing programme)

D – Mineralogical analysis (geomechanical testing programme)

E – Triaxial test results (geomechanical testing programme)

F – Test results in oedometric conditions (geomechanical testing programme)

2 Aims of the study and overview of the testing programme

2.1 Aims of the study and distinction of rock-mechanical and geomechanical testing programmes

For site characterisation, rock-mechanical and geomechanical properties are used for the following applications:

1. Supporting data for the detailed analysis and interpretation of in situ micro-hydraulic fracturing tests
2. Parametrise 3D geomechanical numerical models with (sub-)formation properties to assess the spatial variability of the stress tensor
3. Design of underground repository access structures
4. Hydro-mechanical properties of the host rock Opalinus Clay and its confining units
5. Volumetric behaviour (consolidation and swelling) and hydraulic properties of the host rock Opalinus Clay and its confining units

To address points 1. to 3. «standard» rock-mechanical tests were performed on core material in the stratigraphic interval Malm to Rotliegend, except for Opalinus Clay. «Standard» here means that the tests were performed according to national and international standards, notably the suggested methods of the International Society of Rock Mechanics (*cf.* Section 4.2). Standard tests were performed within the **"rock-mechanical testing programme"**.

In contrast, laboratory testing under points 4. and 5. were conducted using specialised protocols (*cf.* Section 4.3) combining rock-mechanical and soil mechanical aspects. Specifically, these protocols account for 1) the higher requirements of the low-permeability and fluid-sensitive Opalinus Clay and its argillaceous confining units to obtain robust test results, and 2) for the greater relevance of these units to evaluate the safety of a future repository. Tests performed using the specialised protocols are hereafter assigned to the **"geomechanical testing programme"**.

2.2 Overview of testing programme and contractors

2.2.1 Rock-mechanical testing programme

The rock-mechanical testing programme with core material of the STA3-1 borehole comprised the following testing methods:

- Indirect tensile strength (Brazilian)
- Uniaxial compressive strength (UCS)
- Triaxial compressive strength (TRX)

The following laboratory was contracted:

- Gesteinslabor Dr. Eberhard Jahns (Germany). Main contacts were Hansjörg Baumgartner, Sarah Louis and Johanna Menningen.

2.2.2 Geomechanical testing programme

The geomechanical testing programme was specifically designed for Opalinus Clay and its confining units and comprised of the following testing methods with cores from the STA3-1 borehole:

- Triaxial deformation tests with various stress paths (TRX)
- High-pressure oedometric testing (OED), including for some tests constant-head permeability phases (PERM)
- One-dimensional swelling tests (OS), carried out in oedometric conditions, either allowing axial swelling in free stress conditions or at constant stress

Three laboratories were contracted for the geomechanical testing campaign:

- NGI (Norway), main contact was Bahman Bohloli
- Sintef (Norway), main contact was Jørn Stenebråten
- DI (Italy), main contact was Alessio Ferrari

Each laboratory is identified with a letter, used in the test results labelling (A = NGI, B = Sintef, D = DI).

Specialised protocols were developed in recent years to evaluate hydro-mechanical properties of Opalinus Clay in both high-pressure oedometric tests (Favero 2017, Ferrari et al. 2016, Crisci et al. 2019) and triaxial deformation tests (Favero et al. 2018, Giger et al. 2018). In the case of triaxial testing, the testing procedures were further validated in a benchmarking study (Minardi et al. 2019, Minardi et al. 2020).

3 Core sampling, storage and XCT scanning

3.1 Core sampling and conditioning

Cores used for geomechanical or rock-mechanical analyses (hereafter referred to as GM cores) represent one of nine major categories sampled at the borehole. Each of these categories has special requirements to minimise potential effects on laboratory analyses, and hence special conditioning methods. Target exposure time to atmosphere was set to 20 minutes for all GM cores to allow geological description and documentation (incl. core scanner for photographic description). A complete archive of core photographs, and exposure time to atmosphere prior to embedding the cores in resin is made in Nagra's internal QA/QC documentation.

Fig. 3-1: Sampling and storage workflow of GM cores

(a) Inserting core directly into PVC tube (no plastic film). (b) Rack of PVC tubes during curing with clamp bar in core at the front row (left side). (c) Labelled PVC tubes with core and top spacer (used for clamping) embedded in epoxy resin. (d) Custom made core box used for transporting and archiving. Example pictures are from borehole Bülach-1-1 (Nagra 2021a).

The cores were then immediately inserted in PVC tubes, and axially constrained with bar clamps (Fig. 3-1). The annulus was then filled with epoxy (Sikadur-52). The annulus between the core and the PVC tube was chosen to be very small (nominal 3.2 mm) to ensure that no excessive temperature from curing of the epoxy develops[7]. Further details of the conditioning procedure are provided in the field manual (Rufer 2019).

A total of 79 GM cores with a cumulative length of 36 metres were conditioned in this way. Additional 2 cores were sampled later at the core storage facility. This was done to enable permeability testing to complement the in situ testing programme (hydraulic packer tests in the Klettgau Formation) where no conditioned core was secured, and only for hard rocks not sensitive to water exchange (drying).

3.2 Evaluation of core quality using XCT Scanning

To evaluate core integrity prior to shipping to the testing laboratories, all GM cores from Opalinus Clay and its confining units in the Upper Dogger and Lias (Staffelegg Formation) were analysed using medical X-ray computer tomography (XCT). Details of the applied XCT method can be found in Keller & Giger (2019). The obtained image data had a voxel size of 0.25 × 0.25 × 0.4 mm. By stacking individual scans, a virtual cross-section could be obtained for each core (Fig. 3-2). It is noted that the CT-number is a proxy for material density. This enabled the detection of small cracks and a physical representation of the variability of material properties. These cross-sections were the basis for the selection of sub-coring for the geomechanical testing programme (Chapter 6 and Appendix B).

[7] Maximum measured temperature in the laboratory was < 27 °C.

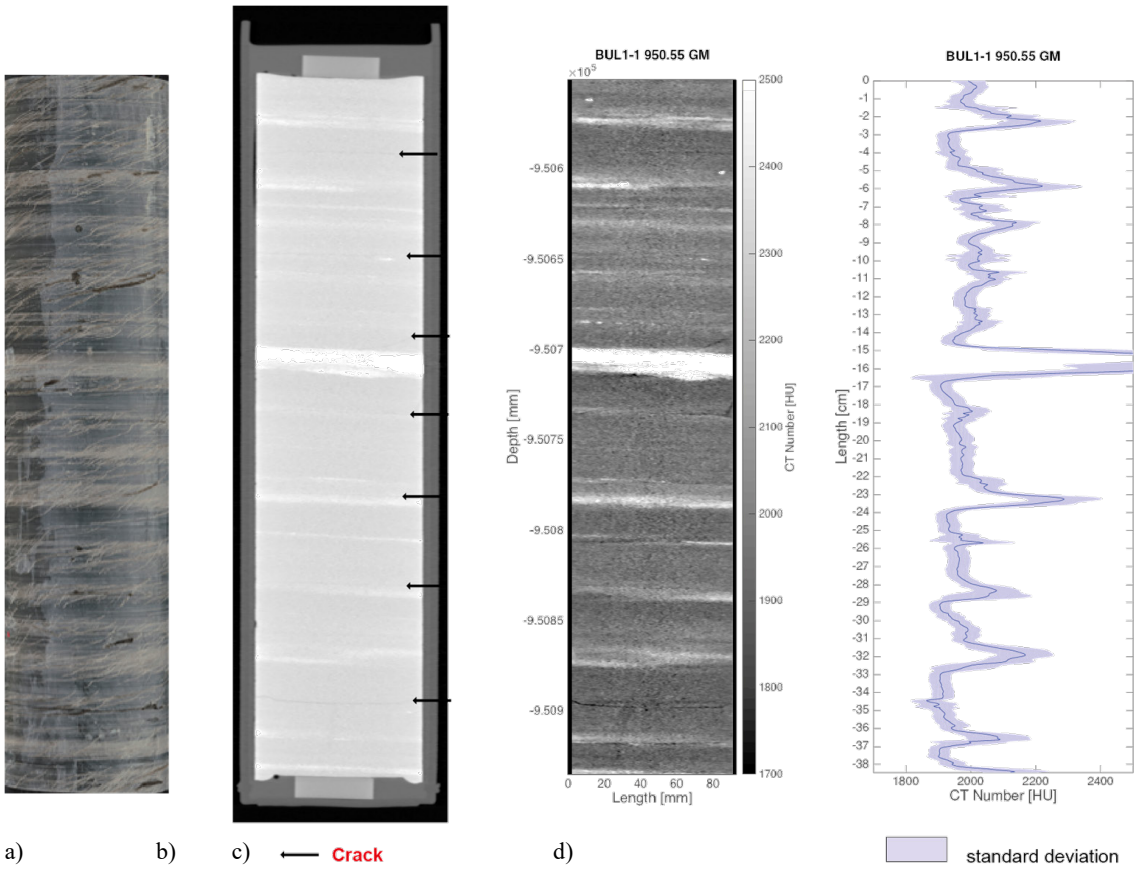

a) b) c) d)

Fig. 3-2: Cross-section of XCT stack

(a) core picture; (b) entire core in PVC tube and resin (both dark grey) and embedded spacers (light grey – subhorizontal cracks are indicated by arrows); (c) optimised image for the core only; (d) vertical profile with CT number (Hounsfield Units). Example pictures are from borehole Bülach-1-1 (Nagra 2021a).

4 Testing methods and overview of executed tests

4.1 Convention of sample geometry

Sedimentary geomaterials typically display transversely isotropic mechanical properties which are related to the orientation of the bedding. To study this anisotropic response, cylindrical specimens were tested in three orientations with respect to bedding (Fig. 4-1).

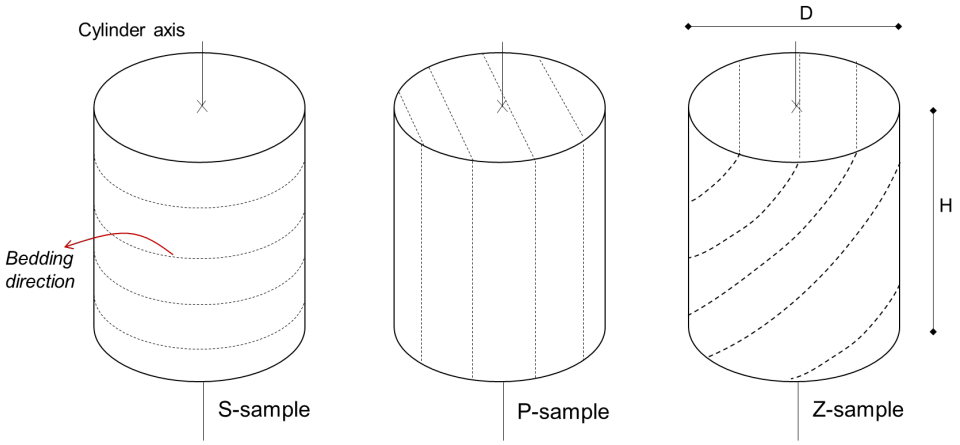

Fig. 4-1: Terminology of specimens in relation to bedding orientation

In this report, the following convention applies:

- S-samples: the cylinder axis is perpendicular to bedding direction
- P-samples: the cylinder axis is parallel to bedding direction
- Z-samples: the cylinder axis is at an angle with respect to bedding.

The convention applies to all kind of tests, however the ratio of diameter (D) to height (H) of the specimen is different. The ratio ranges from $D:H \approx 1/2$ for triaxial and uniaxial tests, to $D:H \approx 1.4$ in Brazilian tests and $D:H \approx 2.5$ for oedometric tests.

4.2 Rock-mechanical testing programme – testing methods

4.2.1 Indirect tensile strength test (Brazilian)

The Brazilian test is a uniaxial compressive strength test aimed for the indirect determination of tensile strength, and tests were done according to ASTM standard D3967-16 (ASTM 2016).

Test specimens have a diameter of 30 mm and a width of 21 mm (thickness:diameter ratio of 0.70). Testing plugs were drilled either perpendicular to bedding (so-called "S" direction) or parallel to bedding (so-called "P" direction). The plugs were drilled with a diamond tipped hollow bit. Cooling during drilling and trimming was performed with the low viscous volatile mineral oil Ilocut EDM 180 (from Castrol). Plug trimming to the required length was carried out with a diamond chop saw with slow constant velocity feeding.

During the test, cylindrical specimens are loaded perpendicular to the cylinder axis (Fig. 4-2). For clarification, it is noted that loading was always done perpendicular to the core axis. In case of the P-samples (Fig. 4-1) loading was parallel to bedding and the tensile force perpendicular to bedding. In case of the S-samples loading and tensile force are both parallel to bedding.

The constant loading rate during testing was approximately 0.30 MPa/s. In case of the P-samples (*cf.* Section 4.1) the specimen was oriented such that loading was parallel to bedding, with the tensile force, consequently, acting perpendicular to bedding. In case of the S-samples loading and tensile force are both perpendicular to bedding. The Brazilian tests were carried out on a high precision digitally controlled electromechanical testing machine with a maximum load range of 100 kN (accuracy class 0.5).

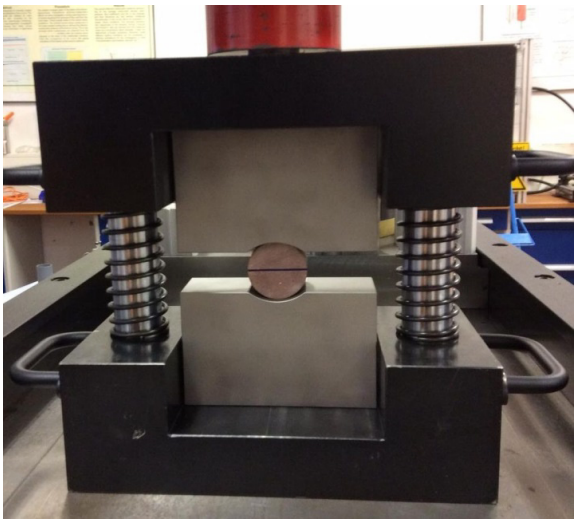

Fig. 4-2: Brazilian testing configuration with curved jaws
Plug diameter is 30 mm.

4.2.2 Unconfined compressive strength test

Unconfined compressive strength (UCS) tests were done according to ASTM standard D7012-14e1 (ASTM 2014).

Test specimens have a diameter of 25.4 mm and a length of at least 50.8 mm (length:diameter ratio of 2:1). Testing plugs were drilled either perpendicular to bedding (so-called "S" direction) or parallel to bedding (so-called "P" direction). The plugs were drilled with a diamond tipped hollow bit. Cooling during drilling and trimming was performed with the low viscous volatile mineral oil Ilocut EDM 180 (Castrol). Plug trimming to the required length was carried out with a diamond chop saw with slow constant velocity feeding. The accuracy in plane parallelism is in accordance with ASTM D4543-19 (ASTM 2019).

The UCS tests were performed on a digitally controlled, servo-hydraulic testing machine with a maximum load range of 600 kN (accuracy class 1) and at a constant strain rate of approximately 10^{-5} s^{-1}.

Axial deformation of the specimen was measured with either one or two LVDT displacement transducers. Measurements were either done directly at the specimen or corrected for load frame deformation. Radial deformation of the specimen is measured diametric with a transverse extensometer (Fig. 4-3).

Throughout this report, the strains are calculated as the ratio of the variation in height (or diameter) to the initial height (or diameter).

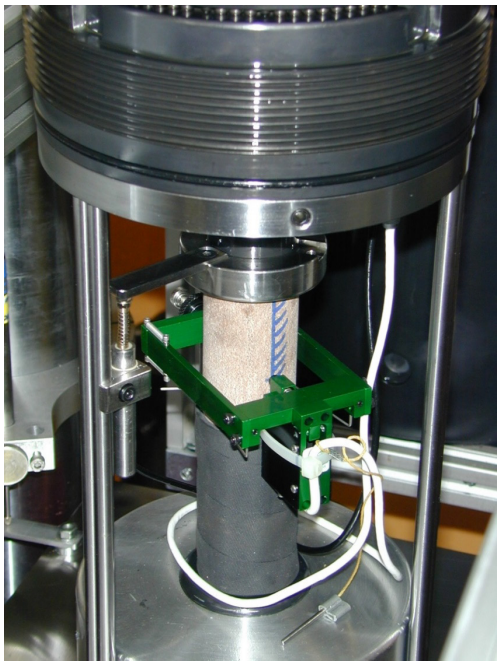

Fig. 4-3: UCS testing configuration

Note axial LVDT and transverse extensometer. Specimen diameter is 25.4 mm.

4.2.3 Triaxial deformation test

Triaxial deformation tests (TRX) were done according to ASTM standard D7012-14e1 (ASTM 2014) for single-stage procedure, but also included an unloading/reloading cyclebefore peak strength (below).

Test specimens have the same dimensions as for the UCS tests (diameter 25.4 mm, length 50.8 mm) and were prepared in the same manner (*cf.* Section 4.2.2). The accuracy in plane parallelism is also in accordance with ASTM D4543-19 (ASTM 2019).

Axial (average of three LVDTs) and radial deformation of the specimen (diametric with one single strain gauge) were measured 'in-vessel' to avoid the load frame deformation being included in the results of the deformation of the individual specimen (Fig. 4-4). The measurement range of the LVDTs is ± 5 mm; their sensitivity in the range between 9 and 60 mV; non-linearity is 0.15% full scale. Three LVDTs were used to observe specimen distortions that may influence the strength measurements in a non-acceptable manner. The differential axial load (strain gauge) also was measured 'in vessel' with a load cell mounted directly below the specimen to eliminate the influence of piston friction effects to the stress measurement. A 600 kN load cell of accuracy class 0.5 was used for the tests.

The artificial brine was composed of demineralised water and 5 g/l NaCl. An exceptions was the anhydrite specimen in test STA3-1-1025 for which no fluid was used. The pistons are perforated to enable drained conditions. Side drains were not used. No spherical seats were used. All the important parameters were recorded automatically with different intervals, adjusted to expected speed of changes. No smoothing or filtering algorithms were applied.

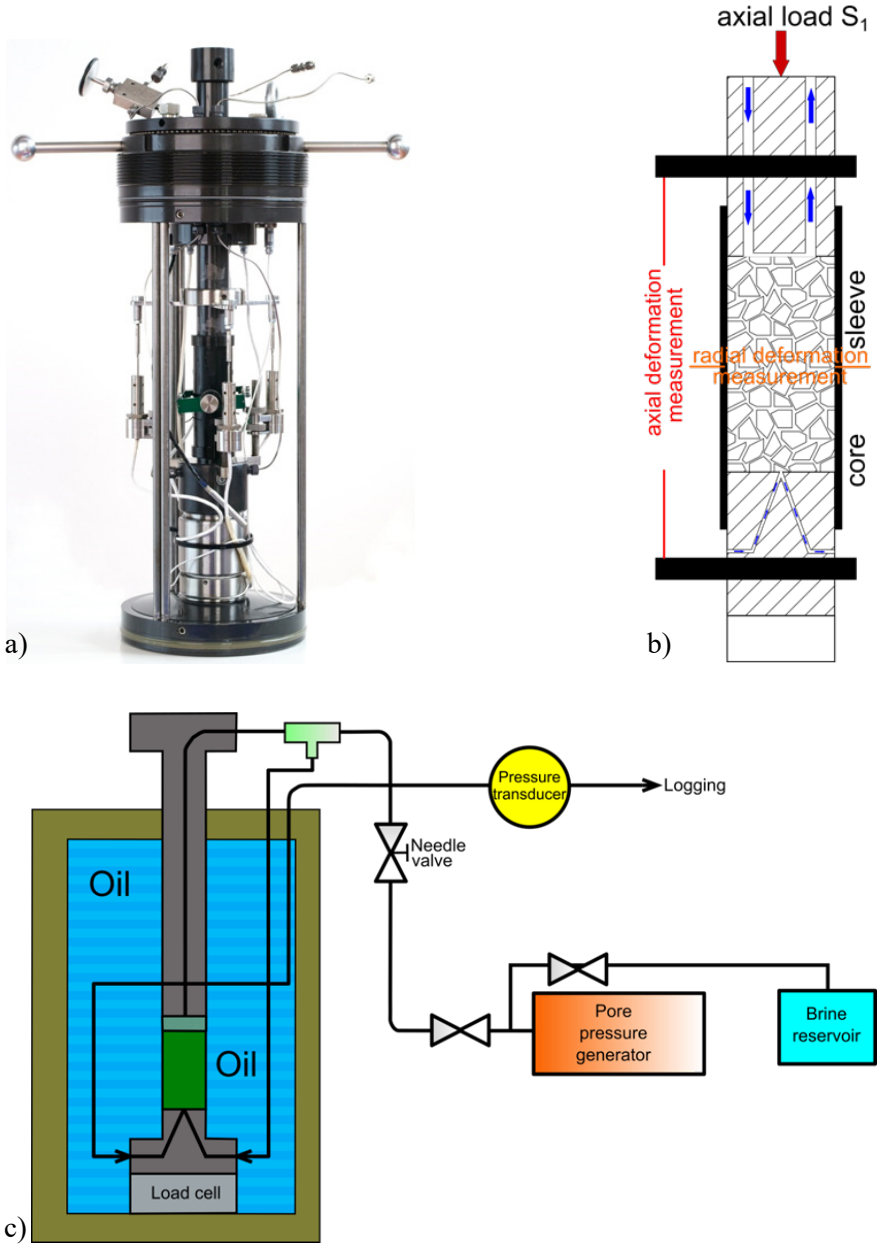

Fig. 4-4: Triaxial testing configuration used for rock-mechanical testing

Specimen in membrane with axial and radial strain sensors, pore fluid line and ultrasonics (a), schematic of the specimen (b) and the pressure cell with pore fluid system (c).

During all phases of the tests, ultrasonic velocities, both P- and S-waves, were logged and monitored according to ISRM standards (Aydin 2014). The piezometer resonance frequency was 1 MHz.

The theoretically possible stress paths in a triaxial testing configuration with two independent controls (axial and radial stress) are illustrated in Fig. 4-5 in mean total stress (p) versus deviatoric stress (q) space, where:

$$p = \frac{\sigma_a + 2\sigma_r}{3} \tag{4-1}$$

$$q = \sigma_a - \sigma_r \tag{4-2}$$

Where σ_a and σ_r are the total axial (direction of the cylinder axis) and radial (direction perpendicular to the cylinder axis) stress, respectively.

The upper part of the plane (compression part) summarises the stress paths that induce axial compression of the tested specimen. The shear path can be induced by either increasing the axial stress σ_a (CTC path), reducing the radial stress σ_r (RTC path) or increasing σ_a and reducing σ_r at the same time (TC path) keeping the mean total stress constant. The stress paths that induce an axial extension of the specimen are illustrated below the p-axis in Fig. 4-5. The axial extension can be induced by either decreasing the axial stress (RTE path), increasing the radial stress (CTE), or decreasing σ_a and increasing σ_r at the same time (TE path) keeping the mean total stress constant. Therefore, when the term 'reduce' is used to define the stress path, it means that one of the two stresses is decreased while the other is kept constant. On the other hand, when the term 'conventional' is used to define the stress path, it means that one of the two stresses is increased and the other is kept constant. It is noted that the illustrations in Fig. 4-5 are the stress paths for total stress only, so the tests can be conducted in either drained or undrained conditions. This means that the submitted loading conditions may differ based on the porewater pressure generation during undrained testing. For the triaxial tests of the rock-mechanical testing programme, only CTC stress paths were executed.

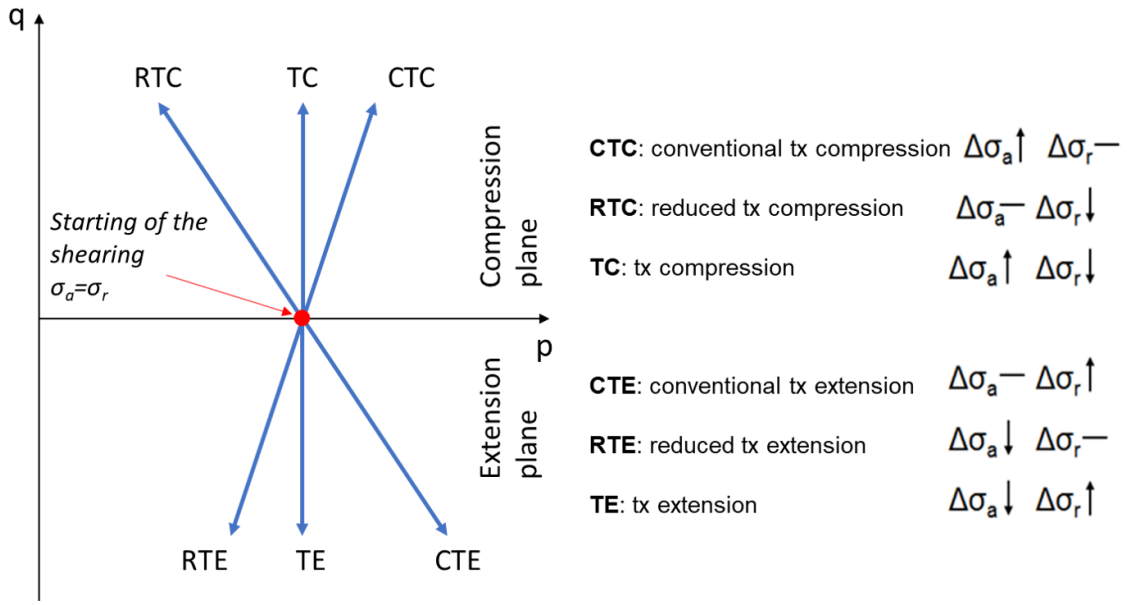

Fig. 4-5: Summary of possible stress paths that can be used to perform triaxial tests

On the right side, it is indicated which of the two stresses (axial σ_a and radial σ_r) is increased or decreased.

Test procedure

The testing procedure consisted of a maximum of four main phases:

1. Isotropic loading phase, during which the radial confining pressure and the axial load are increased simultaneously. The needle valve to the pore pressure generator is opened after the total stress has reached an equivalent value of 2 MPa. Both total mean stress (p) and fluid pressure (u_w) are then increased in concert to their respective target values: 10 to 15 MPa for p and 5 MPa for u_w.
2. *Selected tests only:* the pore-fluid-coupling parameter during isotropic loading (Skempton's B value) is evaluated in undrained conditions. During the Skempton's B test, the change in pore pressure over time (Δu_w) is determined as a function of the change in isotropic pressure increase over time (Δp) (u_w is allowed to equilibrate at least for 20 minutes up to 8 – 24 hours):

$$B = \frac{\Delta u_w}{\Delta p} \tag{4-3}$$

   In the present case two to three Skempton's B tests were carried out per specimen with confining pressure increase Δp of 1 or 2 MPa.
3. *Selected tests only:* a consolidation phase is performed to determine the consolidation coefficient c_{vi}. An isotropic total stress increase (or decrease) is applied to the specimen and the deformations in time are recorded and analysed. The deformation evolves according to the dissipation of the porewater over- (or under-) pressure induced by the load variation. Calculation of the consolidation coefficient c_{vi} (in mm^2/h) is done according to the following equation (Head 1998):

$$c_{vi} = \frac{\pi D^2}{\lambda t_{100}} \tag{4-4}$$

   with D as the plug diameter and t_{100} as the theoretical time to 100% consolidation. The theoretical time t_{100} is found by extrapolating the linear portion of the volumetric strain versus square root of the experimental time curve (with time in h) to the final strain value. Lastly, λ is a constant depending on drainage boundary conditions.
4. The fourth testing phase is the shearing phase or triaxial test, applying a constant deviatoric stress or strain rate. The standard strain rate was 10^{-6} s^{-1} but was adjusted based on theoretical calculations (Head 1998) using the consolidation coefficient determined in phase 3 or considering lithology and water content.

The shearing phase of the triaxial tests was preceded in selected cases by a Skempton's B test for verification of specimen saturation and, subsequently, by a determination of the consolidation coefficient c_v as base for strain rate calculation. However, in the rock mechanics programme of STA3-1 cores, consolidation coefficients were not determined. Instead, strain rates were chosen based on lithological criteria (rock type, water content and mechanical properties based on UCS test results) and previous experiences (*cf.* Nagra 2021a and Nagra 2021b).

Generally, clay-rich rocks, such as clay- and siltstones or marls were tested at lower strain rates than limestones, sandstones and anhydrites. The strain rate of the single-stage triaxial tests ranged between 10^{-5} s^{-1} (1 TRX test), 10^{-6} s^{-1} (7 TRX tests), and 2×10^{-7} s^{-1} (3 TRX tests).

4.3 Geomechanical testing programme – testing methods

4.3.1 Synthetic pore fluid

The artificial porewater (APW) used in the geomechanical tests is based on the recipe derived from the investigations in the Schlattingen borehole (Mäder in Wersin et al. 2013), and the composition is reported in Tab. 4-1. This recipe defines a porewater saturated with respect to calcite and dolomite under atmospheric CO_2 partial pressure (lab conditions).

Towards the end of the geomechanical testing programme, the porewater chemistry was also constrained for the STA3-1 core material (*cf.* Dossier VIII). These investigations confirm the general Na-Cl water type. The salinities in the Dogger section are somewhat higher than in the APW; e.g. chloride concentrations in Opalinus Clay and the adjacent confining units are around 8 g/L (APW: 6.7 g/L). In addition to saturation with carbonate minerals, the investigations suggest that the porewaters are at or close to saturation with respect to the sulphate minerals celestite and gypsum. But the APW was not changed for the final geomechanical tests, to be consistent with earlier tests. Finally, the slightly higher ionic strength in the porewater found in the STA3-1 core is not anticipated to have a significant effect on hydromechanical properties (Witteveen et al. 2013, Ewy 2014, Tuttolomondo 2021).

Tab. 4-1: Recipe used for the preparation of the APW

Compound	$mmol/kg_{H2O}$	g/kg_{H2O}
NaCl	115.26	6.7356
$NaHCO_3$	0.54	0.0456
$CaCl_2\ 2H_2O$	11.91	1.7510
KCl	2.55	0.1902
$MgCl_2\ 6H_2O$	9.17	1.8635
Na_2SO_4	24.00	3.4089

4.3.2 Triaxial deformation test (specialised protocol)

To assess the mechanical properties of the Opalinus Clay and confining units, dedicated testing protocols were established (Minardi et al. 2019).

The extraction of the specimens was carefully performed in order to minimise water content loss during the operation. All involved laboratories used a drilling machine. All labs used hydrocarbons as cooling fluids during the drilling of the specimens.

Computed tomography of the cores after drilling was used to identify the most suitable sections for extracting test specimens *(cf.* Appendix A). The target zones were selected upon Nesol's and Nagra's guidance.

The conventional testing procedure indicated by Nagra to carry out triaxial tests foresaw the following steps (Fig. 4-6):

1. An initial isotropic total stress (0.5 – 1 MPa) is applied to the specimen to ensure contact with the axial piston. The saturation of the specimen is then performed at constant volume to minimise specimen disturbance (i.e. fissure opening during resaturation); axial and radial stresses are progressively increased to keep the specimen's volume constant while it is put in contact with fluid at low back pressure. Next, the fluid back-pressure is increased to at least 2 MPa (the total stresses are also increased to keep the effective stress constant) (*ss1*), to dissolve possible air remaining in the tubing or the material. This procedure allows the determination of the axial and radial swelling pressures. The confining stress is then set equal to the axial stress (*ss2*). A pore pressure increment step is performed either at this stage (*ss3*) or before the shearing phase in order to reach the target confinment.
2. The assessment of the specimens' saturation is carried out by measuring the Skempton's B coefficient (B check test). Two to three isotropic undrained loadings are performed. More steps are applied when unsatisfactory values are obtained.
3. Drained consolidation or swelling of the specimen is performed to reach the target consolidation stress; consolidation effective stresses range between 7 and 20 MPa. The pore fluid pressure is kept constant to 8 – 10 MPa during consolidation.
4. The final stage is the shearing of the specimens at constant axial strain rate. An unloading/ reloading loop is performed, then the specimen is sheared until the specimen's failure and achievement of the post-peak constant deviatoric stress, in undrained or drained conditions.

In the following, the variations from the above mentioned procedure are listed.

Samples B4_STA3_1_857_07S20CTCU and B5_STA3_1_857_07S7CTC were saturated in isochoric conditions. Then, after the swelling pressure stabilised, the pore pressure was increased in steps of 2 MPa, keeping the isochoric condition, and time was allowed for the total axial and radial stresses to equilibrate. The procedure was adopted to check the influence of the pore pressure on the swelling pressure measurement.

To evaluate potential effects of the water chemistry on the sample mechanical response, deionised water was used during testing of sample B7_STA3_1_857_07S13CTCU_DI. The saturation was first conducted in isochoric condition, where swelling pressure increased to a total axial stress of 23 MPa, whereupon the isochoric condition was stopped and constant stress/pressure maintained (19.9 MPa confining pressure). The change in the boundary condition was selected to avoid an excess pressure generation during saturation, which may have been induced by the deionised water, but still obtain effective stress levels at the end of saturation comparable to other test results.

Samples A5_STA3_1_812_44S13CTCU and A6_STA3_1_812_44S13CTCU were saturated at constant isotropic effective stress (p' = 12 MPa), until strains reached equilibrium. Following the B checks, two isotropic drained phases were conducted: a loading and an unloading over the same stress amplitude. Both were used to estimate the consolidation coefficient. The undrained shearing phase of test A5 was conducted at a strain rate of 1×10^{-7} s^{-1}, a rate similar to that used in other undrained tests in Opalinus Clay, in the current and in the previous testing campaigns. On the other hand, test A6 was deliberately conducted at a strain rate 5 times lower than test A5, hence at a strain rate 2×10^{-8} s^{-1}. The latter is a strain rate usually adopted for drained shearing. The comparison between the results of the two tests allow to evaluate the potential impact of the shearing rate on the mechanical response.

The laboratories involved in the triaxial testing programme with specialised protocols, prepared cylindrical specimens respecting the diameter (D) to height (H) ratio $D:H \approx 0.5$. In particular, the specimen nominal diameters are:

- Lab A: $D = 25.0$ mm
- Lab B: $D = 25.0$ mm

The labs used two drainage systems, both radial drainage and drainage at the two edges. The strain rates to apply during shearing were defined according to the drainage conditions and the specimen dimensions (i.e., drainage length). Water content after testing was determined by oven-drying at 105 °C for several days until constant weight.

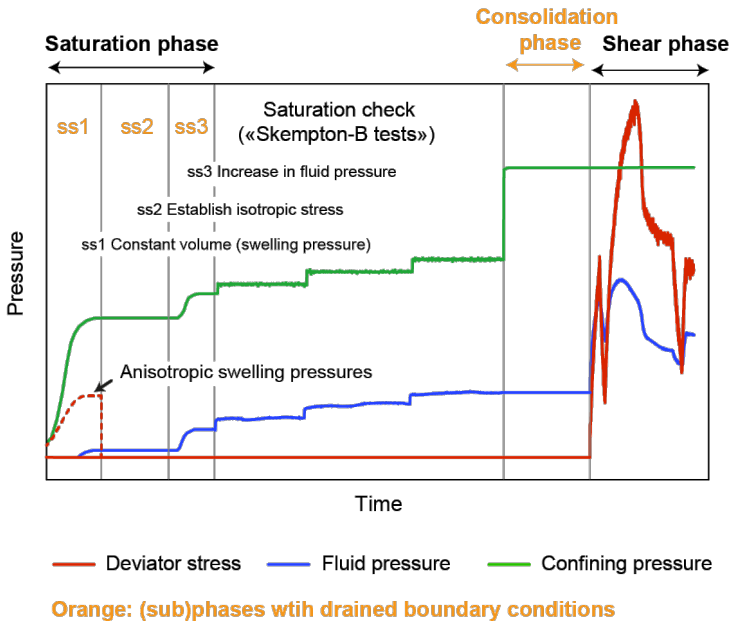

Fig. 4-6: Pressure – time sequence of triaxial deformation tests (specialised protocol)

Conventional testing procedure for undrained boundary conditions during the shear phase.

4.3.3 Oedometric test (high-pressure, specialised protocol)

Specimens for oedometric testing are of cylindrical shape, with a diameter (D) to height (H) ratio $D:H \geq 2.5$. The nominal dimensions of the specimens are:

- Lab D: $D = 35.0$ mm; $H = 12.5$ mm

The operators cut a pre-defined section of the core with a saw, through the PVC tube to minimise exposure of the geomaterial to the atmosphere. Then, the obtained slice is cut into a smaller piece to be handled within a lathe machine. No air nor water is used during the sawing process. Planarity and parallelism of the bases are verified, and the dimensions of sawn specimens are measured. In addition, Lab A covered the cut parts with a hydrocarbon oil and performed lathing at high humidity to limit the humidity gradient between the specimen and the laboratory atmosphere. After the final specimen diameter was reached, the specimen was wiped free of oil (using oil-only absorbent).

The specimen is then put into the oedometric ring, a rigid metallic ring to constrain the radial strains; silicon grease was placed on the internal surface of the ring to reduce the friction between the specimen and the metallic ring.

The specimen disks are loaded axially, and deformation is recorded with time.

Specimens are resaturated within the apparatus in isochoric conditions. The axial deformations are kept constant by increasing the axial stress. Pore pressure is applied from the bottom side of the specimen at 50 kPa. When the swelling pressure generated by saturation at isochoric conditions stabilises, pore pressure equal to 50 kPa is applied at the top side of the specimen. Displacements are monitored throughout this stage of the test. Once the axial stress has stabilised, the mechanical loading phase of the test can start.

The loading is performed in steps, starting from the axial swelling stress attained at the end of the resaturation phase. The incremental loading steps are performed by doubling the axial stress reached during the previous step. Each step lasted at least 24 hours. A few doubling steps (depending on the swelling stress) are performed to achieve an axial stress of 10 – 15 MPa. For selected tests, a constant-head permeability test (PERM) is performed at this stage, increasing the pore pressure at the bottom side and measuring the fluid flow through the specimen. The axial stress and pressure gradient are kept constant during the permeability test until steady-state conditions are achieved. Then, the bottom fluid pressure is reduced back to 50 kPa. Enough time is given for the displacement to stabilise (minimum of 24 hours). After that, the sample is loaded up to 20 MPa. Finally, unloading was performed in steps, following the same loading steps. Unloading was continued to the minimum possible stress level, below the swelling pressure stress level. This procedure differs from the one applied in the previous testing campaigns, since the load is stopped to a lower effective stress, while the unloading is prolongated.

After completion of the test, the oedometer cell is dismantled, and the specimen is dried in the oven to measure the water content (oven-drying at 105 °C for several days until constant weight).

4.4 Lithostratigraphy and test overview

4.4.1 Lithostratigraphy of tested core material

A brief summary is provided here on lithological characteristics of the formations of which cores were used in geomechanical testing. Further details on lithology can be found in Dossier III ('TBO Stadel-3-1: Lithostratigraphy').

- **«Felsenkalke» + «Massenkalk»**: Bedded (Felsenkalke) to poorly or non-bedded limestones (Massenkalk).
- **Schwarzbach Formation**: Calcareous to argillaceous marls.
- **Wildegg Formation**: Calcareous marl with interlayers of limestone.
- **«Herrenwis Unit»**: A sedimentary succession consisting of coralligeneous sediments in the upper part (from which a test sample was taken) and encrinite in the lower part.
- **Wedelsandstein Formation**: Predominantly argillaceous siltstone grading downward into (silty) claystone. The quartz content decreases with depth. The tested samples are from the upper (743 m) and central part (755 m) of the formation.

- «**Murchisonae-Oolith Formation**»: A very heterogeneous succession of siltstone, argillaceous marl to claystone and limestone beds. The tested interval (768 m) is a rather homogeneous argillaceous siltstone.
- **Opalinus Clay**: Silty claystone with silty to sandy lenses. The following subdivision was specified:
  - **779.26 – 807.34 m Subunit 1**: **«Sub-unit with silty calcareous beds» (28.08 m)**: Claystone to silty claystone with discrete heterogeneities, in particular silty calcareous beds and nodules.
  - **807.34 – 821.09 m Subunit 2**: **«Upper silty sub-unit» (13.75 m)**: Claystone to silty claystone with frequent lenses, typically centimetres wide and several millimetres thick (flaser structure).
  - **821.09 – 868.06 m Subunit 3**: **«Mixed clay-silt-carbonate sub-unit» (46.97 m)**: Silty claystone, devoid of marked characteristics typical for the other subunits.
  - **868.06 – 887.94 m Subunit 4**: **«Clay-rich sub-unit» (19.88 m)**: Homogeneous claystone with high clay-mineral content (mostly > 60 wt.-%).
- **Staffelegg Formation**: Marl and claystone, some of it bituminous, and including various thin limestone horizons, some of them iron-oolitic. The tested interval (902 m) belongs to the Frick Member and is an argillaceous siltstone.
- **Klettgau Formation**: Heterogeneous succession dominated by playa sediments with mostly silty claystone and dolocretes. The tested interval (950 m) is from the Ergolz Member.
- **Bänkerjoch Formation**: Succession of anhydrite, dolomitic marl, dolostone and sandstone. Both tested samples are anhydrites, with the one from 968 m characterised as chickenwire texture (anhydrite as nodules in argillaceous matrix).
- **Schinznach Formation**: Succession of dolomites and dolostones, partly dolomitised limestones and micritic limestones, and bituminous claystones.
- **Zeglingen Formation**: Evaporitic sequence with anhydrite, rock salt and dolostone. The tested samples are a dolostone (1'105 m) and halite (1'154 m).
- **Kaiseraugst Formation**: Succession of claystone to marly, partly bituminous and dolomitic marl, with interbeds of limestone, dolostone and sandstone.
- **Weitenau Formation**: Siliciclastic pre-Mesozoic sediments. Siltstone with few beds of sandstone (mostly fine-grained and argillaceous). Fanglomerates, as found in all nearby boreholes, are missing.

4.4.2 Test overview

A total of 97[8] rock-mechanical and geomechanical tests were conducted on a total of 23 cores from borehole STA3-1 (Tab. 4-2). The number of tests in the geomechanical testing programme is smaller than in the rock-mechanical testing programme. However, typical testing times in the geomechanical programme were 12 to 30 days for TRX+ tests and 20 to 35 days for OED+ tests. This is one order of magnitude longer than the typical TRX test in the rock-mechanical testing programme.

[8] The 2 constant-head permeability tests (PERM) performed as part of the oedometric tests (OED+) are not counted separately in the total number of tests, but they are listed as such in Tab. 4-2 for overview.

Cores without proper initial conditioning (PVC = 0 in Tab. 4-2) were generally only used for lithologies not sensitive to water exchange, i.e. without any macroscopic indication of damage at the time of sampling in the storage facility.

Tab. 4-2: Overview of performed tests

The red border illustrates the clay-mineral rich interval of Opalinus Clay and confining units (focus of geomechanical testing programme). PVC indicates whether cores were conditioned in resin and core barrel on site (1) or later wrapped in aluminium foil off-site (0). TRX = triaxial test, UCS = unconfined compressive strength test, TS = indirect tensile strength test (Brazilian), TRX+ = TRX with specialised protocols, OED+ = Oedometric test with specialised protocols (high-pressure), OS = swelling test in oedometric conditions.

Core-ID	**Formation**	**Top**	**Length**	**Bottom**		**Rock-mechanical testing programme**			**Geomechanical testing programme**		
						Standard rock-mechanical tests			**Special protocols**		**Other**
STA3-1		[m]	[cm]	[m]	**PVC**	**TRX**	**UCS**	**TS**	**TRX+**	**OED+**	**OS**
476.23/50-GM	«Felsenkalke» + «Massenk.»	476.23	50	476.73	1		3				
516.74/50-GM		476.23	50	476.73	1	1	3	1			
534.97/50-GM	Schwarzbach	534.97	50	535.47	1		3	1			
556.26/50-GM		556.26	50	556.76	1	1	3	1			
644.20/50-GM	Wildegg	644.20	50	644.70	1	1	3	1			
680.50/50-GM		680.50	50	681.00	1		3				
704.28/40-GM	«Herrenwis Unit»	704.28	40	704.68	1	1	3	1			
743.88/50-GM	Wedelsandstein	743.88	50	744.38	1		3				
755.82/49-GM		755.82	49	756.31	1	1	2	1			
768.72/50-GM	«Murchisonae-Oolith»	768.72	50	769.22	1					1	
812.19/50-GM	Opalinus Clay	812.19	50	812.69	1				6	2	2
856.99/40-GM		856.99	40	857.39	1				7		
902.07/50-GM	Staffelegg	902.07	50	902.57	1	1	3	1			
950.05/50-GM	Klettgau	950.05	50	950.55	1	1	3	1			
968.53/36-GM	Bänkerjoch	968.53	36	968.89	1		3				
1025.57/40-GM		1025.57	40	1025.97	1	1	3				
1031.58/45-GM	Schinznach	1031.58	45	1032.03	1		3				
1077.19/34-GM		1077.19	34	1077.53	1	1	3				
1105.25/46-GM	Zeglingen	1105.25	46	1105.71	1		3				
1154.48/50-GM		1154.48	50	1154.98	1		3				
1195.16/33-GM	Kaiseraugst	1195.16	33	1195.49	1	1	3	1			
1237.50/39-GM	Weitenau	1237.50	39	1237.89	1	1	2	1			
1274.32/50-GM		1274.32	50	1274.82	1		3				
Total					**23**	**11**	**58**	**10**	**13**	**3**	**2**

5 Rock-mechanical testing

5.1 Indirect tensile strength test (Brazilian)

A total of 10 Brazilian tests were performed (Tab. 5-1). The splitting tensile strength (MPa) is calculated according to the following formula (curved jaws):

$$S_z = \frac{1272 * F}{\pi * d * l} \tag{5-1}$$

with the compressive force F (in kN); the specimen diameter d (in mm) and the specimen length l (in mm). It is noted that the values of S_z are negative.

Tab. 5-1: Test results from indirect tensile strength tests

For specimen geometry see Fig. 4-1.

Test-ID	**Specimen geometry**	**Average depth**	**Bulk density**	**Water content**	**Tensile strength**
		[m]	[g/cm^3]	[wt.-%]	[MPa]
STA3-1_516TS_S1	S	516.81	2.675	0.35	-7.7
STA3-1_534TS_S1	S	535.37	2.650	1.37	-3.6
STA3-1_556TS_S1	S	556.33	2.598	3.22	-3.3
STA3-1_644TS_S1	S	644.22	2.619	2.17	-3.5
STA3-1_704TS_S1	S	704.34	2.699	0.35	-3.6
STA3-1_755TS_S1	S	755.89	2.498	5.38	-3.7
STA3-1_902TS_S1	S	902.29	2.539	3.33	-2.8
STA3-1_950TS_S1	S	950.24	2.435	3.25	-2.6
STA3-1_1195TS_S1	S	1'195.23	2.637	2.59	-5.1
STA3-1_1237TS_S1	S	1'237.50	2.561	4.98	-3.5

The test results yielded values from -7.7 MPa to -2.6 MPa for S-samples. Most TS specimens failed along primary central tensile fractures. Photographs of the specimens before and after testing can be found in Appendix A.

5.2 Unconfined compressive strength tests (UCS)

A total of 58 UCS tests were performed by two laboratories (Tab. 5-2). Photographs of the specimens before and after testing can be found in Appendix A.

At the linear portion of the axial load cycle, an unloading/reloading cycle was performed by reducing the axial stress to 1/3 of the actual load, and hysteresis was observed. The cycle was performed for determining the elastic properties of the rock. The Young's modulus E (in GPa) was determined as an average reload modulus using the slope of the rising portion of the hysteresis as the ratio between the axial load change $\Delta\sigma_a$ (in MPa) and the induced axial strain $\Delta\varepsilon_a$ (dimensionless) according to the equation:

$$E = \frac{\Delta\sigma_a}{\Delta\varepsilon_a} \tag{5-2}$$

The Poisson's ratio (ν) is calculated as the negative ratio between the delta in radial $\Delta\varepsilon_r$ and axial strain $\Delta\varepsilon_a$:

$$\nu = -\frac{\Delta\varepsilon_r}{\Delta\varepsilon_a} \tag{5-3}$$

An example of calculation of tangent E modulus is reported in Fig. 5-1.

Following the hysteresis, the axial load was again increased until peak strength was reached, and the specimen was allowed to fail. The compressive peak strength was derived from the peak value of the axial load.

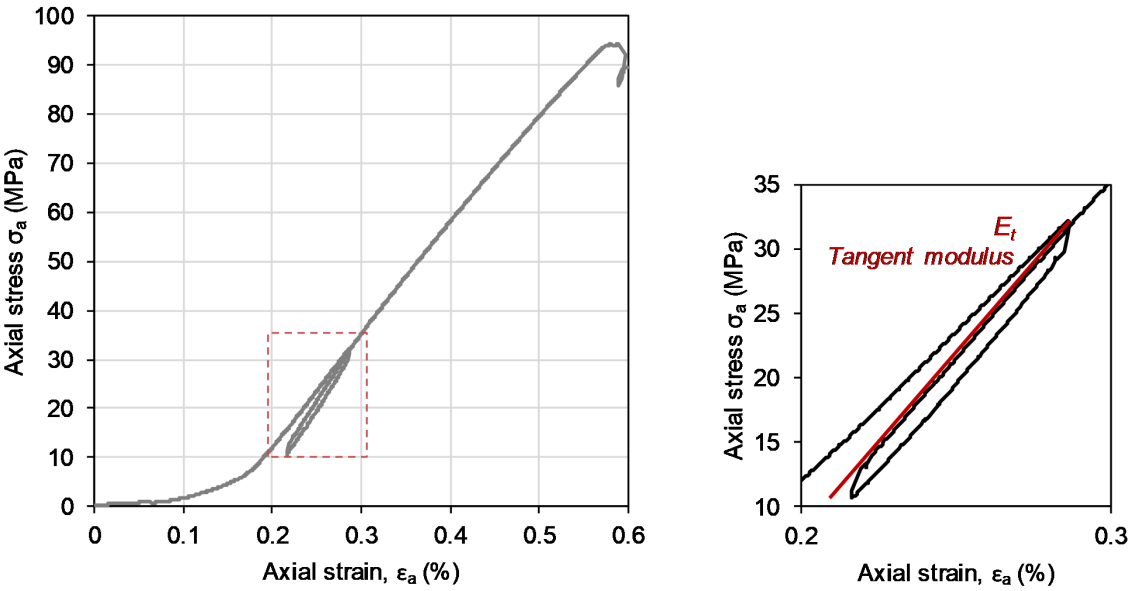

Fig. 5-1: Stress – strain diagram for UCS test

On the right zoom into the unloading/reloading loop, and the definition of tangent and secant Young's moduli. Example from test BUL1-1_661UCS_S1 (Nagra 2021a).

Tab. 5-2: Test results from UCS tests

Young's modulus refers to E_{50}. For specimen geometry see Fig. 4-1.

Test-ID STA3-1	**Specimen geometry**	**Average depth**	**Bulk density**	**Water content**	**Young's modulus**	**Poisson's ratio**	**Peak strength**	**Strain at peak strength**
		[m]	[g/cm^3]	[wt.-%]	[GPa]	[-]	[MPa]	[%]
476UCS_S1	S	476.30	2.69	0.06	39.00	0.14	182.2	0.51
476UCS_S2	S	476.47	2.70	0.04	40.65	0.21	58.0	0.29
476UCS_S3	S	476.67	2.69	0.04	41.71	0.16	137.0	0.54
516UCS_S1	S	516.75	2.67	0.43	36.41	0.18	192.0	0.67
516UCS_S2	S	516.99	2.70	0.23	42.11	0.19	207.9	0.68
516UCS_S3	S	517.17	2.69	0.23	43.27	0.21	140.8	0.49
534UCS_S1	S	534.98	2.65	1.32	22.87	0.27	120.8	0.93
534UCS_S2	S	535.23	2.67	0.64	34.67	0.20	210.7	0.83
534UCS_S3	S	535.40	2.64	1.57	20.07	0.25	101.5	1.07
556UCS_S1	S	556.26	2.61	2.91	13.17	0.25	69.0	1.12
556UCS_S2	S	556.41	2.61	2.89	12.62	0.25	59.7	0.97

Tab. 5-2: continued

Test-ID STA3-1	Specimen geometry	Average depth	Bulk density	Water content	Young's modulus	Poisson's ratio	Peak strength	Strain at peak strength
		[m]	[g/cm^3]	[wt.-%]	[GPa]	[-]	[MPa]	[%]
556UCS_S3	S	556.70	2.58	3.02			54.1	0.96
644UCS_S1	S	644.22	2.61	2.25	16.40	0.22	77.4	0.98
644UCS_S2	S	644.39	2.61	2.52	14.44	0.24	62.3	0.91
644UCS_S3	S	644.63	2.63	1.94	17.76	0.23	76.7	0.72
680UCS_S1	S	680.52	2.63	1.83	21.53	0.23	110.0	0.84
680UCS_S2	S	680.69	2.60	2.40	16.35	0.23	75.5	0.82
680UCS_S3	S	680.86	2.60	2.79	14.83	0.26	85.7	1.17
704UCS_S1	S	704.28	2.69	0.61	29.40	0.26	55.2	0.33
704UCS_S2	S	704.44	2.70	0.43	32.99	0.21	71.5	0.43
704UCS_S3	S	704.62	2.66	0.81	22.68	0.30	35.5	0.35
743UCS_S1	S	743.89	2.52	4.04	8.95	0.19	35.1	0.68
743UCS_S2	S	744.08	2.56	3.41	12.09	0.19	38.1	0.63
743UCS_S3	S	744.31	2.54	3.84	10.57	0.20	39.8	0.75
755UCS_S1	S	755.84	2.51	5.36	6.50	0.24	36.3	1.06
755UCS_S3	S	756.27	2.51	5.22	7.26	0.24	37.1	0.98
902UCS_S1	S	902.07	2.55	3.13	14.97	0.19	55.2	0.66
902UCS_S2	S	902.32	2.54	3.22	13.79	0.17	53.9	0.73
902UCS_S3	S	902.47	2.59	2.28	19.32	0.22	64.0	0.53
950UCS_S1	S	950.05	2.50	5.58	5.08	0.36	25.5	0.99
950UCS_S2	S	950.28	2.44	4.49	7.00	0.23	31.7	0.93
950UCS_S3	S	950.46	2.43	4.43	8.03	0.25	40.5	0.93
968UCS_S1	S	968.60	2.69	3.16	8.73	0.20	14.3	0.55
968UCS_S2	S	968.72	2.86	0.66	27.43	0.23	41.9	0.36
968UCS_S3	S	968.76	2.80	1.48	16.93	0.14	31.4	0.48
1025UCS_S1	S	1025.58	2.84	0.29	44.39	0.15	213.1	0.58
1025UCS_S2	S	1025.64	2.89	0.14	43.11	0.15	164.37	0.52
1025UCS_S3	S	1025.78	2.94	0.03	42.72	0.16	137.4	0.39
1031UCS_S1	S	1031.60	2.43	7.37	27.51	0.22	84.2	0.49
1031UCS_S2	S	1031.76	2.47	6.10	30.22	0.23	106.1	0.54
1031UCS_S3	S	1031.96	2.50	5.34	27.44	0.30	78.9	0.49
1077UCS_S1	S	1077.19	2.75	0.08	44.08	0.18	255.2	0.76
1077UCS_S2	S	1077.33	2.73	0.19	43.54	0.17	220.0	0.66
1077UCS_S3	S	1077.46	2.74	0.23	42.96	0.17	254.4	0.69
1105UCS_S1	S	1105.29	2.58	1.89	32.49	0.21	165.4	0.78
1105UCS_S2	S	1105.42	2.80	0.66	35.86	0.27	88.1	0.55
1105UCS_S3	S	1105.63	2.73	1.72	34.58	0.20	160.8	0.71
1154UCS_S1	S	1154.49	2.28	1.03	12.80	0.14	21.4	1.05
1154UCS_S2	S	1154.68	2.23	1.01	12.52	0.17	22.6	1.27
1154UCS_S3	S	1154.88	2.18	0.46	13.70	0.20	26.4	4.08
1195UCS_S1	S	1195.17	2.67	1.46	23.17	0.17	78.0	0.56
1195UCS_S2	S	1195.31	2.64	2.01	18.20	0.23	69.63	0.68
1195UCS_S3	S	1195.31	2.65	2.10	16.90	0.13	64.92	0.66
1237UCS_S1	S	1237.54	2.57	4.44	13.69	0.17	54.64	0.58
1237UCS_S3	S	1237.83	2.55	4.43	16.60	0.24	64.89	0.62
1274UCS_S1	S	1274.32	2.57	4.16	15.96	0.20	68.03	0.73
1274UCS_S2	S	1274.57	2.58	4.02	17.00	0.18	66.97	0.63
1274UCS_S3	S	1274.76	2.57	4.16	16.19	0.22	61.67	0.63

The relatively large lithologic variability of tested specimens is reflected by the test results, ranging just over one order of magnitude both for Young's moduli and strength.

5.3 Triaxial deformation tests

A total of 11 triaxial tests were performed. Photographs of the specimens before and after testing can be found in Appendix A.

Basic properties and test conditions are provided in Tab. 5-3. The water content reported refers to the final, post-test measurement. With some exceptions, tests were conducted undrained with an initial fluid pressure of either 7 or 10 MPa. The anhydrite sample STA3-1_1025TRX_S1 was carried out "dry" without the pore-fluid system and at a strain rate of $1 \times 10^{-5}\,s^{-1}$. Confining pressure in all tests was 15 MPa except in the single "dry" test (10 MPa).

Skempton's B values were constrained in 2 tests[9].

Ultrasonic velocities were recorded throughout the tests, and the tabulated values in Tab. 5-3 were constrained at the start of the shear phase.

In test STA3-1_516_TRX_S1, the maximum differential stress q was 258.1 MPa at a pore pressure of 6.5 MPa. Post-peak strength could not be determined due to the strong deformation of the sample and a very sudden drop of force. The sample also showed very little axial deformation and little pore pressure built up (Fig. 5-2).

Tab. 5-3: Basic properties and triaxial test results from consolidation and saturation stage

For specimen geometry see Fig. 4-1.

Test-ID	**Specimen geometry**	**Average depth**	**Bulk density**	**Water content**	**Pore pressure**	**Confining pressure**	**Skempton's B**	**P-wave velocity**	**S-wave velocity**
		[m]	[g/cm^3]	[wt.-%]	[MPa]	[MPa]	[-]	[m/s]	[m/s]
STA3-1-516	S	516.75	2.68	1.01	5.0	15.0	-	5'880	3'120
STA3-1-556	S	556.26	2.62	3.90	5.0	15.0	-	4'015	2'275
STA3-1-644	S	644.63	2.62	2.74	7.0	15.0	0.47	4'495	2'410
STA3-1-704	S	704.44	2.70	0.97	5.0	15.0	-	6'186	3'176
STA3-1-755	S	756.26	2.53	6.25	7.0	15.0	-	3'079	1'934
STA3-1-902	S	902.32	2.55	4.44	7.0	15.0	0.57	3'755	2'200
STA3-1-950	S	950.46	2.44	5.99	5.0	15.0	-	3'667	2'143
STA3-1-1025	S	1'025.64	2.93	0.21	-	10.0	-	6'064	3'355
STA3-1-1077	S	1'077.19	2.76	1.02	5.0	15.0	-	6'467	3'394
STA3-1-1195	S	1'195.17	2.67	2.23	5.0	15.0	-	4'876	2'610
STA3-1-1237	S	1'237.54	2.56	5.40	5.0	15.0	-	3'883	1'844

[9] The tabulated values in Tab. 5-3 are not corrected for potential equipment compliance.

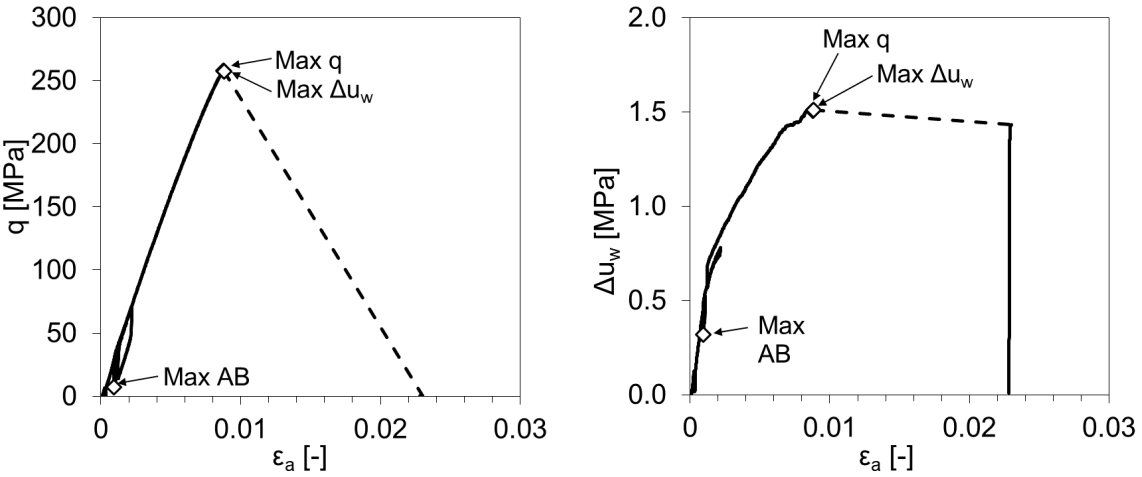

Fig. 5-2: Sample with strong deformation and a very sudden drop of strength post peak
Test STA3-1_516_TRX_S1

Tab. 5-4: Triaxial test results from the shear phase

Test-ID	**Stress path**	**Strain Rate**	**Young's modulus**	**Poisson's ratio**	**Deviatoric stress at peak** ($q = \sigma 1 - \sigma 3$)	**Radial total stress at peak** ($\sigma 3$)	**Pore pressure at peak**	**Axial strain at peak**	**Post-peak** q	**Pore pressure at post-peak**
		[1/s]	[GPa]	[-]	[MPa]	[MPa]	MPa]	[%]	[MPa]	[MPa]
STA3-1-516	CTCU	1E-06	34.5	0.21	258.08	15	6.53	0.92	-	-
STA3-1-556	CTC	1E-06	7.16	0.47	64.78	15	7.03	1.61	44.43	6.24
STA3-1-644	CTCU	2E-07	10.9	0.46	94.53	15	8.86	1.53	49.45	3.7
STA3-1-704	CTCU	1E-06	33.2	0.35	156.22	15	7.12	0.72	95.20	3.18
STA3-1-755	CTCU	2E-07	6.6	0.38	27.49	15	12.98	0.45	19.29	7.5
STA3-1-902	CTCU	2E-07	9.2	0.45	55.24	15	4.83	1.27	31.54	0.0
STA3-1-950	CTCU	1E-06	10.1	0.44	52.20	15	9.71	1.43	35.59	3.3
STA3-1-1025	CTCU	1E-05	42.7	0.20	198.59	10	-	0.68	64.99	-
STA3-1-1077	CTCU	1E-06	42.0	0.26	303.42	15	6.63	1.00	84.98	2.1
STA3-1-1195	CTCU	1E-06	26.6	0.42	84.99	15	8.02	0.83	41.79	4.9
STA3-1-1237	CTCU	1E-06	15.5	0.30	55.66	15	6.14	0.57	31.43	4.3

6 Geomechanical testing programme

In the STA3-1 geomechanical testing campaign, 13 triaxial tests were performed with specialised protocols. Two geometries (Section 5.1) were selected: S- and P-samples.

In addition, 3 one-dimensional compression tests (including 2 constant-head permeability tests) were performed in oedometric conditions. Two one-dimensional swelling tests were perfomed under constant stress.

In the following sections, the test results of the experimental campaign are presented. First, the main geotechnical and intrinsic properties are reported (Section 6.1). Then, in Sections 6.2 and 6.3, the results of tests in triaxial and oedometric conditions are reported.

6.1 Geotechnical and intrinsic properties of tested cores

6.1.1 Water content and Native activity

The laboratories involved in the testing campaign also determined basic properties of the tested specimens. The water content of the specimens before and after testing was determined, and the results are reported in Fig. 6-1.

For the triaxial tests, the first phase of each test consisted in imposing saturated conditions on the specimen by injecting water in isochoric conditions and measuring the generated swelling pressure (conventional testing procedure).

The water content before and after the tests generally differs, and in the case of undrained boundary conditions, the difference may primarily be attributed to resaturation in the rig. Additional sources of discrepancy between the water content before and after the tests can be attributed to the handling of the specimen when dismantling the tests (e.g. loss of solid mass while removing the specimen from the sleeve, drained unloading phases which allow further swelling and water content increase).

The water content and the Native activity of the material were also measured on trimming pieces from a part of the section from which testing specimens were extracted. The Native activity of a specimen corresponds to the value of relative humidity in equilibrium with the specimen's native state, with no variation of the initial water content[10].

The measurements were done by placing a piece of freshly cut material within a closed container and measuring the resulting (relative) humidity generated within the container (Ewy 2015) by the use of a psychrometer.

Results are reported in Fig. 6-2. All cores exhibit high Native activity, above 65%, indicating good to excellent preservation conditions.

[10] In a specimen in contact with controlled relative humidity, if water content increases, then that relative humidity value is greater than the Native activity value of the shale. Conversely, if there is a water content decrease, then that relative humidity value is less than the Native activity.

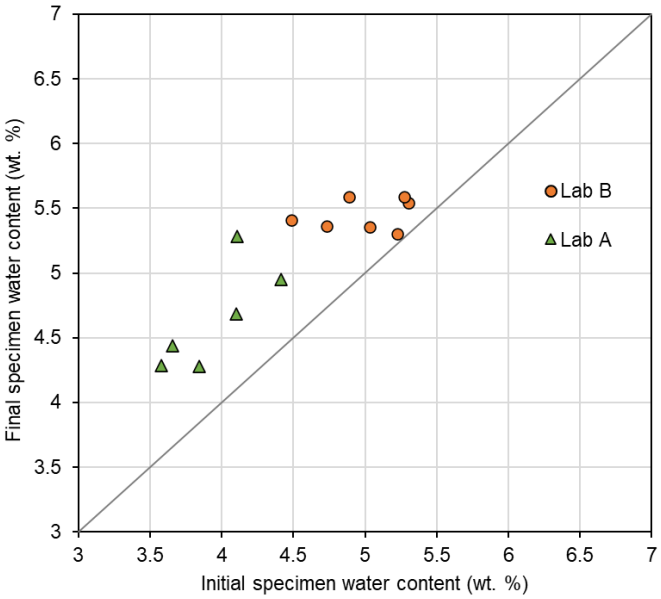

Fig. 6-1: Initial (at test) versus final water content of specimens in triaxial tests (Opalinus Clay)

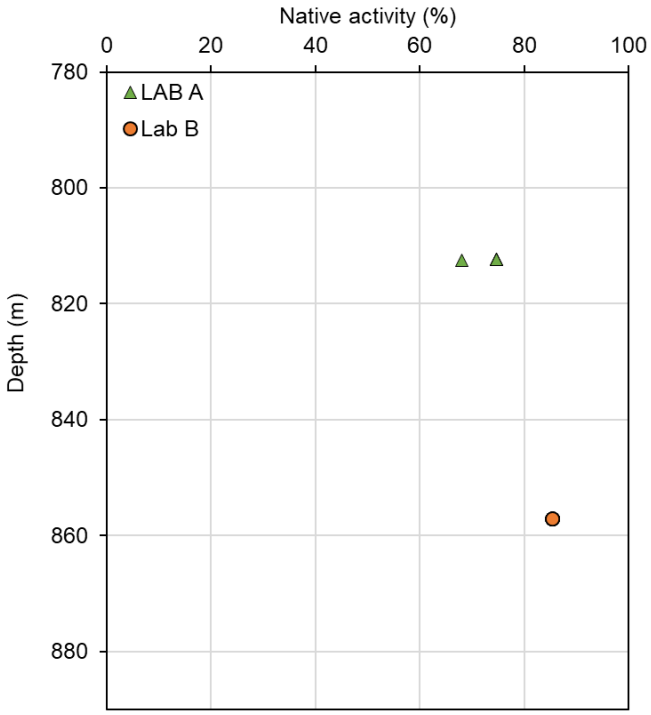

Fig. 6-2: Native activity of trimming material versus depth of collection

Results grouped by laboratory.

6.1.2 Atterberg limits, plasticity index, grain size distribution

In the context of the oedometric testing campaign Lab D performed geotechnical characterisation of the tested core. They determined Atterberg limits, plasticity index and grain size distribution.

Atterberg limits were determined according to ASTM D4318-17 (ASTM 2017a); the material was manually crushed with a rubber-tipped pestle. Only the portion with grain dimension lower than 0.425 mm was used.

Grain size distributions were determined according to ad-hoc procedures developed by the laboratories, in line with Nagra's indications. The main aspects of the procedure of Lab D are here summarised. Lab D adopted a procedure implemented during previous projects involving Opalinus Clay and which is based on the ASTM D6913-17 (ASTM 2017b) and D7928-17 (ASTM 2017c); a gentle pre-crushing was performed manually with a rubber-tipped pestle, to separate the aggregates avoiding the breakage of individual particles. Before the test, the material was submerged in distilled water for 24 hours and sieved using water. Grain size distribution was determined by wet sieving for particles larger than 0.075 mm, and by sedimentation (by the use of a hydrometer) for the smaller particles.

Atterberg limits and granulometric fractions are summarised in Tab. 6-1. The results of the granulometric fractions show a clay fraction lower than the clay mineralogical content determined by XRD (App. D).

Granulometric fractions (sand, silt and clay) are distinguished (as by standard) on the dimension of the particles. It has to be pointed out that there could be particles in the silt granulometric fraction which are clay-mineral particles or aggregates with a larger size than the clay – silt threshold; on the other hand, there may be particles in the clay granulometric fraction which are minerals other than clays having fine particles dimension. All the previous considerations contribute to the difference between granulometric and mineralogical clay fractions.

Tab. 6-1: Atterberg limits and grain size fractions for the tested core

Core ID	**Lab**	**Core interval**	w_L	w_P	*PI*	**Gravel**	**Sand**	**Silt**	**Clay**
		[cm]	[-]	[-]	[-]	[%]	[%]	[%]	[%]
STA3-1 768.72/50-GM	D	24 – 30	0.26	0.17	0.09	2.4	29.5	45.2	22.9

6.2 Triaxial tests with specialised protocols

An overview of the performed tests is presented in Tab. 6-2. Each test is labelled with an ID indicating the main features of the test.

For example, the triaxial test ID A1_STA3_1_812_32_S7CTCU indicates the laboratory that performed the test (A), a testing sequential number (1), the borehole name (STA3-1), the specimen depth (812.32 m), the specimen geometry (S), effective confinement before shearing (7 MPa), the stress path (CTCU).

It is reported in Tab. 6-2 for each tested specimen:

- Specimen ID, as described above
- Core depth [m]
- Geological formation, as presented in Section 4.4.1

- Specimen geometry
- Total confining stress, p_0 [MPa] at the beginning of the shearing phase
- Pore pressure [MPa] at the beginning of the shearing phase
- Effective confining stress p'_0 [MPa] at the beginning of the shearing phase
- Stress path, as presented in Fig. 4-5
- Indication of shearing in drained conditions (*d*)
- Initial void ratio, computed using a reference solid density[11] of 2.70 g/cm^3
- Initial porosity, computed using a reference solid density of 2.70 g/cm^3
- Initial and final water content.

The initial part of the ID (hereafter Specimen ID), including the laboratory and the sequential number is afterwards used as short code to quickly identify a specific test point in the entire set of results.

Tab. 6-2: Conducted triaxial tests

Specimen ID, shearing phase characteristics, specimen initial (and final) conditions.

Specimen ID	**Specimen location and geometry**			**Shearing phase characteristics**				**Specimen initial conditions**			
	Core depth [m]	**Formation**	**Specimen geometry**	**Total confining stress,** p_0 [Mpa]	**Pore pressure,** u_{w0} [MPa]	**Effective confining stress** p'_0 [MPa]	**Stress path**	**Initial void ratio,** e_0 [-]	**Initial porosity,** n_0 [-]	**Initial water content,** w_0 [%]	**Final water content,** wf [%]
A1_STA3_1_812_32_S7CTCU	812.32	Opalinus Clay	S	16	9	7	CTCU	0.128	0.114	4.41	4.95
A2_STA3_1_812_32S13CTCU	812.32		S	22	9	13	CTCU	0.115	0.103	4.10	4.68
A3_STA3_1_812_33S20CTCU	812.33		S	29	9	20	CTCU	0.122	0.109	4.11	5.28
A4_STA3_1_812_33S5CTC	812.33		S	14	9	5	CTC	0.104	0.094	3.58	4.29
A5_STA3_1_812_44S13CTCU	812.44		S	22	9	13	CTCU	0.110	0.099	3.84	4.28
A6_STA3_1_812_44S13CTCU	812.44		S	22	9	13	CTCU	0.104	0.094	3.65	4.44
B6_STA3_1_857_02P11TC	857.015		P	20	9	11	TC	0.118	0.106	4.89	5.59
B2_STA3_1_857_02P7CTCU	857.015		P	16	9	7	CTCU	0.115	0.104	4.73	5.37
B7_STA3_1_857_07S13CTCU_DI	857.065		S	22	9	13	CTCU	0.130	0.115	5.27	5.59
B5_STA3_1_857_07S7CTC	857.065		S	16	9	7	CTC	0.121	0.108	4.49	5.41
B4_STA3_1_857_07S20CTCU	857.065		S	29	9	20	CTCU	0.129	0.114	5.23	5.30
B3_STA3_1_857_07S13CTCU	857.065		S	22	9	13	CTCU	0.126	0.112	5.03	5.36
B1_STA3_1_857_07S7CTCU	857.065		S	15	9	7	CTCU	0.130	0.115	5.30	5.54

[11] Solid density measurements were conducted on specimens used for mineralogical analysis and are available in Appendix D.

6.2.1 Saturation and consolidation phase

6.2.1.1 Swelling pressure

In the conventional triaxial procedure, the specimen saturation was conducted imposing isochoric conditions and monitoring the evolution of the axial and radial stress. The effective stress reached at the end of the saturation phase is called swelling pressure, and the results (grouped by S- and P-geometries, respectively) are reported in Fig. 6-3 versus the specimen initial water content (before saturation). For specimens with S-geometry, the radial direction corresponds to the one of the bedding, while the axial direction is perpendicular to it. Swelling pressure was found to be higher in the axial direction.

On the other hand, in P-samples, the axial direction corresponds to the bedding direction, while the radial stress is obtained by maintaining close to zero the average of the deformation in the two radial directions, perpendicular and parallel to bedding.

It has to be noted that the experimental configuration adopted by Lab B, does not allow to sustain a confining pressure higher than the axial pressure. In STA3-1 saturation tests, P-samples showed a tendency of the confining pressure to rise above the axial pressure. Hence, the axial pressure was adjusted to the confining value, and the two values coincide in Fig. 6-3.

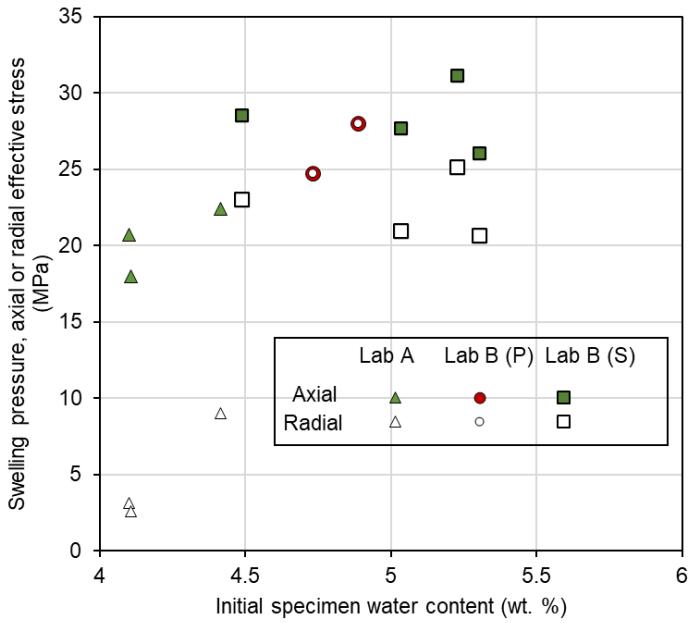

Fig. 6-3: Radial and axial swelling pressure versus initial specimen water content

S-samples and P-samples (Opalinus Clay).

Results from tests B4 and B5 (multiple pore pressure increments during saturation) reported in Fig. 6-3 refer to the first equalisation phase. The variation of the swelling pressure in terms of axial and radial effective stress at the multiple pore pressure values was limited few hundreds of kPa, to a maximum of 1 MPa.

6.2.1.3 B check tests

In each test, the specimen saturation was verified by performing Skempton's B checks. B values were computed over multiple steps. If the difference in B values among the steps was less than 10%, the average of the measurements was considered as the B coefficient and associated with the average effective confinement level at which B segments were performed. The values are reported in Fig. 6-4 for all results.

The compressibility of the apparatus can affect the accuracy of the measured B values. Wissa (1969) proposed a correction to the B value to consider the compressibility of the dead volume of water (i.e., the water in the drainage system) and the compressibility of the system (tubes and transducers). However, several researchers (e.g. Ghabezloo & Sulem 2010) show that the compressibility of modern types of steel tubes and transducers has a negligible impact on the B measurements compared to the dead water volume impact. Therefore, the results of the testing campaign have been analysed considering the dead water volume in each apparatus, and B values results ($B_{correct}$) were computed as (Wissa 1969, Favero et al. 2018):

$$B_{correct} = \frac{1}{\frac{1}{B_{obs}} - \frac{V_L}{V}\frac{K}{K_f\left(1-\frac{K}{K_S}\right)}} \tag{6-1}$$

where B_{obs} is the measured B value, V_L is the volume of fluid in the porewater lines, V is the volume of the specimen, K is the bulk modulus of the specimen, K_f the bulk modulus of the pore fluid and K_s the bulk modulus of the solid phase. Bulk and solid moduli K = 6 MPa and Ks = 50 MPa were considered for the corrections. The correction was applied for results of Lab A and Lab B. It has to be noted that the dead volume in the apparatus from Lab B is ~ 700 mm^3, while those from Lab A is 2'100 mm^3. The results for the measured and corrected B values are reported in Fig. 6-4. An average value of 0.88 was calculated and marked as a dotted line in the graph.

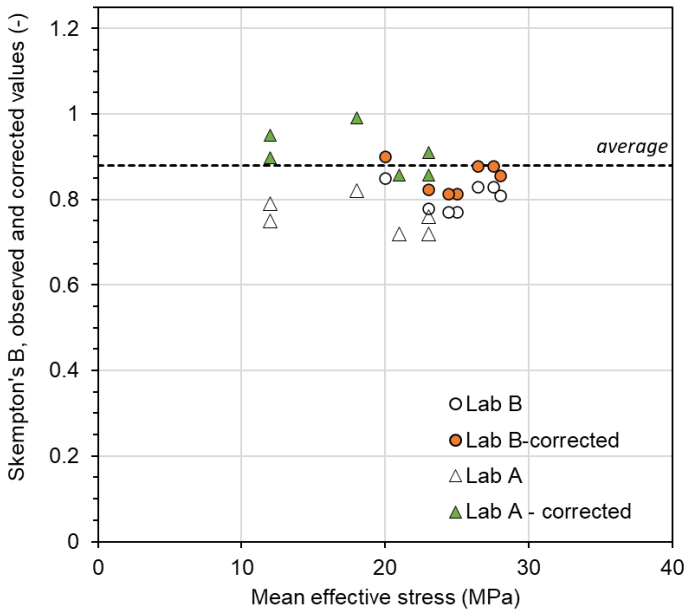

Fig. 6-4: Average Skempton's B values

B values versus the corresponding effective mean stress; data from STA3-1 (Opalinus Clay): Observed and corrected values accounting for dead water volume.

6.2.1.4 Consolidation phase

Drained consolidation phases were performed to achieve the target effective confining stress for shearing, and allow for determining the consolidation coefficient, according to Head (1998). The time to consolidate was obtained applying the square root of time method in the evaluation of the evolution of the volumetric strain. It is noted that the method refers to an instantaneous loading of the sample. However, in most test adopting a conventional method, the stress level at the end of saturation is higher than the target value for shearing, hence an unloading (with consequent swelling of the sample) was performed. Performing quasi-instantaneous unloading is challenging, given the stress levels involved, and often a ramp of several hours needs to be used. Therefore, the consolidation coefficient obtained from these results may be underestimated. It is further noted that the values were obtained by considering the time to consolidate excluding the time required to load.

In tests A5 and A6, two isotropic drained phases were conducted: a loading and an unloading over the same stress amplitude. Both phases were used to estimate the consolidation coefficients, and yielded similar values, with difference within 10 – 15%. Only the value for the first loading phase is reported in Fig. 6-5.

The obtained values for all tested specimens of Opalinus Clay are reported in Fig. 6-5 versus the mean effective stress at the end of the consolidation phase.

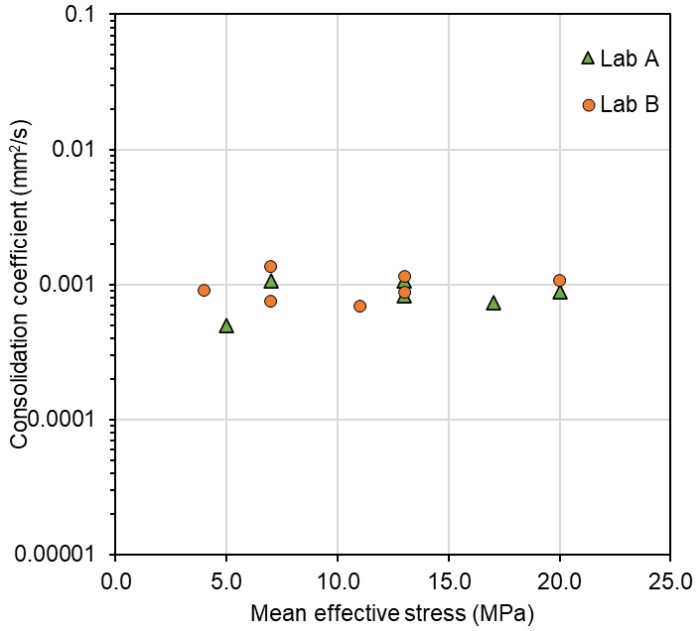

Fig. 6-5: Consolidation coefficient for Opalinus Clay specimens (all geometries)

6.2.2 Shearing phase

This section provides the results of the shearing phase of tests. The stress paths are reported in the $q - p'$ plane, where q is the deviatoric stress (Eq. 4-2) and p' is the mean effective stress, obtained by subtracting the porewater pressure u_w from the total stress (Eq. 4-1).

6.2.2.1 Stress paths of Opalinus Clay subunits

This section focuses on the stress paths obtained on Opalinus Clay specimens during the shearing phase of the tests. The behaviour of the tested specimens is characterised by a pronounced non-linearity before the peak stress and softening response after the peak. A similar evolution of the deviatoric stress (q) and porewater pressure (u_w) with the axial effective strain is observed among the tests (see Appendix B). The effective stress paths obtained on Opalinus Clay specimens are here grouped by the lithological sub-units (Fig. 6-6), as presented in Section 4.4.1.

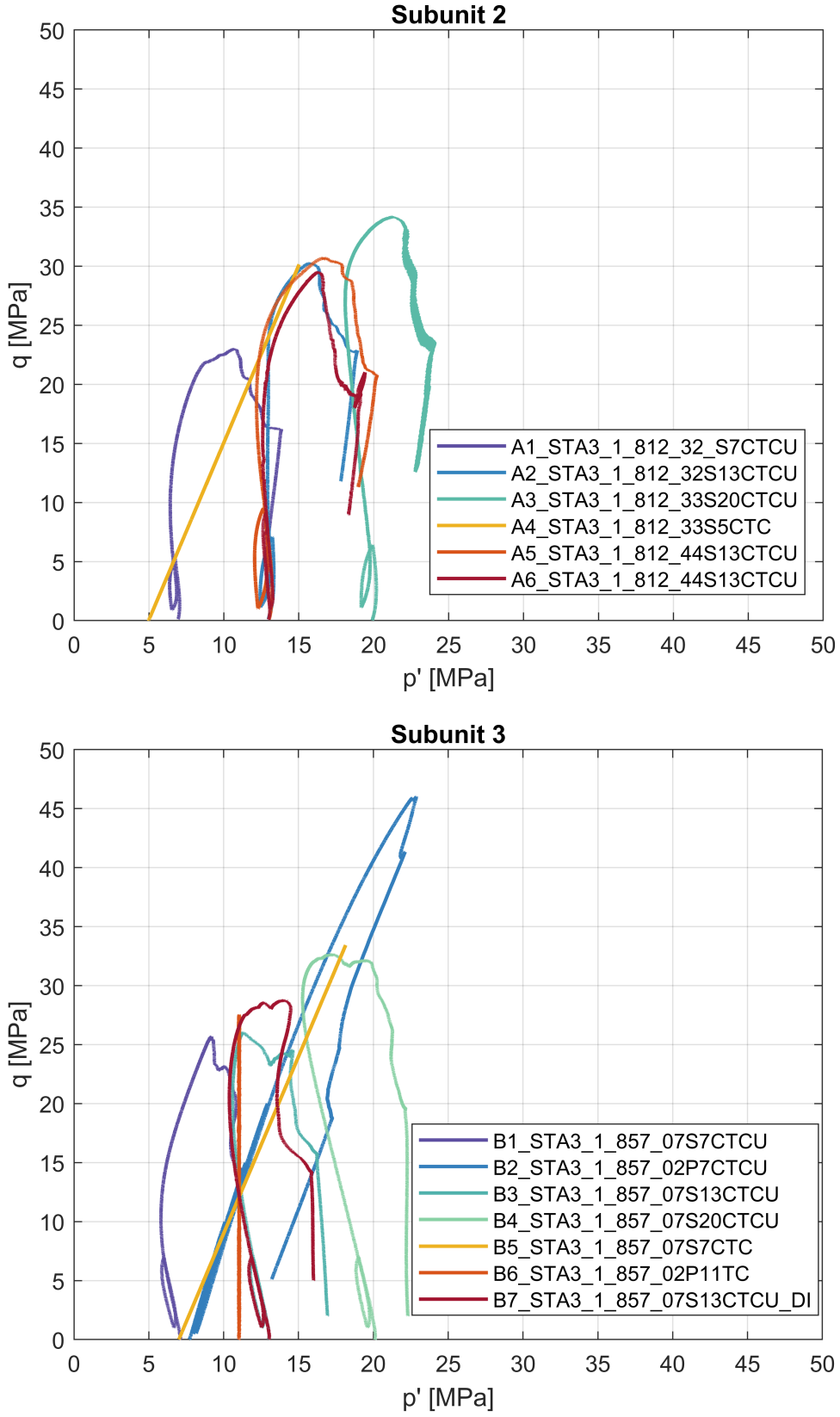

Fig. 6-6: Effective stress paths of tested specimens grouped by the lithological (sub-)unit

6.2.2.2 Elastic phase

The analysis of the elastic parameters for Opalinus Clay samples is presented in this section. Unloading/reloading cycles were performed to estimate the elastic response of the material during an unloading phase. As requested in the testing procedure, the cycles were carried out during the shearing of the specimens before the achievement of the peak stress.

During unloading and reloading, shales present a hysteretic and non-linear behaviour. Depending on the strain amplitude of the unloading/reloading loop, the secant moduli may vary considerably. The strains are calculated as the ratio of the variation in height (or diameter) to the initial height (or diameter). To eliminate the dependency of the moduli on the amplitude of the unloading loop, the elastic modulus for all analysed tests was computed as the secant modulus during unloading for a pre-fixed strain range, 0.02 – 0.04% from the beginning of the unloading phase (Fig. 6-7). The strain calculation refers to the initial specimen height. The strain amplitude was selected as common to all the analysed test results.

Small-strain moduli were also evaluated from the stress cycles (Fig. 6-7) according to the procedure presented in Giger et al. (2018). An example of elastic moduli evaluation is reported in Fig. 6-7, with reference to test BUL1_1_950_62S9CTCU_B (BUL1-1 testing campaign; Nagra 2021a). The top graph in Fig. 6-7 shows the evolution of the secant moduli with the axial strain range used for their computation, for the unloading phase. A clear non-linear decrease of the modulus is observed with the axial strain, which reflects the non-linearity of the material's response. This feature highlights the importance of the axial strain range adopted to perform unloading/reloading cycles. Different ranges lead to different moduli, making a comparison among the tests difficult and misleading. Generally, larger strain ranges lead to lower moduli (Minardi et al. 2019).

A summary plot comparing small strain moduli and secant moduli is provided in Fig. 6-8. It is highlighted that small strain moduli are always higher than the secant moduli computed over the common strain range. Secant moduli from P- and S-samples are provided in Fig. 6-9, sorted by specimen final water content. In the case of P-tests, generally higher values of the undrained elastic moduli with respect to S-tests are observed.

In terms of radial response, the relationship between axial and radial deformations during the unloading phase of the cycles performed before the achievement of the peak stress was used ($-\Delta\varepsilon_r/\Delta\varepsilon_a$) for the assessment of the undrained equivalent of the drained Poisson's ratio (ν). In the undrained conditions, deviations from the theoretical value of 0.5, typically obtained from the linear isotropic elasticity, are due to the anisotropic features of the material and possible poro-elastic effects. The computed parameters for the drained and undrained unloading loops are reported in Fig. 6-10 (also, Appendix E), divided by specimen geometry (S and P) and along with the corresponding elastic moduli.

For P-samples, usually the radial sensors detect the anisotropic response, with higher deformation in the direction perpendicular, compared to the direction parallel to the bedding plane. As a consequence, the Poisson's ratios computed using the strain perpendicular to bedding are higher than those parallel to bedding. In the current campaign, limited evidences on P- samples were obtained.

Ultrasonic velocities of P (*Vp*) and S (*Vs*) waves were also measured by Lab A and Lab B. Both laboratories measured the velocity of P and S waves in the axial direction (*Vp* and *Vs*). In 1 test, Lab B measured P wave velocity also in the direction orthogonal to the cylinder axis (*Vph*).

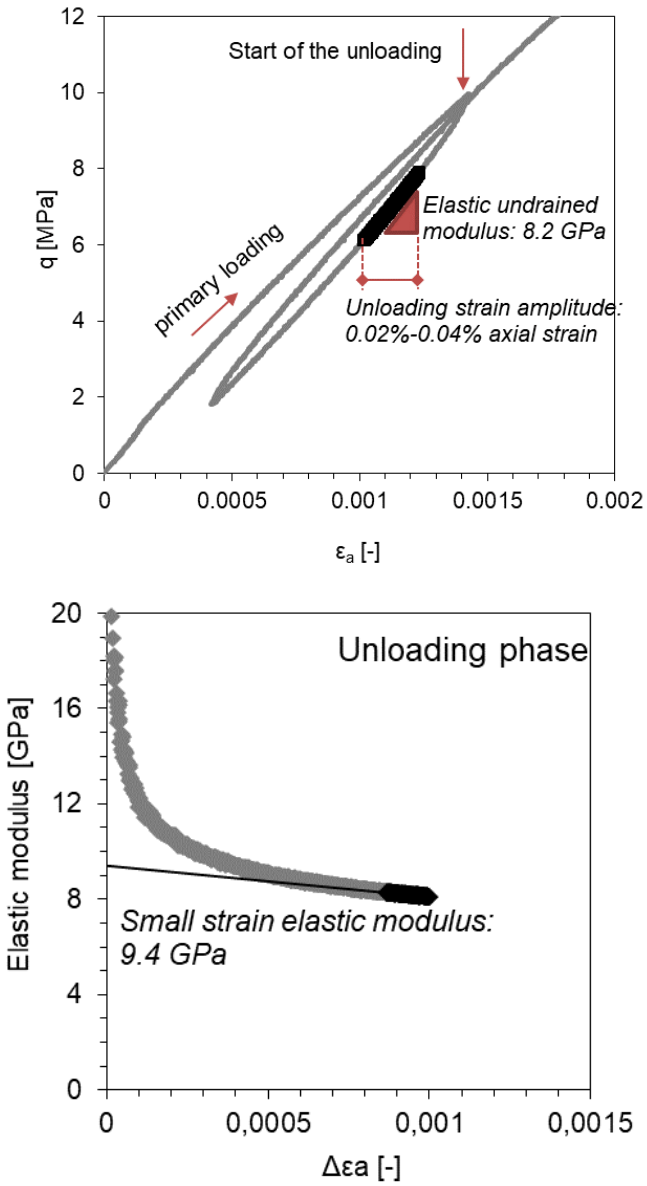

Fig. 6-7: Unloading/reloading cycle and small strain elastic modulus in triaxial tests

Determination of the elastic undrained moduli (E_u) during the unloading phase, for a pre-determined strain amplitude (top); small strain elastic modulus obtained on the unloading phase (bottom) (test BUL1_1_950_62S9CTCU_B; Nagra 2021a).

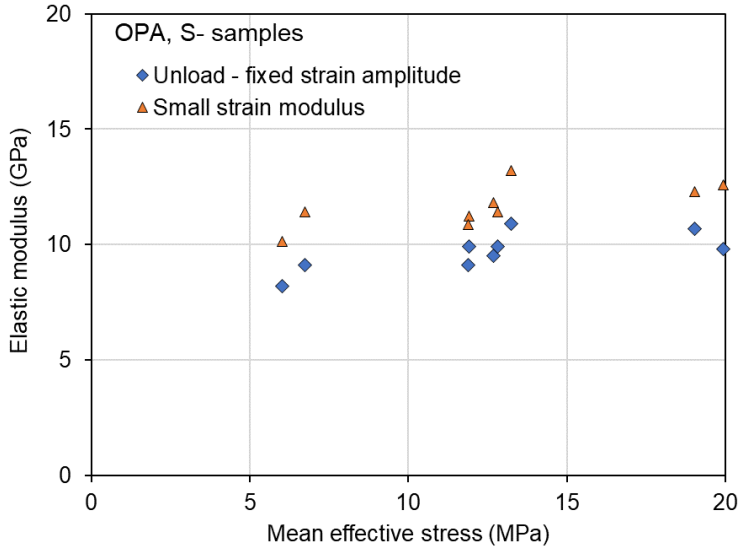

Fig. 6-8: Elastic undrained moduli calculated over an unloading (UL) path: modulus of a fixed strain interval and small strain extrapolation (S-samples)

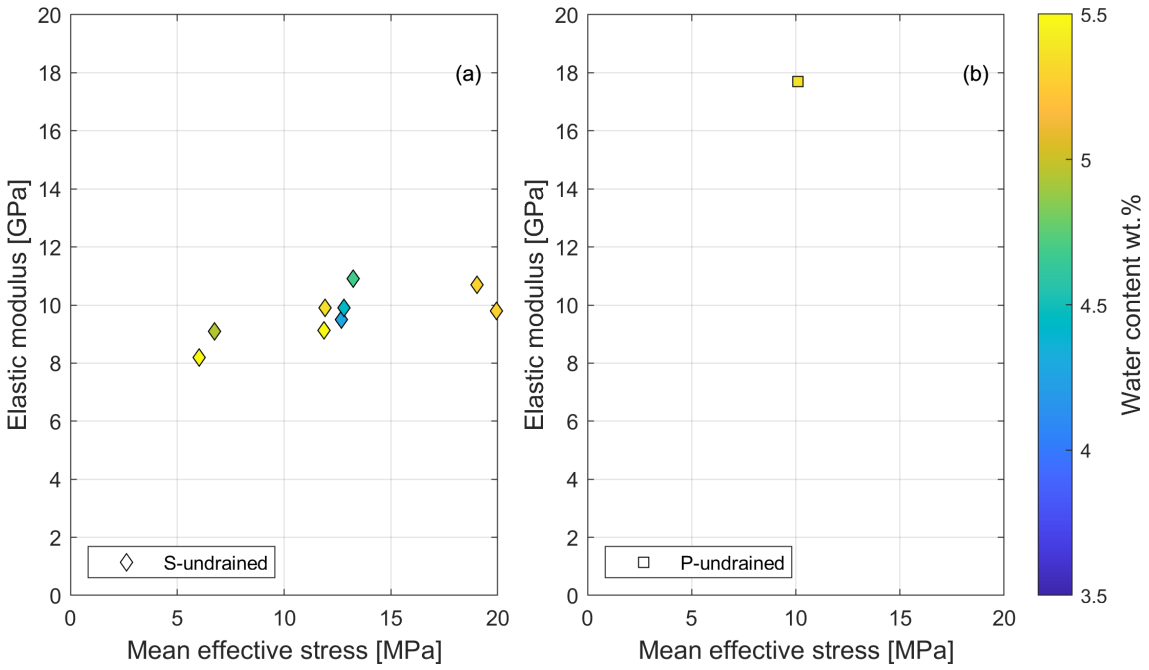

Fig. 6-9: Elastic undrained moduli, sorted by specimen final water content

Moduli are calculated over a fixed strain interval during an unloading (UL) path: P- and S-geometries, sorted by water content at the end of the test (final).

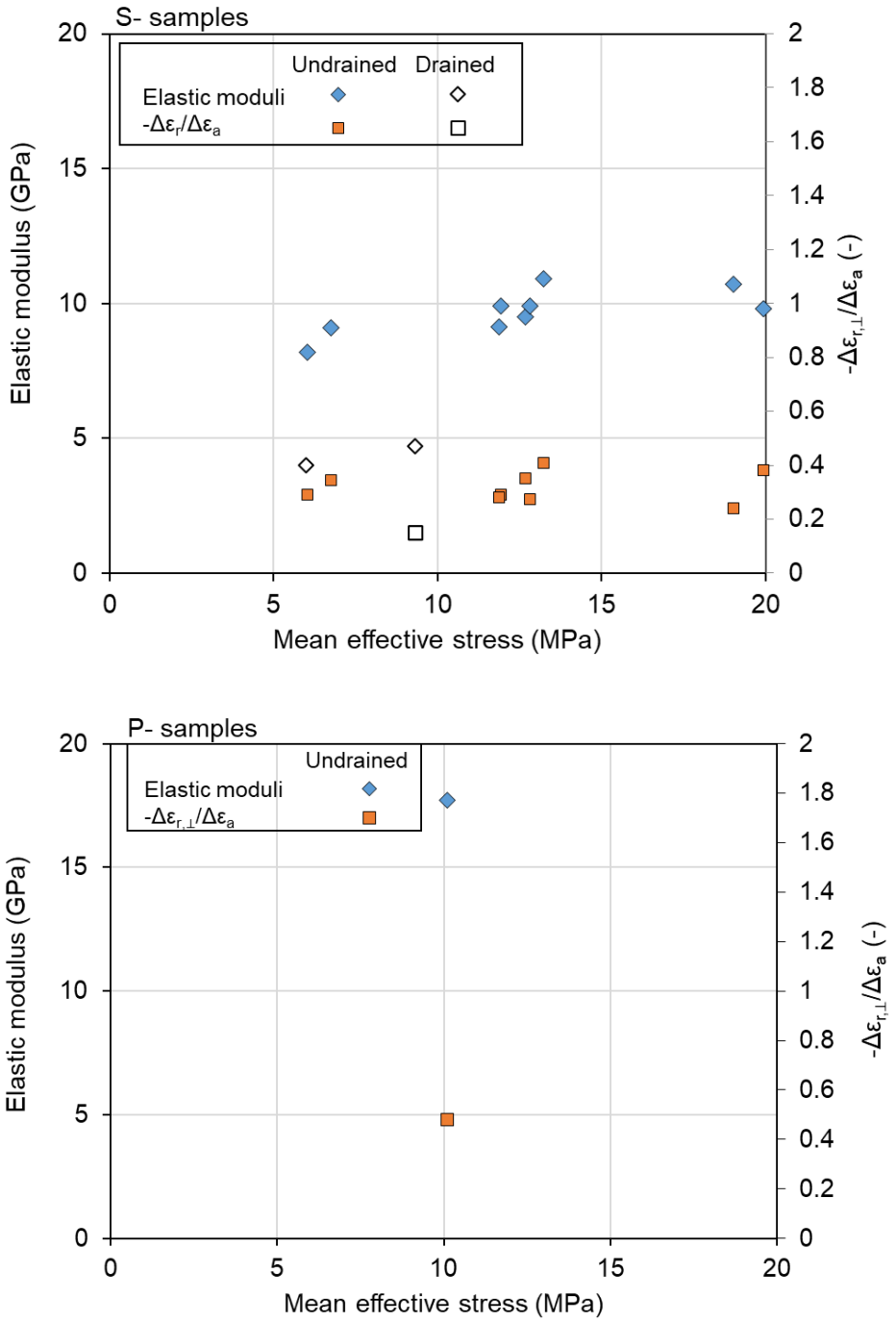

Fig. 6-10: Elastic drained and undrained properties

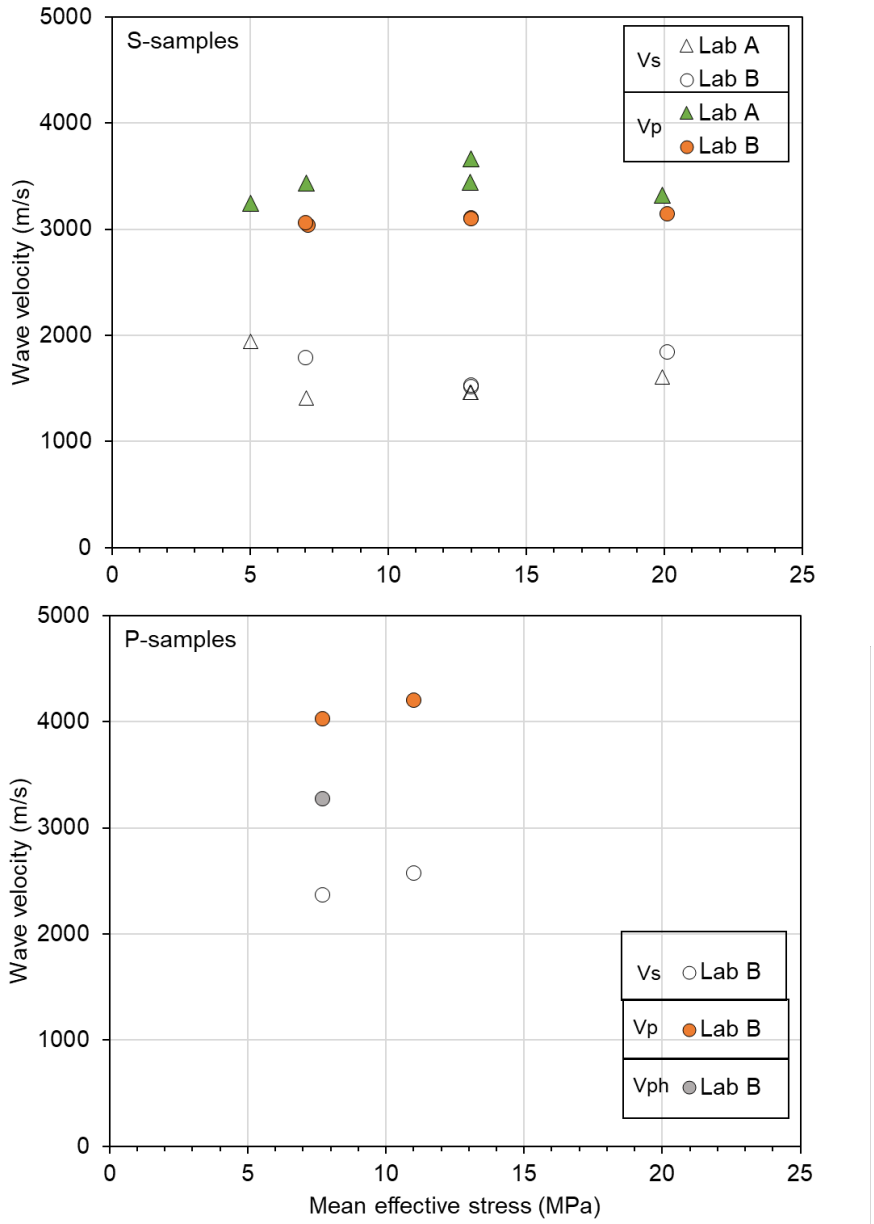

Fig. 6-11: Wave velocities at the beginning of the shearing phase

Results are divided by specimen geometry (data in Appendix E).

6.2.2.3 Pore pressure evolution

In Fig. 6-12, the stress levels ($p' - q$), at which the maximum value of the AB parameter and the maximum pore pressure u_w are reached, are plotted along with the peak shear strength for all test results (data in Appendix B). q is the deviatoric stress, p' is the mean effective stress, Δu_w is the variation of pore fluid pressure from the beginning of the shearing, AB is the ratio between Δu_w and q. The results are divided by specimen geometry.

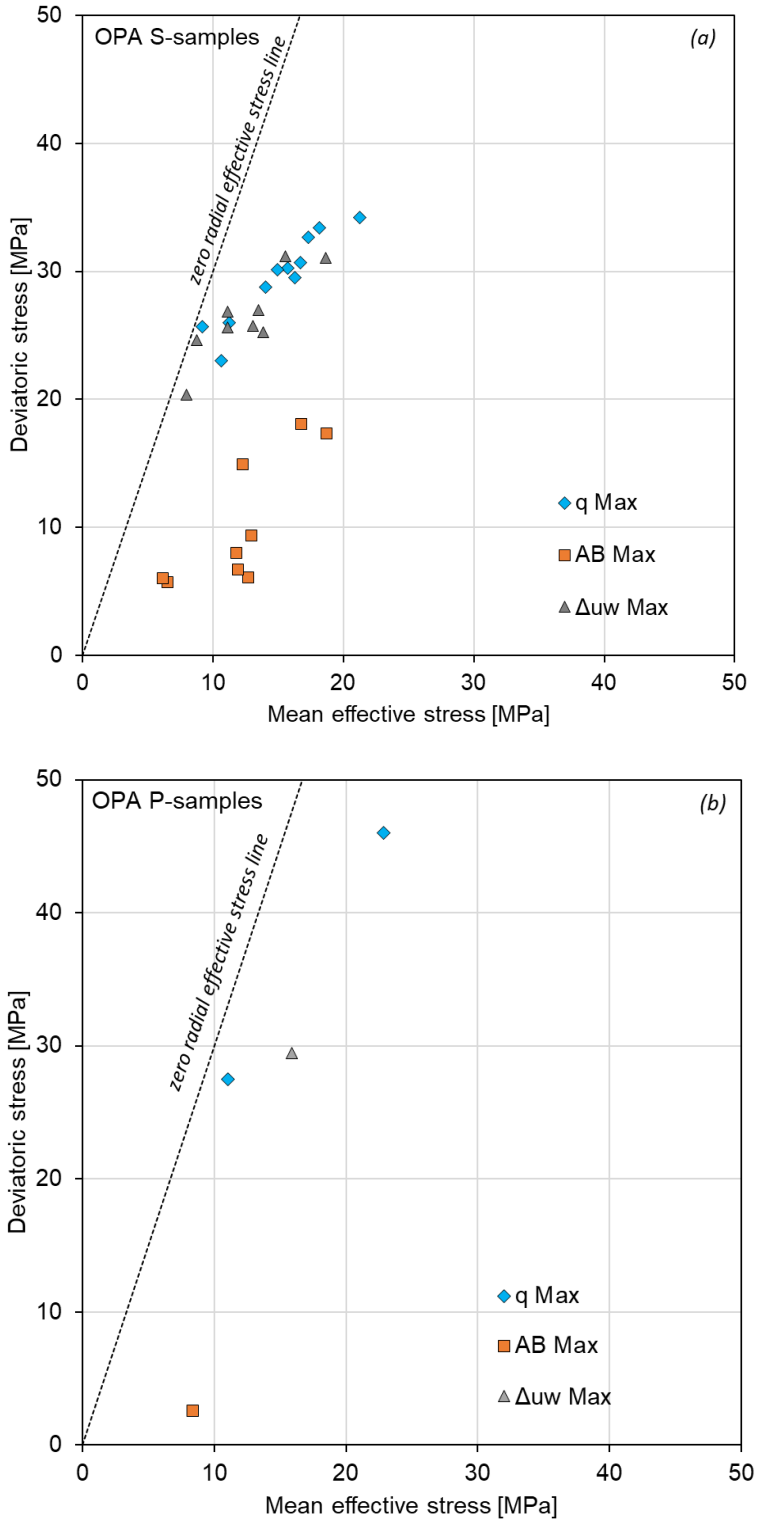

Fig. 6-12: Stress level at which the maximum deviatoric stress, the maximum value of pore pressure and the maximum value of the *AB* parameter are achieved

Opalinus Clay results, all geometries (a) S-samples, (b) P-samples.

6.2.2.4 Shear strength

For all tested specimens, during shearing, a peak in deviatoric stress was achieved, before softening occurred, followed by near-constant deviatoric stress. The peak value is reported below, as the *peak shear strength*, while the constant deviatoric stress achieved during continuing shearing (axial strain up to 1.5 – 3%) is hereafter referred to as *post-peak shear strength*.

In Fig. 6-13, peak (a) and post-peak shear strength (b) are reported in the $p' - q$ plane. The dotted lines highlight the pair of $p' - q$ values, at which radial effective stress equals zero. This line would correspond to the same boundary conditions as a UCS test if pore fluid pressure was zero. The stress states on the left side of this line cannot be achieved (negative radial effective stress) in a triaxial apparatus.

In Fig. 6-14 the peak shear strength results are analysed, sorted by the water content (Fig. 6-14a) of the specimens (obtained at the end of the test) and by the clay mineral content (Fig. 6-14b), where available. The plot includes the results of S-samples of Opalinus Clay. The results are reported also in Fig. 6-15 in terms of radial versus axial effective stress.

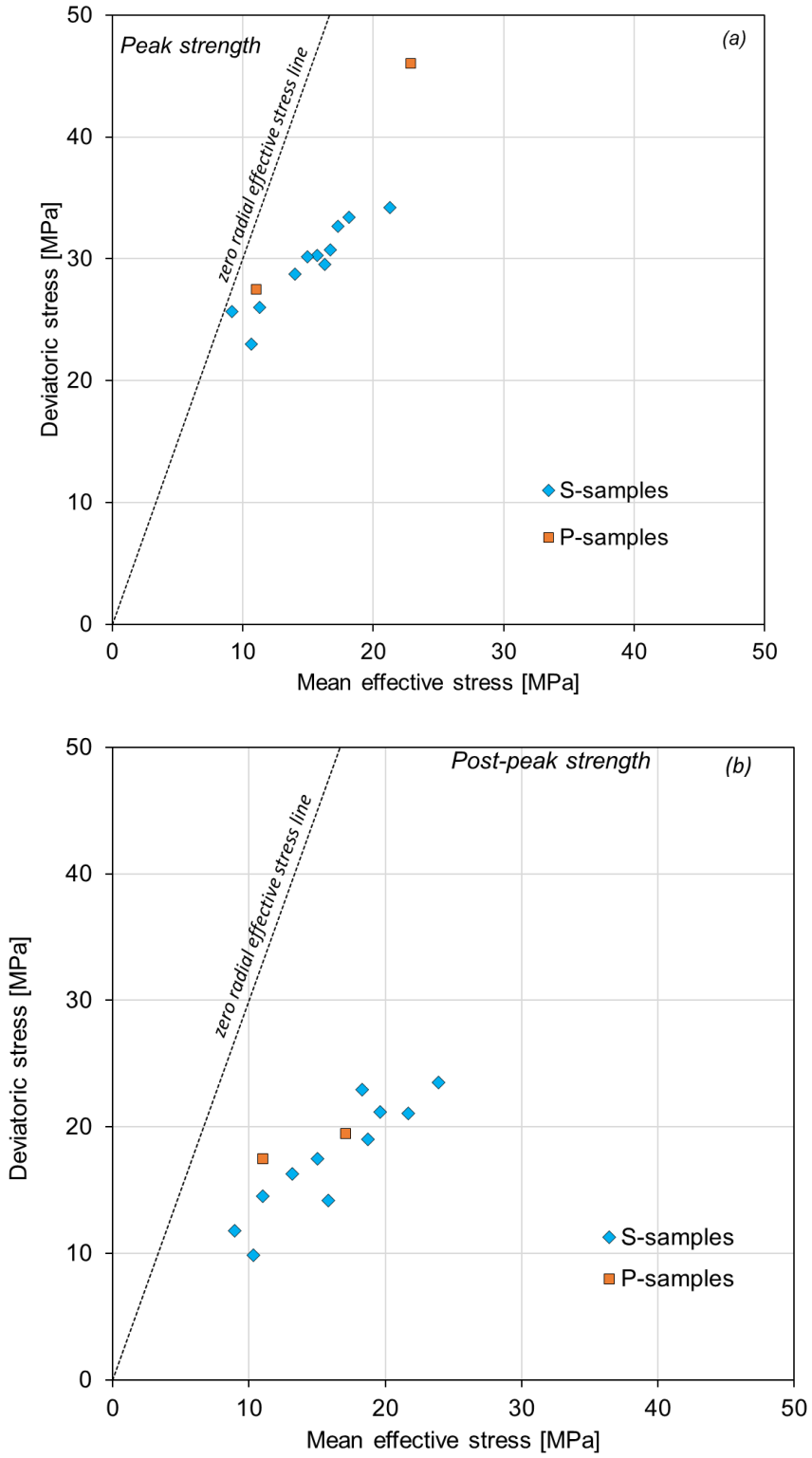

Fig. 6-13: Peak (a) and post-peak (b) shear strength of Opalinus Clay STA3-1 specimens
Results divided by geometry.

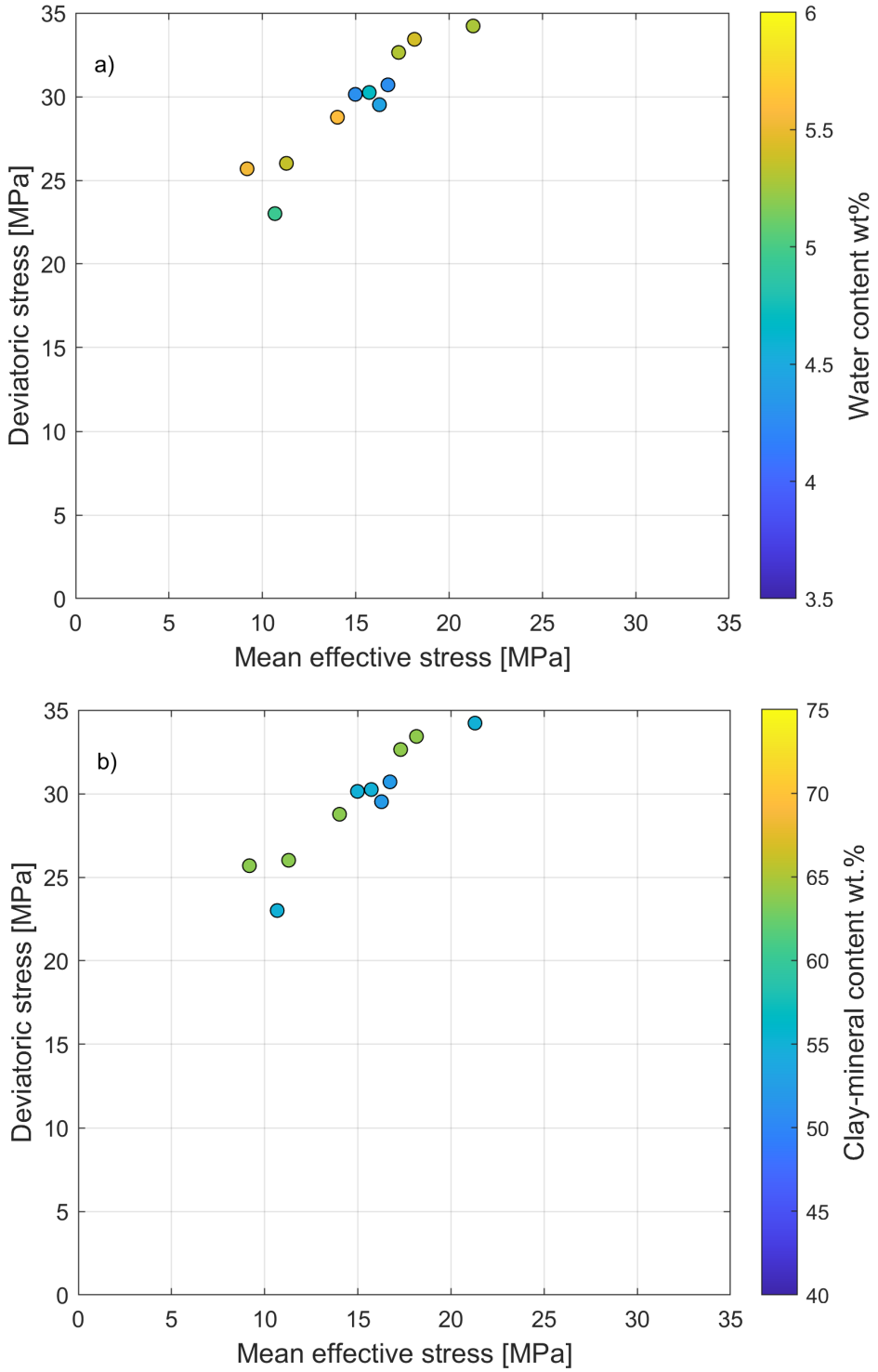

Fig. 6-14: Peak shear strength of Opalinus Clay specimens

Results in mean effective versus deviatoric stress, sorted by (a) water content and (b) clay mineral content, when available. Only S-samples are reported.

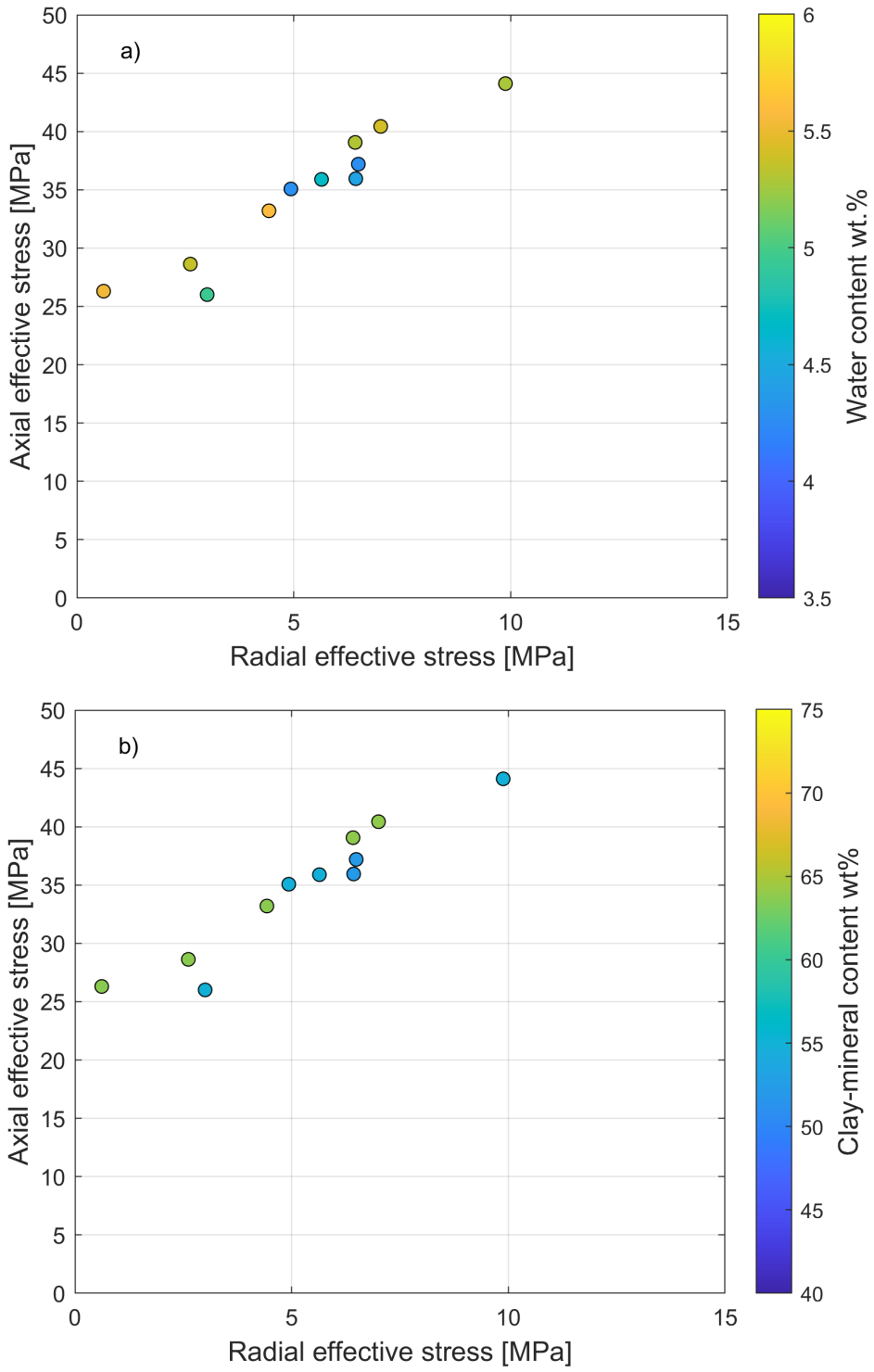

Fig. 6-15: Peak shear strength of Opalinus Clay specimens

Results in radial versus axial effective stress, sorted by (a) water content and (b) clay mineral content, when available. Only S-samples are reported.

6.3 Oedometric tests, one-dimensional swelling and complementary permeability tests

This section includes the results obtained on:

- High-pressure oedometric tests (OED), including 2 constant-head permeability tests
- One-dimensional swelling tests (OS), at constant stress
- Constant-head permeability tests (PERM) obtained in oedometric conditions

6.3.1 Overview of the performed tests and initial specimen conditions

An overview of the performed tests is provided in Tab. 6-3.

Tab. 6-3: Tests performed in oedometric conditions and complementary permeability tests

For specimen geometry see Fig. 41.

[a] Total stress reported in brackets for swelling under constant stress. [b] High-pressure oedometric test.

ID	OS [a]	OED [b]	Perm	Depth [m]	Laboratory	Specimen geometry	Formation
D1_OED_STA3_1		×	×	768.99	D	S	«Muchisonae-Oolith Fm.»
A1_OED_STA3_1		×		812.56	A	S	Opalinus Clay
A2_OED_STA3_1		×	×	812.56	A	P	Opalinus Clay
A1_OS_STA3_1	(0.2)			812.64	A	S	Opalinus Clay
A2_OS_STA3_1	(1.0)			812.49	A	P	Opalinus Clay

The tests in oedometric conditions were labelled by indicating the letter of the laboratory that performed the test (e.g. Lab A), a sequential number (01) and the type of test (OED = oedometric, PERM = constant-head permeability).

6.3.2 Oedometric test results

The settlement over time curve for each loading increment is analysed adopting an extension to the consolidation theory tailored on shales response (Ferrari et al. 2016). The solution combines a modified form of the classical Biot theory (Biot 1941), to account for the behaviour of shales in oedometric conditions, and an extended one-dimensional consolidation theory, to consider the poroelastic behaviour of shales and time-dependent loading conditions. For each loading step, the method allows for the identification of the primary consolidation settlement, related to the water overpressure dissipation, the secondary compression coefficient, the hydraulic conductivity.

As an example, the results of one oedometric test are reported in Fig. 6-16, in terms of oedometric curves. The graph presents the void ratio (e) obtained at the end of the primary consolidation, versus the vertical effective stress (σ'_v). The initial void ratio (e_0), the swelling pressure attained at the end of the resaturation phase (S_p) and the unloading (C_s) indexes are marked in the figure.

Since the load was limited to 20 MPa, the yield stress and the compressibility index cannot be constrained.

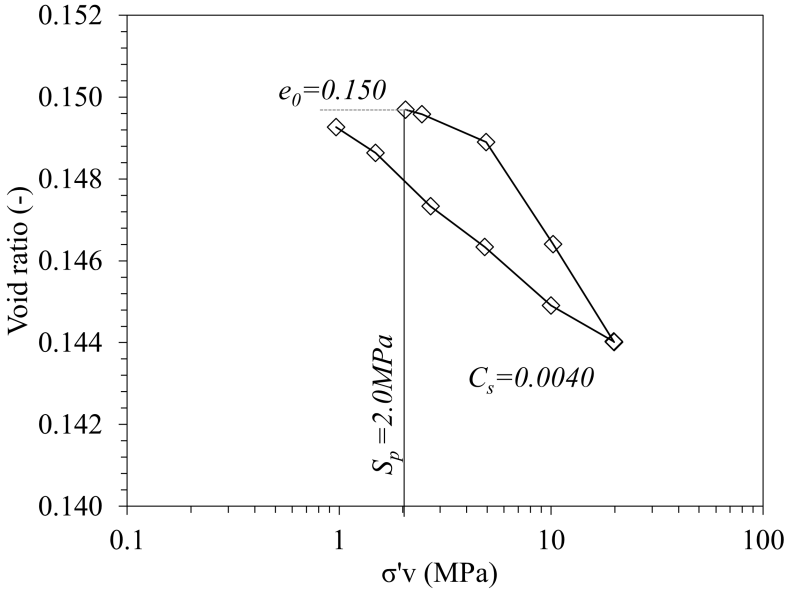

Fig. 6-16: Oedometric curve in void ratio versus vertical effective stress plane

Results from D1_OED_STA3_1.

The results from the performed tests are summarised in Tab. 6-4. Corresponding plots are reported in Appendix F. Tab. 6-4 also includes the effective stress level at which the constant-head permeability test was performed, where applicable.

Tab. 6-4: Oedometric test results

For specimen geometry see Fig. 4-1.

Specimen ID	**Specimen geometry**	**Specimen depth**	e_0	Cc	S_P	$\sigma'_{v,y}$	Cs	**PERM test** at σ'_v (or p')
		[m]	[-]	[-]	[MPa]	[MPa]	[-]	[MPa]
D1_OED_STA3_1	S	768.99	0.15	-	2.0	-	0.0040	19.2
A1_OED_STA3_1	S	812.56	0.102	-	4.3	-	0.0035	-
A2_OED_STA3_1	P	812.56	0.105	-	0.3	-	0.0008	15

It is noted that swelling pressure values are generally lower than those obtained in triaxial conditions. This is attributed to a more precise strain control available in the triaxial setups.

6.3.3 Hydraulic conductivity: direct and indirect measurements

From the consolidation theory application, hydraulic conductivity at each loading step can be derived. In Fig. 6-17, the hydraulic conductivity of P- and S-samples obtained from consolidation theory are reported. The ranges of values obtained upon primary loading are represented as the average plus bars: the plot considers the values obtained for a range of vertical effective stress comparable to what is expected in situ (5 – 20 MPa). The results are combined with constant-head permeability measurements and labelled with the values of vertical effective stress or mean

effective stress at which the test was performed. Data of hydraulic conductivity computed from the consolidation and those from constant-head tests are reported in Tab. 6-5, including the results of the PERM tests.

The reason for the discrepancies between the constant-head tests and the results obtained from the consolidation coefficient could not be resolved.

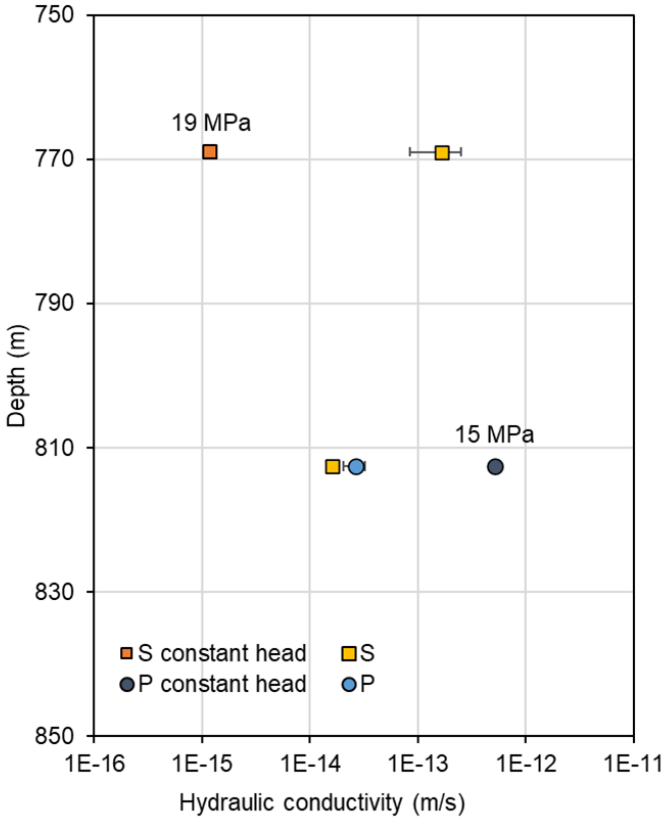

Fig. 6-17: Hydraulic conductivity versus depth

Results obtained from the analysis consolidation test, for the range of effective vertical stress 5 – 20 MPa, and constant-head tests in oedometric conditions.

Tab. 6-5: Hydraulic conductivity test results: from consolidation and constant-head tests

Specimen ID	**Speci-men geo-metry**	**Depth**	**Consolidation stages**		**Constant-head tests**	
			Average k (4 – 20 MPa)	Standard deviation	k	σ'_v *or* p'
		[m]	[m/s]	[m/s]	[m/s]	[MPa]
D1_OED_STA3_1	S	768.99	1.7E-13	8.3E-14	1.18E-15	19.2
A1_OED_STA3_1	S	812.56	1.6E-14	4.7E-16		
A2_OED_STA3_1	P	812.56	2.6E-14	6.0E-15	5.19E-13	15

7 Representativeness of test results

A critical question revolving around any rock-mechanical or geomechanical laboratory programme is how representative the chosen specimens are for a given formation. This depends on several factors, notably material heterogeneity.

One possible way to address this is to compare wave velocities derived from the sonic scanner in situ (Fig. 7-1, blue line) and ultrasonic velocities constrained in triaxial tests on cores in the laboratory (*cf.* Tab. 5-3 and E-1, orange squares in Fig. 7-1). Such correlations can be used for both i) checking the plausibility of test results and ii) estimating the variability of material properties in (sub-)formations. Therefore, the tests conducted in the rock-mechanical testing programme with formations other than Opalinus Clay (and confining units) are used as guidance to estimate rock-mechanical formation properties.

In contrast, the ambition of the geomechanical testing programme (of Opalinus Clay in particular) is to cover the relevant spectrum of material properties by actual laboratory testing. Whether this was achieved is primarily assessed by comparing the basic properties and mineralogy of tested specimens with the larger database (*cf.* Dossier VIII). In this larger database, water content and mineralogy were constrained every 2 to 3 m along the 109 m thick interval of Opalinus Clay, and each measurement reflects a mean value over a 25 cm core interval.

The water content of geomechanically tested specimens was measured on trimming material from the specimen preparation and on the specimens themselves (before and after testing). For a same specimen, these values were averaged, and the error bars constructed to include the variability in the measurements. Those results are reported versus the specimens sourcing depth in Fig. 7-2. Based on the water content, the comparison with the larger database reveals that the spectrum of water contents is covered by the geomechanical tests.

The bulk mineralogy was also assessed for the tested specimens. However, it is noted that for a given depth interval, multiple «twin specimens» were sourced to constrain stress-dependent properties of the same material. As the material's variability in the horizontal direction in the Opalinus Clay is generally considered very small compared to the variability in the vertical direction, only one specimen was generally used for a given depth interval as a reference mineralogy for other specimens. This assumption was verified with repeated analyses of two plugs from an identical depth interval. Therefore, the bulk mineralogy obtained on one specimen was attributed to the other specimens from the same vertical interval of the core. The clay-mineral content (wt.-%) is reported in Fig. 7-3 against depth, together with the large database obtained from University of Bern (*cf.* Dossier VIII).

The comparisons of Figs. 7-2 and 7-3 demonstrate that tested specimens in the geomechanical testing programme capture the material variability and can thus be considered representative of the entire formation.

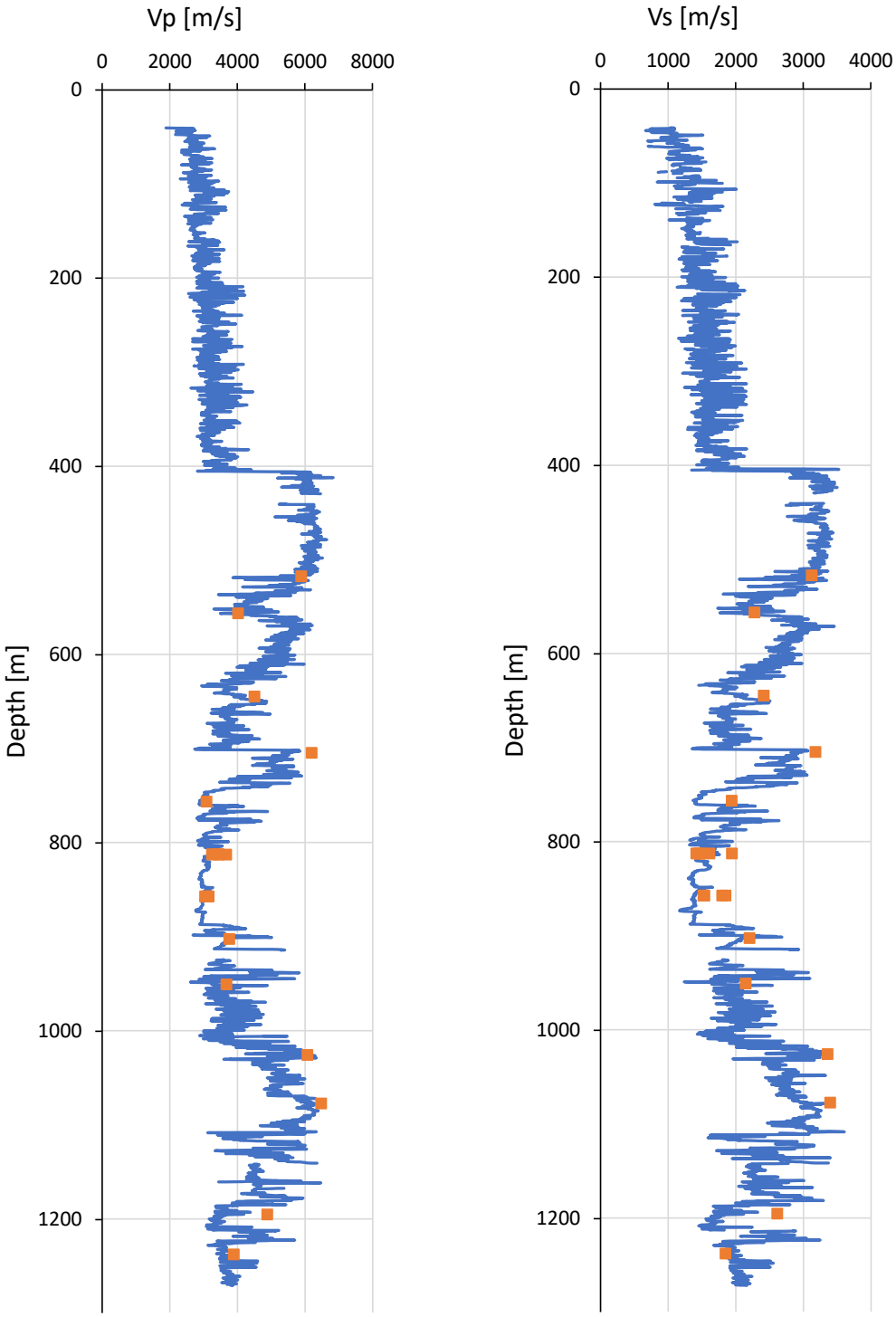

Fig. 7-1: Compressional (a) and shear-wave velocities (b) from borehole and lab testing

Blue line: continuous measurements from borehole sonic scanner (kHz frequency). Orange squares: lab measurements (MHz frequency).

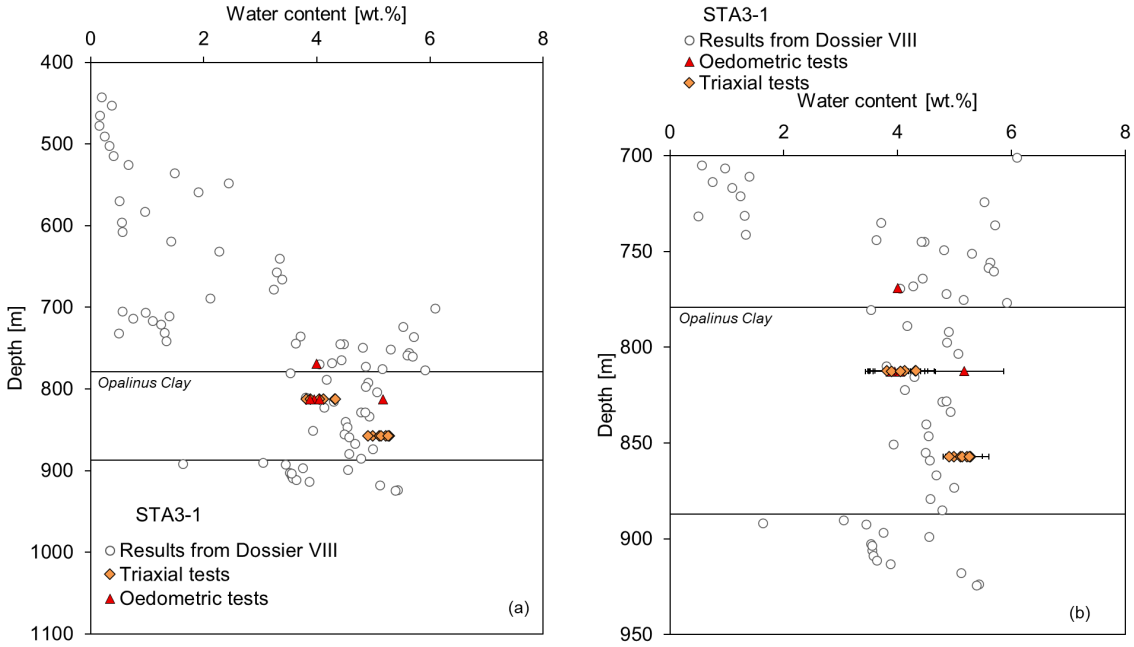

Fig. 7-2: Water content vs. depth from the large database and from tested specimens

Results include those from Dossier VIII for the STA3-1 borehole (a) and zoom into the Opalinus Clay and confining units' section (b).

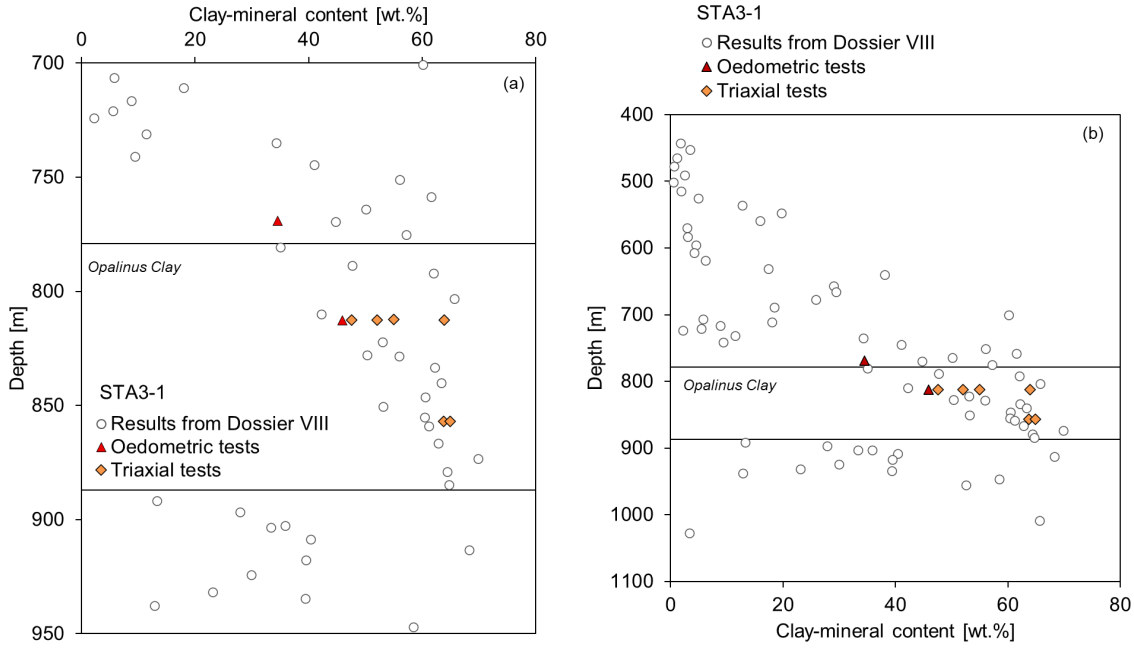

Fig. 7-3: Clay-mineral content vs. depth from the large database and from tested specimens

Results include those from Dossier VIII for the STA3-1 borehole (a) and zoom into the Opalinus Clay and confining units' section (b).

8 References

ASTM (2014): D7012-14e1: Standard test method for compressive strength and elastic moduli of intact rock core specimens under varying states of stress and temperatures. ASTM International, West Conshohocken, PA.

ASTM (2016): D3967-16: Standard test method for splitting tensile strength of intact rock core specimens. ASTM International, West Conshohocken, PA.

ASTM (2017a): D4318-17e1: Standard test methods for liquid limit, plastic limit, and plasticity index of soils. ASTM International, West Conshohocken, PA.

ASTM (2017b): D6913/D6913M-17: Standard test methods for particle-size distribution (gradation) of soils using sieve analysis. ASTM International, West Conshohocken, PA.

ASTM (2017c): D7928-17: Standard test method for particle-size distribution (gradation) of fine-grained soils using the sedimentation (hydrometer) analysis. ASTM International, West Conshohocken, PA.

ASTM (2019): D4543-19: Preparing rock core as cylindrical specimens and verifying conformance to dimensional and shape tolerances. ASTM International, West Conshohocken, PA.

Aydin, A. (2014): Upgraded ISRM suggested method for determining sound velocity by Ultrasonic Pulse Transmission Technique. Rock Mechanics and Rock Engingeering 47, 255-259.

Biot, M.A. (1941): General theory of three-dimensional consolidation. Journal of Applied Physics 12/2, 155-164.

Crisci, E., Ferrari, A., Giger, S.B. & Laloui, L. (2019): Hydro-mechanical behaviour of shallow Opalinus Clay shale. Eng. Geol. 251, 214-227. https://doi.org/10.1016/j.enggeo.2019.01.016.

Ewy, R.T. (2014): Shale swelling/shrinkage and water content change due to imposed suction and due to direct brine contact. Acta Geotech. 9, 869-886. https://doi.org/10.1007/s11440-013-0297-5.

Ewy, R.T. (2015): Shale/claystone response to air and liquid exposure, and implications for handling, sampling and testing. International Journal of Rock Mechanics and Mining Sciences 80, 388-401. https://doi.org/10.1016/j.ijrmms.2015.10.009

Favero, V. (2017): Multiphysical behaviour of shales from Northern Switzerland. https://doi.org/10.5075/epfl-thesis-7539, urn:nbn:ch:bel-epfl-thesis7539-7.

Favero, V., Ferrari, A. & Laloui, L. (2018): Anisotropic behaviour of Opalinus Clay through consolidated and drained triaxial testing in saturated conditions. Rock Mechanics and Rock Engineering 51, 1305-1319.

Ferrari, A., Favero, V. & Laloui, L. (2016): One-dimensional compression and consolidation of shales. Int. J. Rock Mech. Min. Sci. 88, 286-300. https://doi.org/10.1016/j.ijrmms.2016.07.030.

Ghabezloo, S. & Sulem, J. (2010): Effect of the volume of the drainage system on the measurement of undrained thermo-poro-elastic parameters. International Journal of Rock Mechanics and Mining Sciences 47, 60-68. https://doi.org/10.1016/j.ijrmms.2009.03.001.

Giger, S.B., Ewy, R.T., Favero, V., Stankovic, R. & Keller, L.M. (2018): Consolidated-undrained triaxial testing of Opalinus Clay: Results and method validation. Geomechanics for Energy and the Environment 14, 16-28.

Head, K.H. (1998): Manual of soil laboratory testing. Volume 3: Effective stress tests. Second Edition John Wiley and Sons.

Isler, A., Pasquier, F. & Huber, M. (1984): Geologische Karte der zentralen Nordschweiz 1:100'000. Herausgegeben von der Nagra und der Schweiz. Geol. Komm.

Keller, L.M. & Giger, S.B. (2019): Petrophysical properties of Opalinus Clay drill cores determined from Med-XCT images. Geotech. Geol. Eng. 37/4, 3507-3522. https://doi.org/10.1007/s10706-019-00815-2.

Minardi, A., Ferrari, A. & Laloui, L. (2019): Benchmark study on triaxial testing of Opalinus Clay: Analysis and comparative evaluation of tests results. Nagra Arbeitsbericht NAB 19-18.

Minardi, A., Giger, S.B., Ewy, R.T., Stankovic, R., Stenebråten, J., Soldal, M., Rosone, M., Ferrari, A. & Laloui, L. (2020): Benchmark study of undrained triaxial testing of Opalinus Clay shale: Results and implications for robust testing. Geomechanics for Energy and the Environment 25, 100210.

Nagra (2014): SGT Etappe 2: Vorschlag weiter zu untersuchender geologischer Standortgebiete mit zugehörigen Standortarealen für die Oberflächenanlage. Geologische Grundlagen. Dossier II: Sedimentologische und tektonische Verhältnisse. Nagra Technischer Bericht NTB 14-02.

Nagra (2021a): TBO Bülach-1-1: Data Report. Dossier IX: Rock-mechanical and Geomechanical Laboratory Testing. Nagra Arbeitsbericht NAB 20-08.

Nagra (2021b): TBO Trüllikon-1-1: Data Report. Dossier IX: Rock-mechanical and Geomechanical Laboratory Testing. Nagra Arbeitsbericht NAB 20-09.

Pietsch, J. & Jordan, P. (2014): Digitales Höhenmodell Basis Quartär der Nordschweiz – Version 2013 (SGT E2) und ausgewählte Auswertungen. Nagra Arbeitsbericht NAB 14-02.

Rufer, D. (2019): Field manual: Drill core sampling for analytical purposes. Nagra Arbeitsbericht NAB 19-13.

Tuttolomondo, A. (2021): Effective stress for unsaturated active clays and in-situ effective stress estimation methodology. EPFL PhD Thesis n° 8291.

Wissa, A.E.Z. (1969): Pore pressure measurement in saturated stiff soils. Journal of the Soil Mechanics and Foundations Division 95, 1063-1074.

Wersin, P., Mazurek, M., Waber, H.N., Mäder, U.K., Gimmi, T., Rufer, D. & de Haller, A. (2013): Rock and porewater characterisation on drillcores from the Schlattingen borehole. Nagra Arbeitsbericht NAB 12-54.

Witteveen, P., Ferrari, A. & Laloui, L. (2013): An experimental and constitutive investigation on the chemo-mechanical behaviour of a clay. Geotechnique 63/3, 244-255.

Appendix A Photo documentation of the rock mechanical testing programme

TS (average depth of sample) **STA3-1**

before testing **after testing**

516.82 m

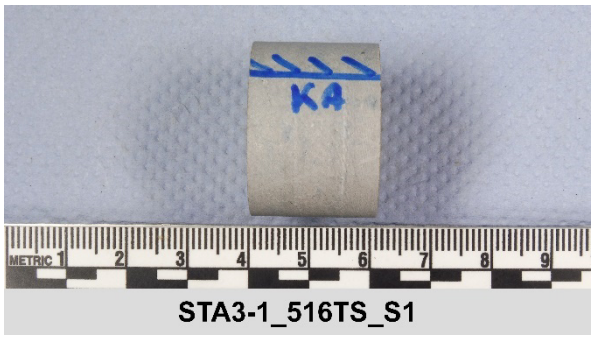

535.38 m

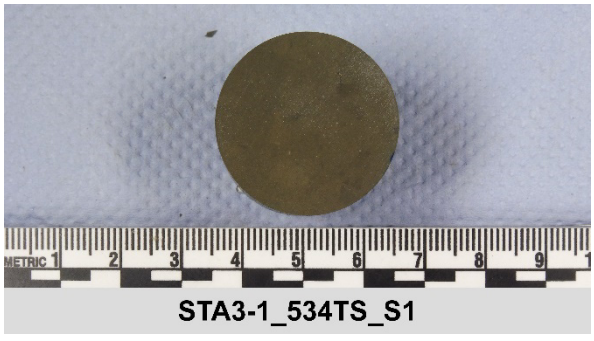

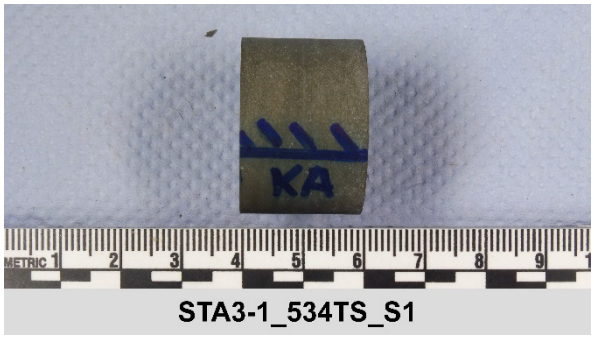

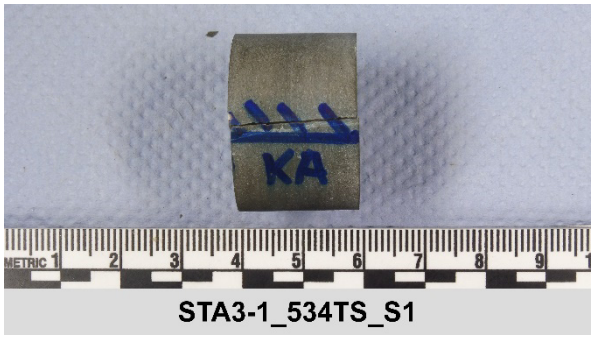

before testing **after testing**

556.34 m

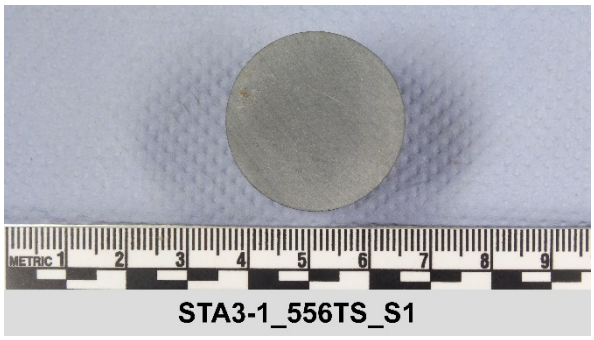

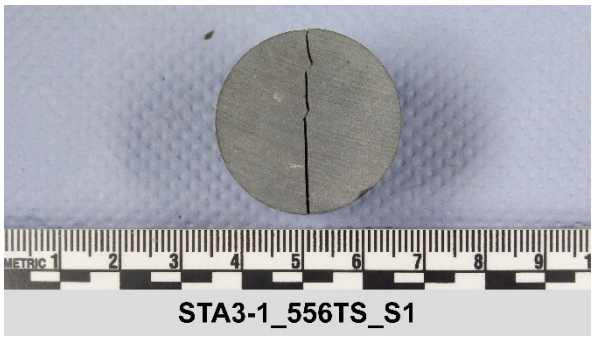

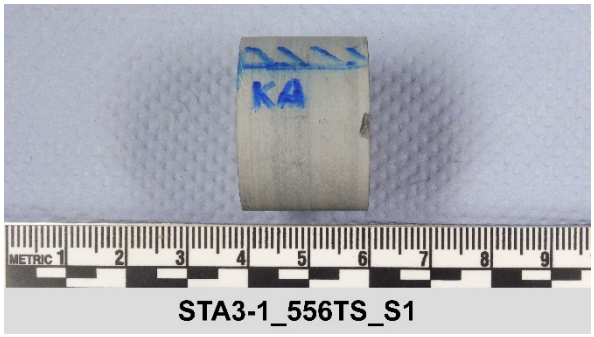

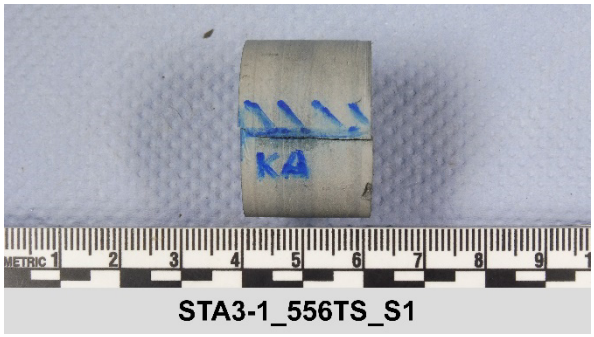

644.23 m

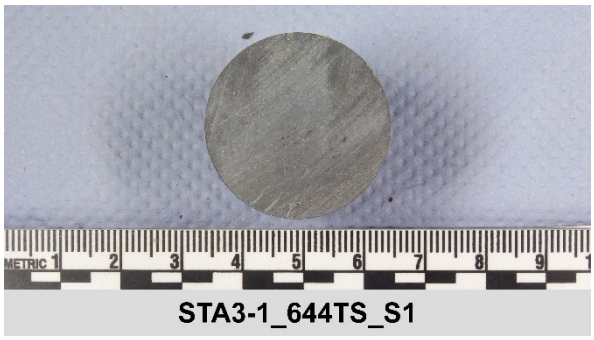

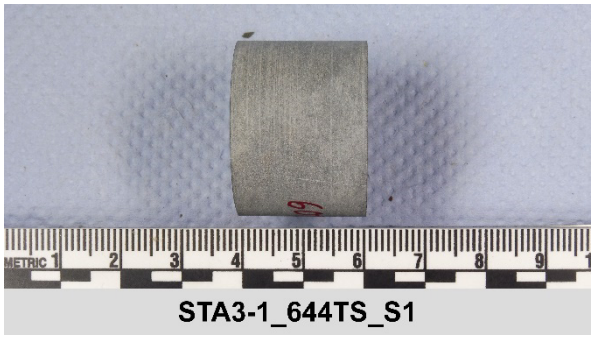

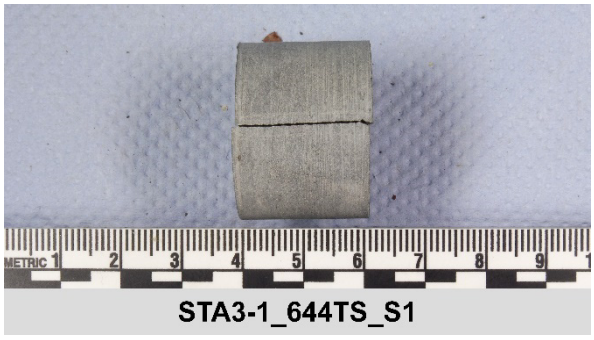

before testing **after testing**

704.35 m

755.90 m

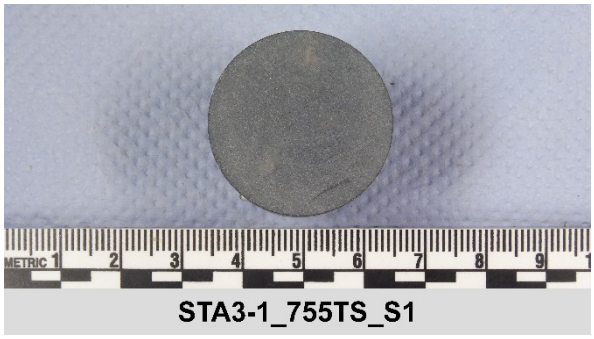

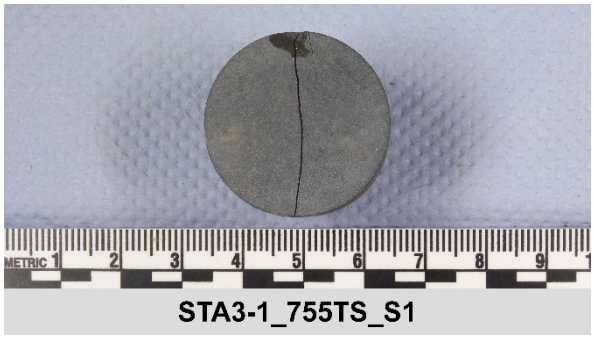

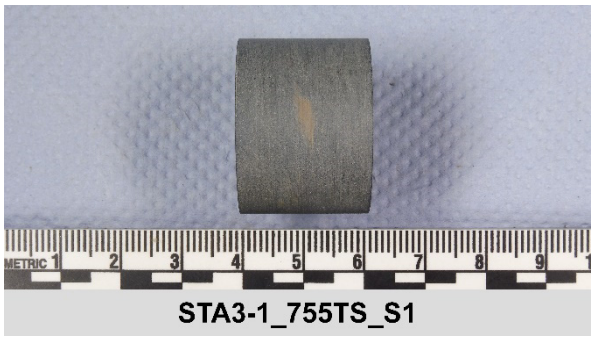

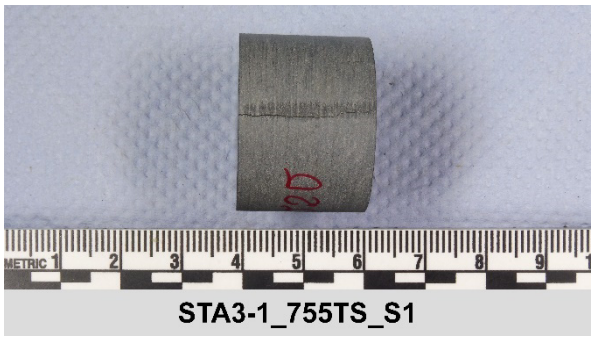

before testing **after testing**

902.30 m

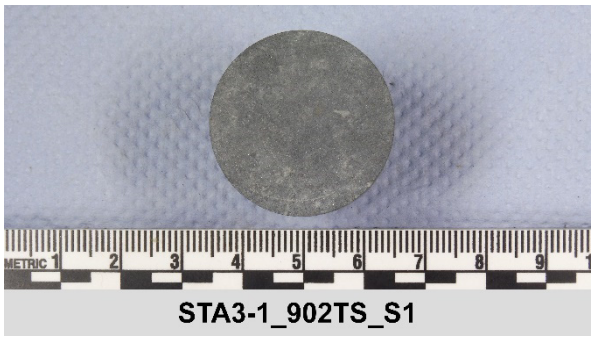

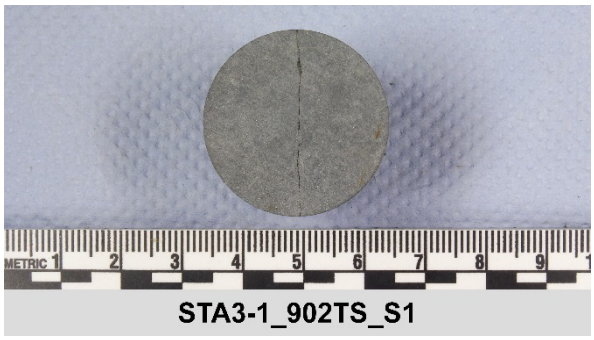

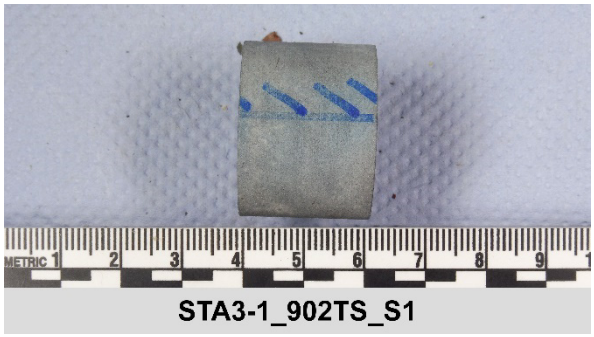

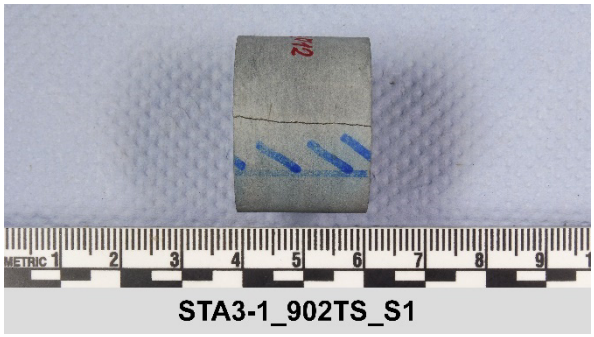

950.25 m

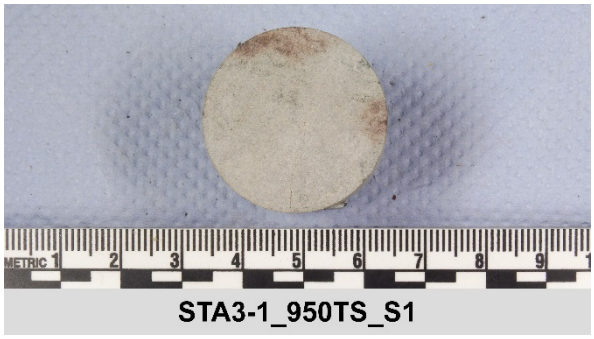

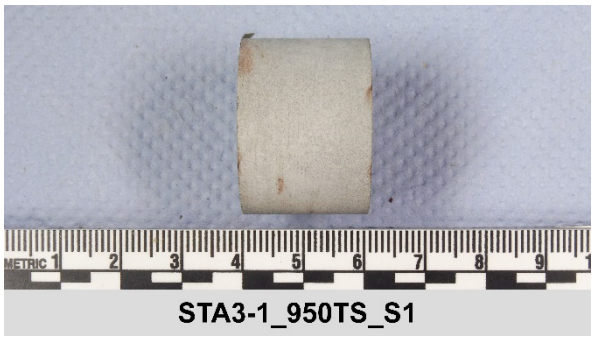

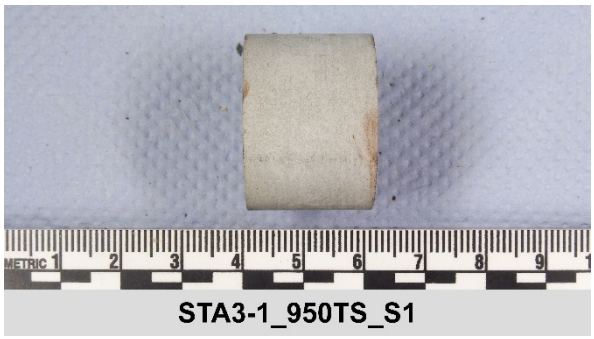

before testing **after testing**

1195.24 m

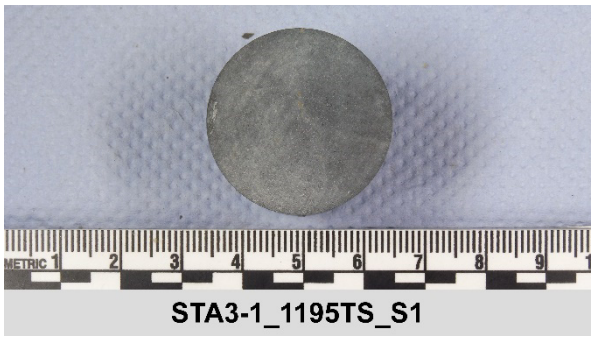

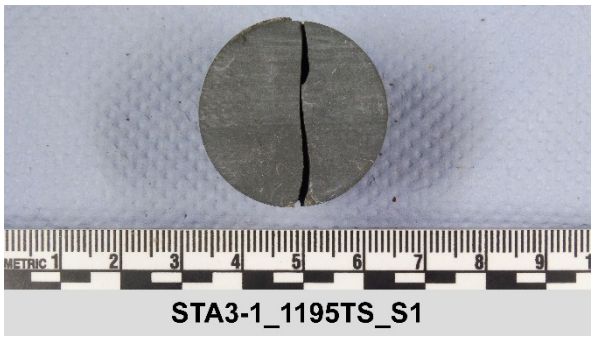

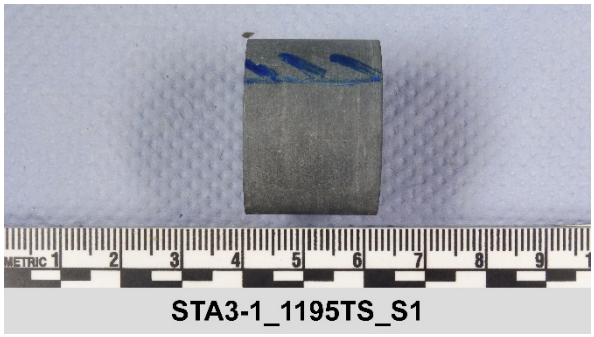

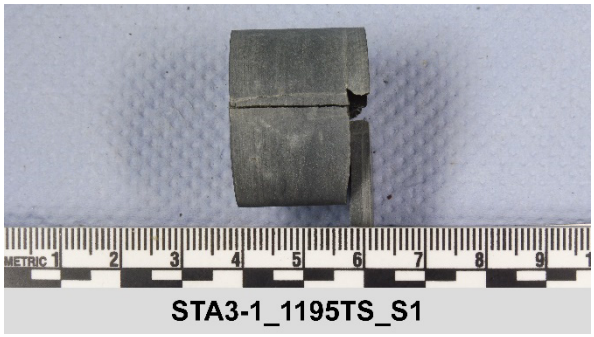

1237.51 m

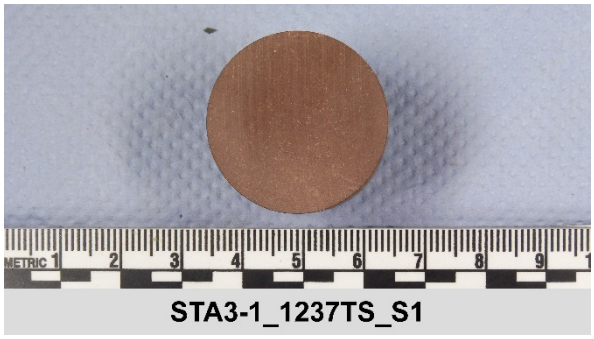

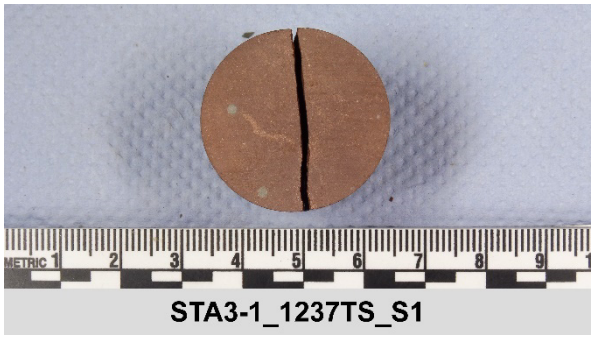

UCS (depth of sample top) **STA3-1**

before testing **after testing**

476.33 m

476.50 m

476.70 m

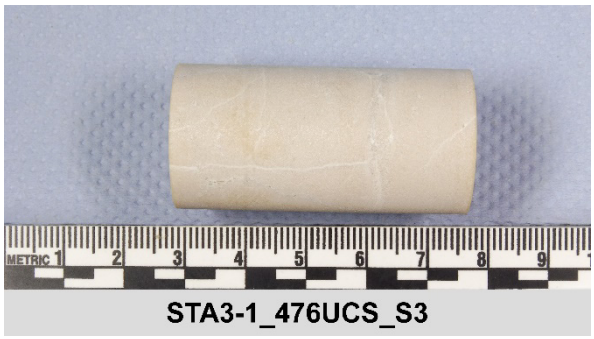

516.78 m

before testing **after testing**

517.02 m

517.20 m

535.01 m

535.26 m

before testing **after testing**

535.43 m

556.29 m

556.44 m

556.73 m

before testing **after testing**

644.25 m

644.42 m

644.66 m

680.55 m

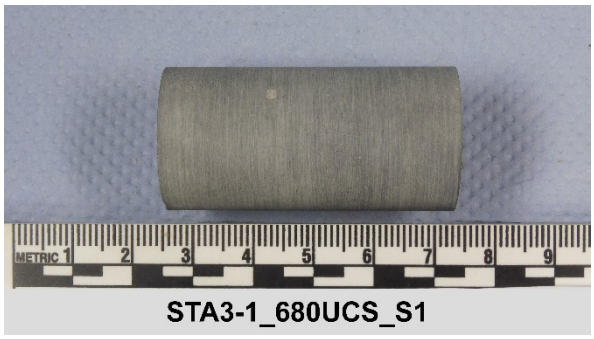

before testing **after testing**

680.72 m

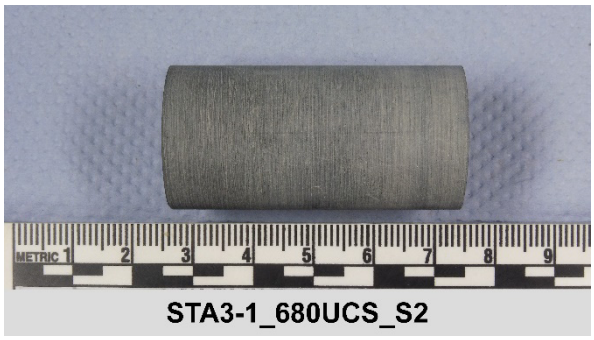

680.89 m

704.31 m

704.47 m

before testing **after testing**

704.64 m

743.92 m

744.11 m

744.34 m

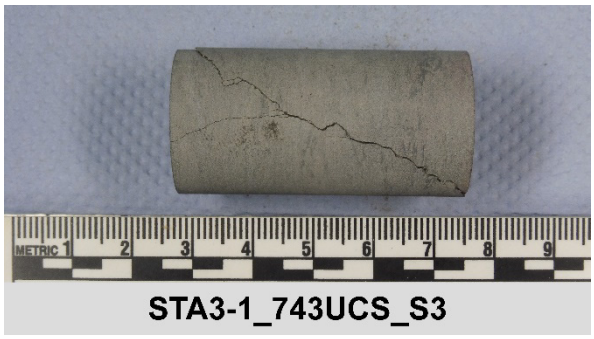

before testing **after testing**

755.87 m

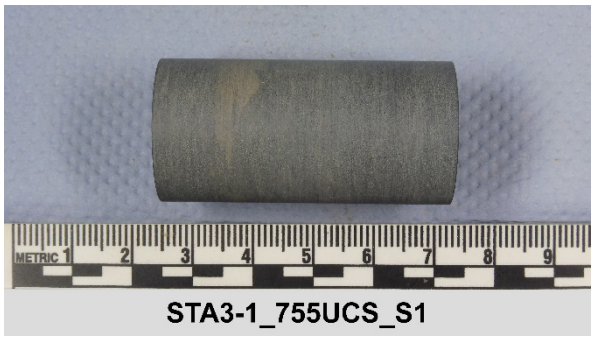

756.29 m

902.10 m

902.35 m

before testing **after testing**

902.50 m

950.08 m

950.31 m

950.49 m

before testing **after testing**

968.63 m

968.75 m

968.79 m

1025.61 m

before testing **after testing**

1025.67 m

1025.81 m

1031.63 m

1031.79 m

before testing **after testing**

1031.99 m

1077.22 m

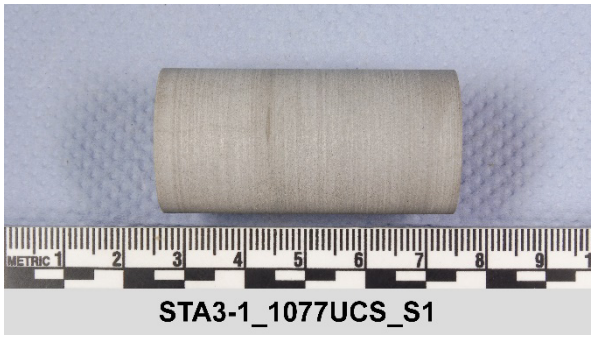

1077.69 m

1077.49 m

before testing **after testing**

1105.32 m

1105.45 m

1105.66 m

1154.52 m

before testing **after testing**

1154.71 m

1154.91 m

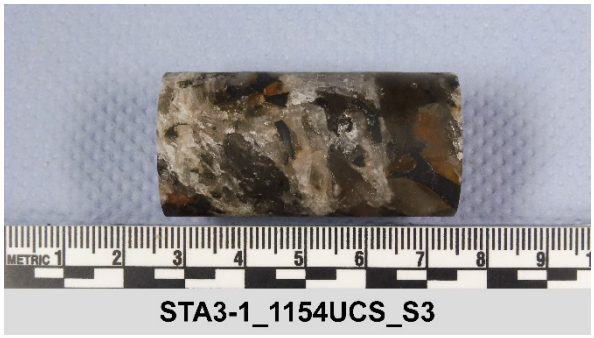

1195.20 m

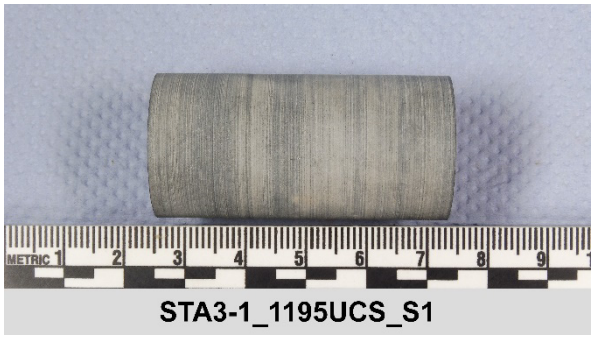

1195.34 m

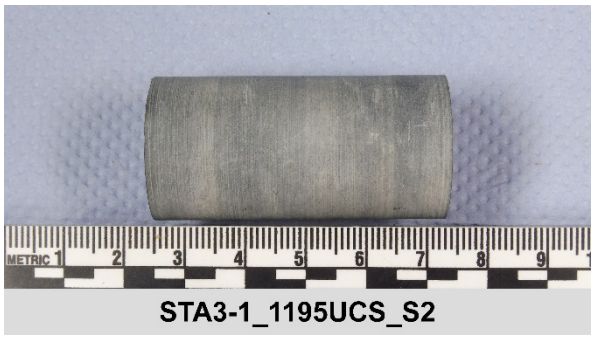

before testing **after testing**

1195.45 m

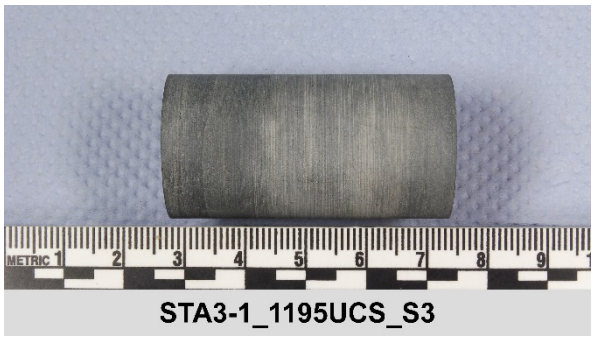

1237.57 m

1237.86 m

1274.35 m

before testing **after testing**

1274.60 m

1274.79 m

TRX (depth of sample top)

before testing

STA3-1

after testing

516.78 m

556.29 m

644.66 m

704.47 m

before testing **after testing**

756.29 m

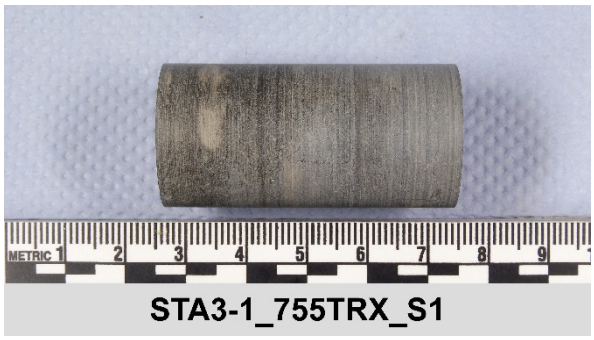

902.35 m

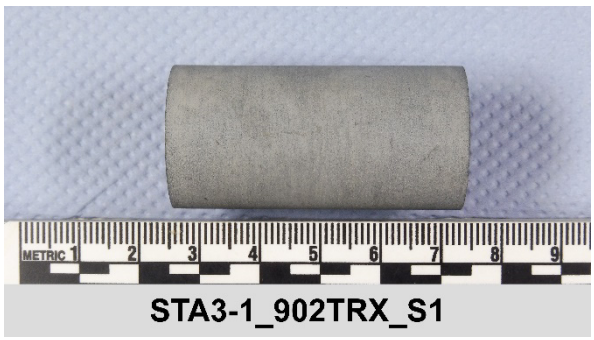

950.49 m

1025.67 m

before testing **after testing**

1077.22 m

1195.20 m

1237.57 m

Appendix B XCT cross-sections with selection of test specimens

The computed tomography scans of the tested cores are here reported, and the sections used in the testing programme are indicated.

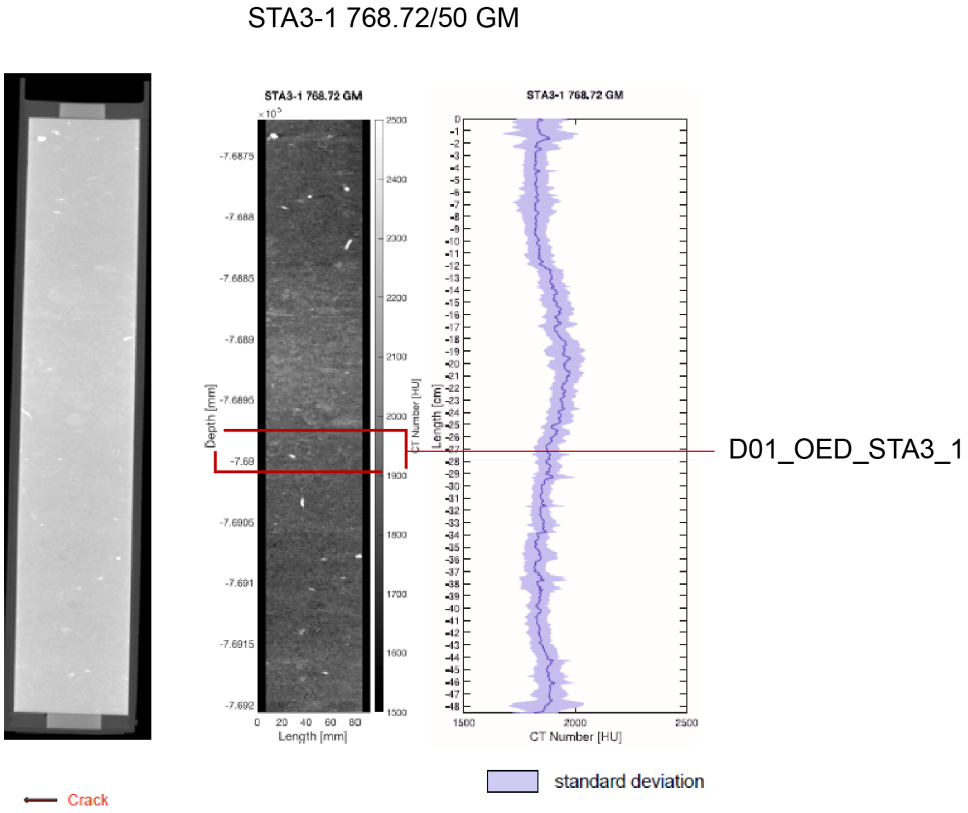

STA3-1 812.19/50 GM

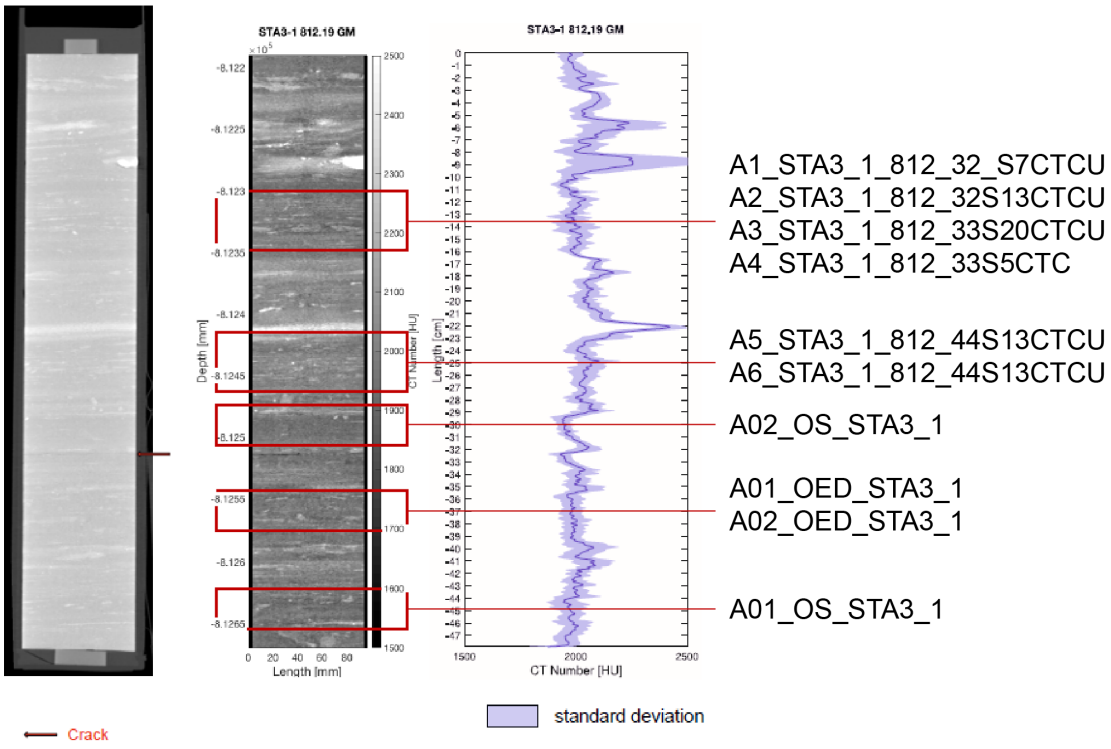

STA3-1 856.99/40 GM

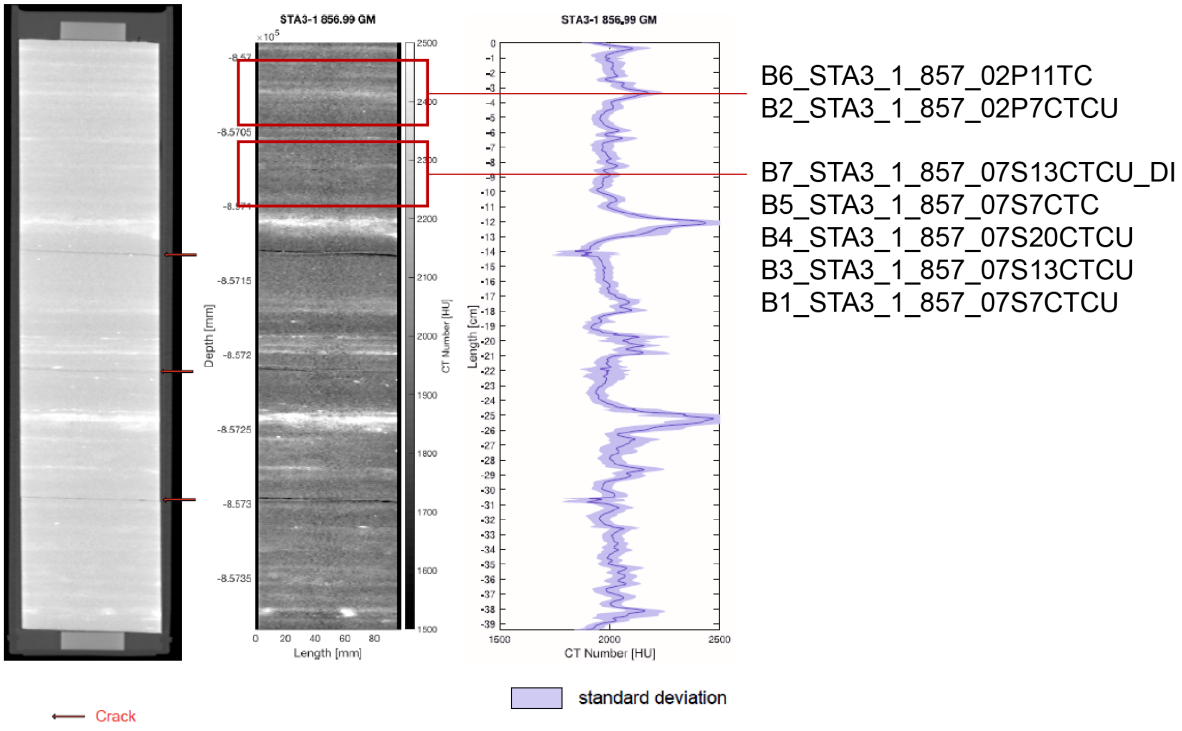

Appendix C Diagnostic plots of triaxial tests (geomechanical testing programme)

For each triaxial test, the diagnostic plots are here reported (order of tests according to Tab. E-2). The plots include: the evolution of axial and radial strains with deviatoric stress q, the pore pressure change Δu_w during shearing versus the axial strain ε_a, the stress path in the p'-q plane, the pore pressure variation Δu_w and the AB parameter evolution with q. In all the plots, the conditions at which the maximum deviatoric stress (Max q), the maximum pore pressure change (Max Δu_w) and the maximum AB (Max AB) (excluding evolution during unload/reload loops) are marked, as mentioned in Section 6.2.2.4. Testing conditions are reported in Tab. 6-2.

A1_STA3_1_812_32_S7CTCU

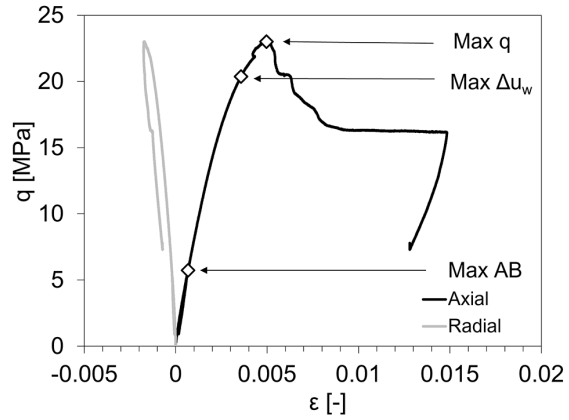

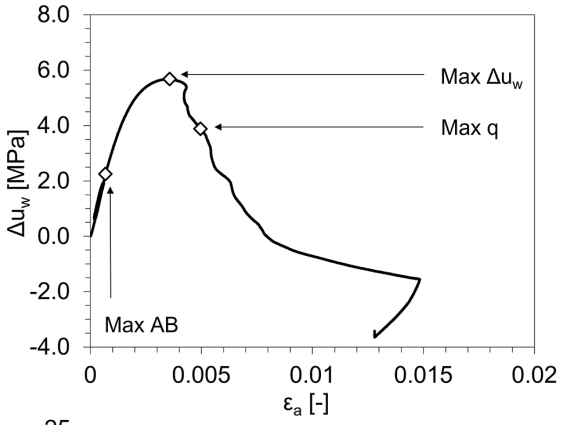

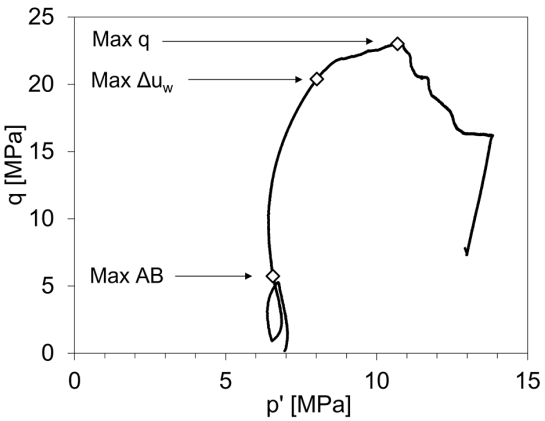

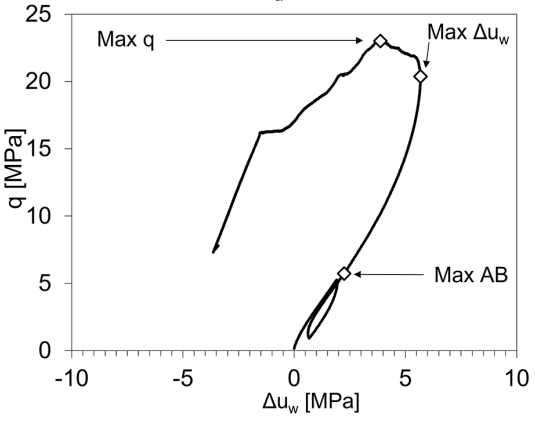

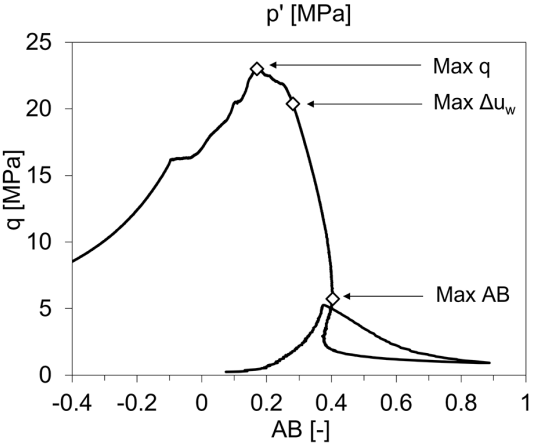

A2_STA3_1_812_32S13CTCU

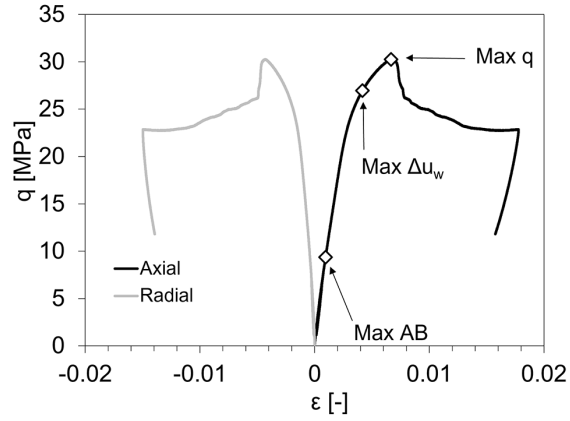

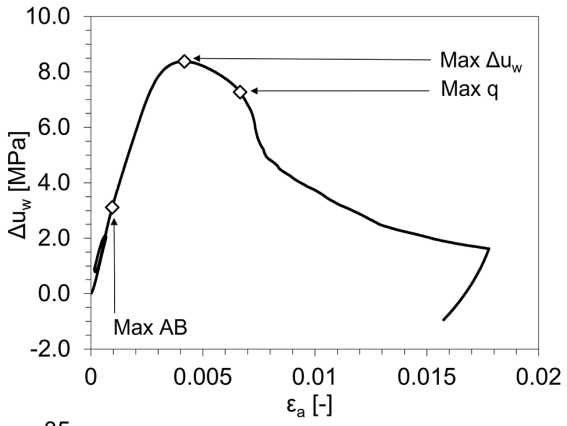

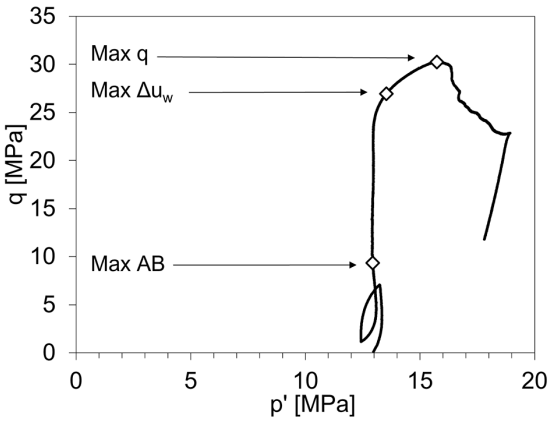

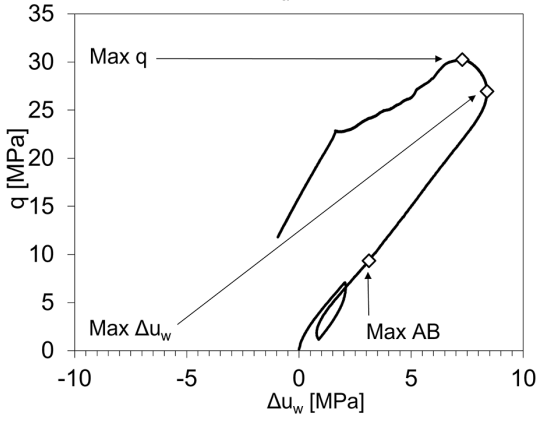

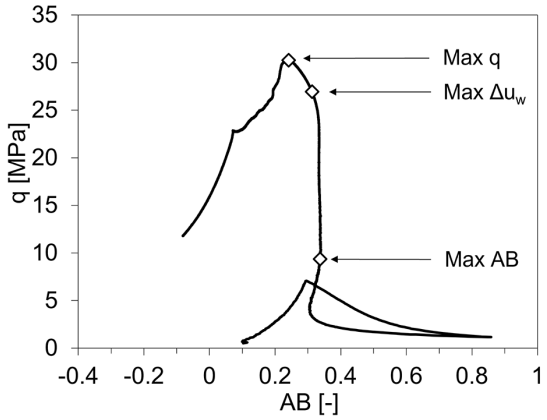

A3_STA3_1_812_33S20CTCU

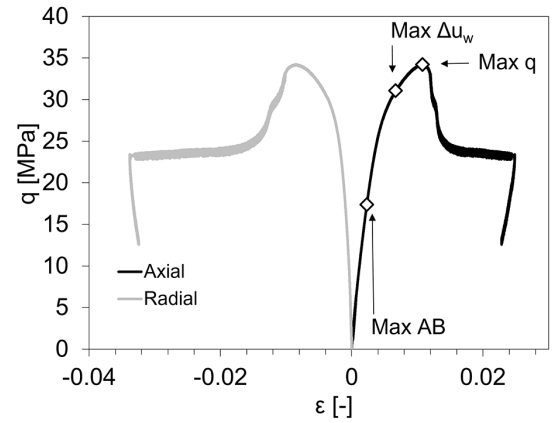

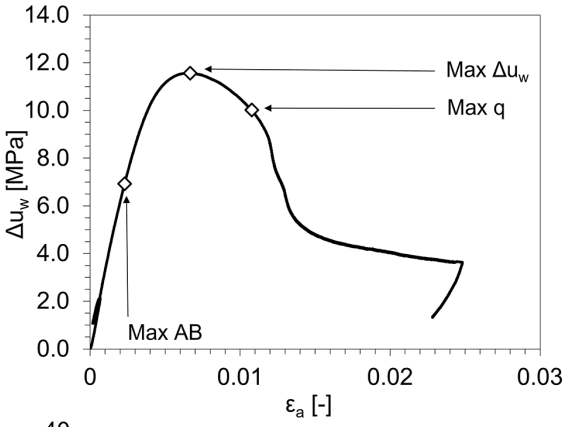

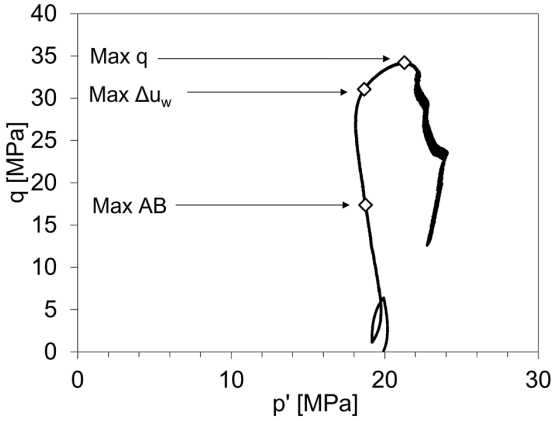

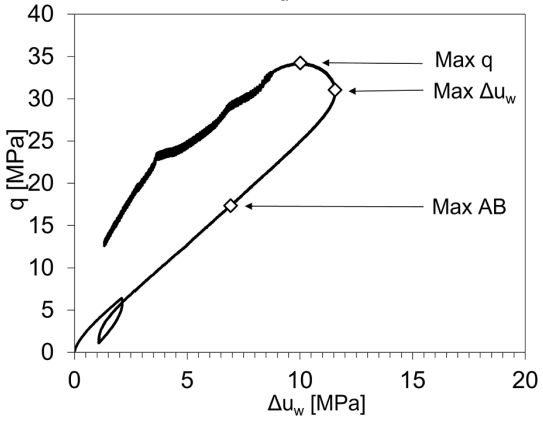

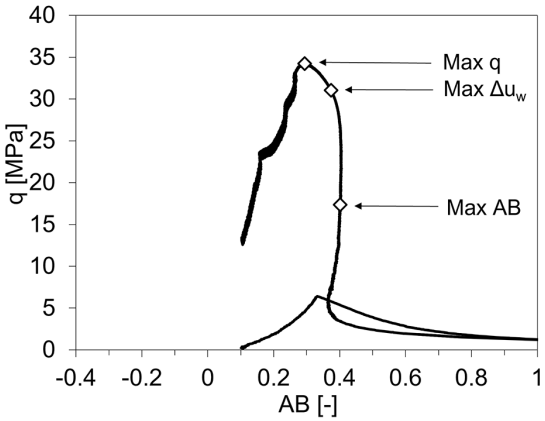

A4_STA3_1_812_33S5CTC

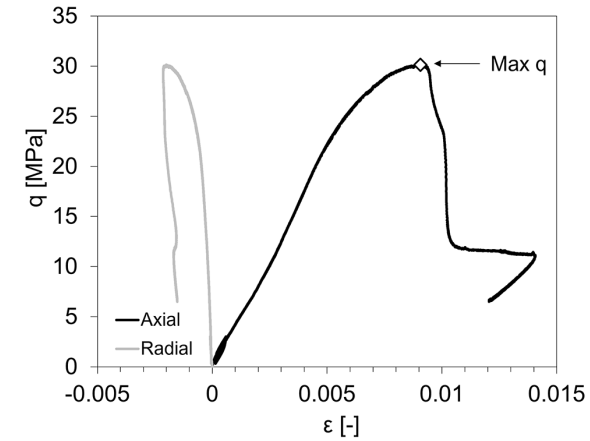

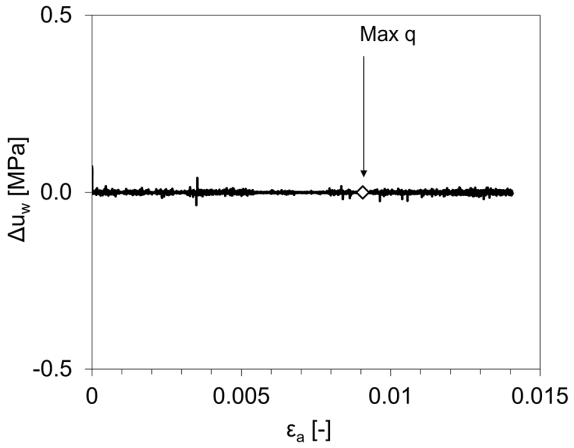

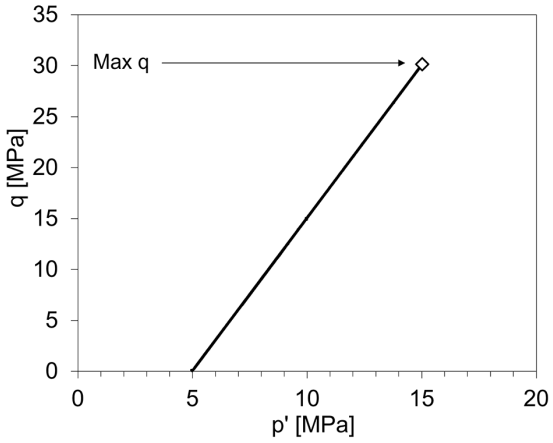

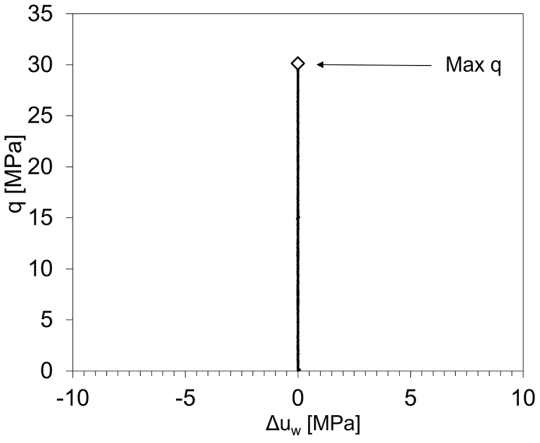

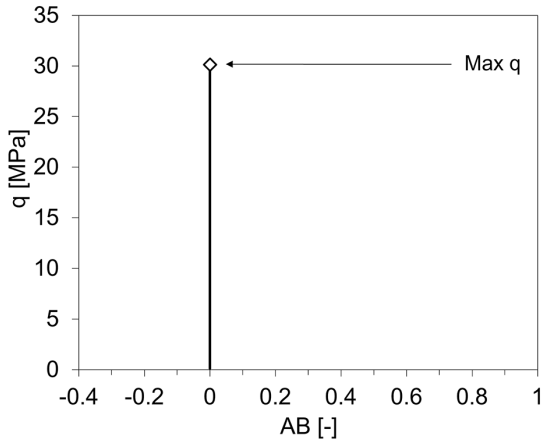

A5_STA3_1_812_44S13CTCU

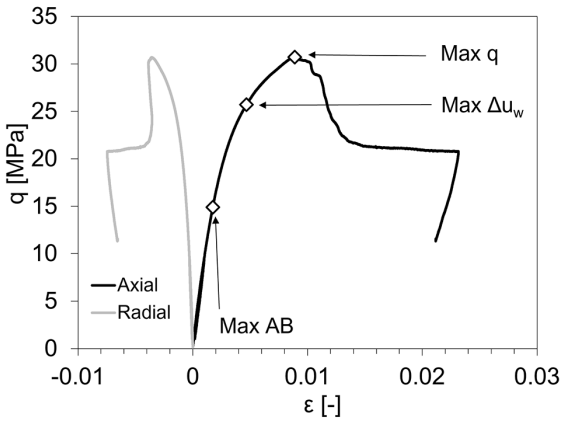

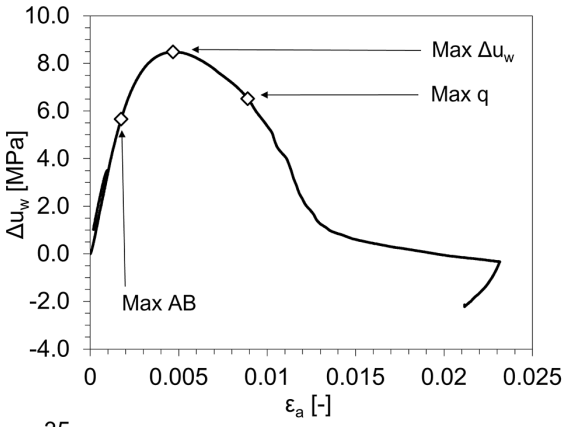

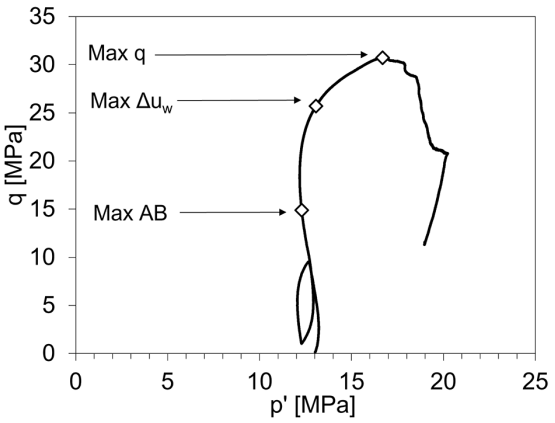

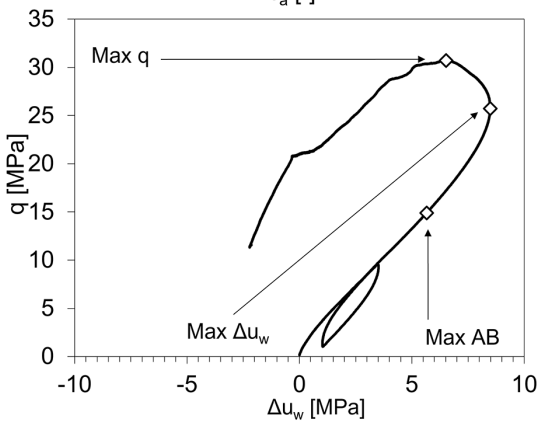

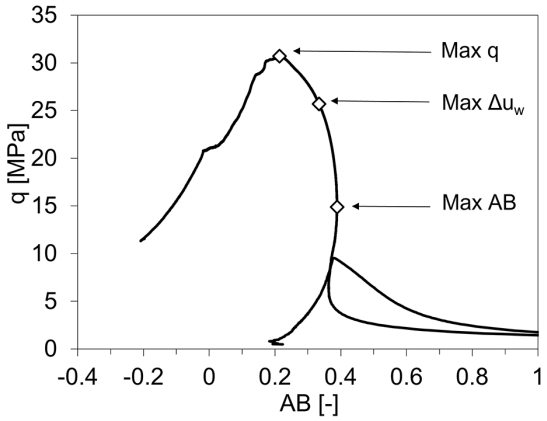

A6_STA3_1_812_44S13CTCU

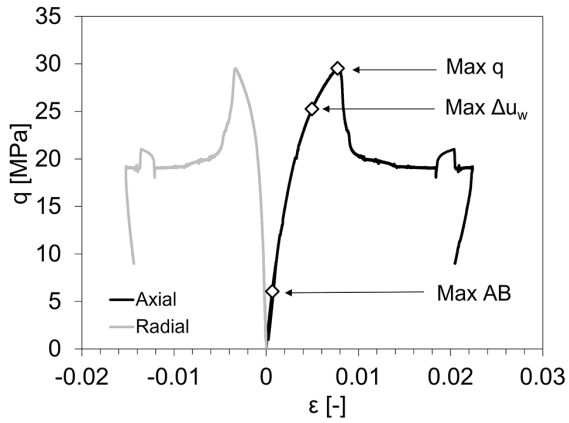

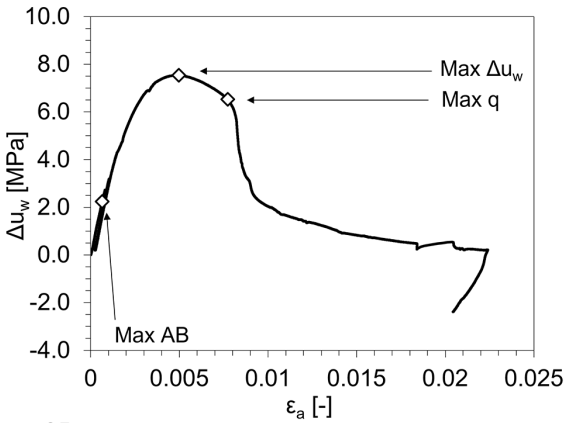

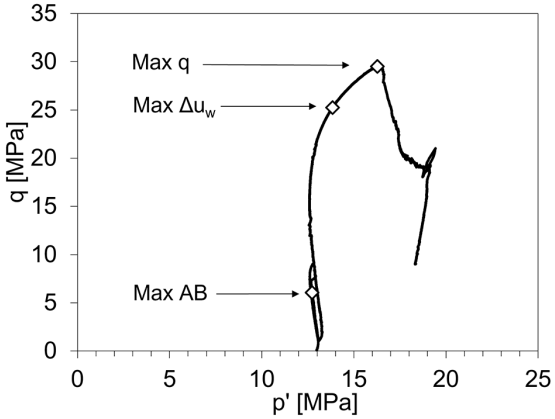

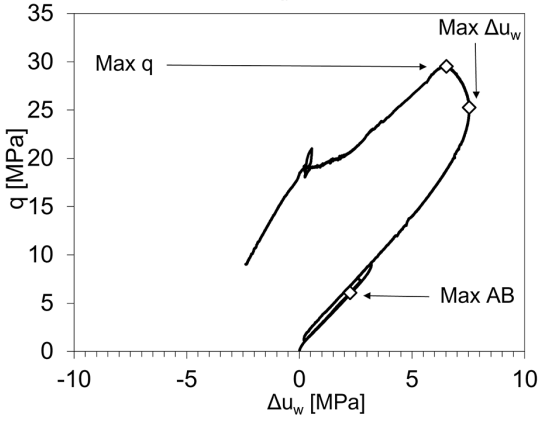

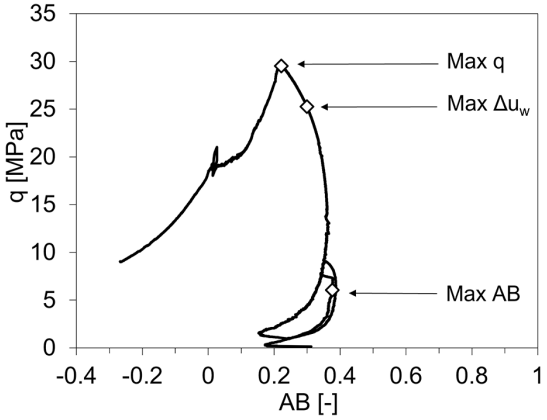

B6_STA3_1_857_02P11TC

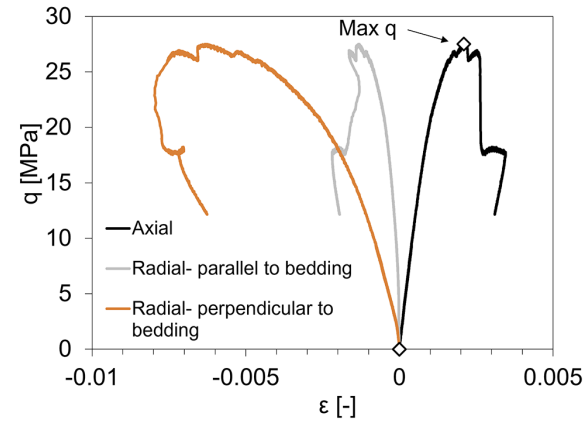

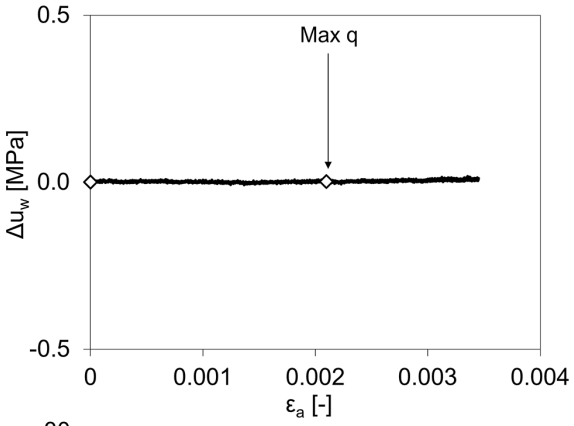

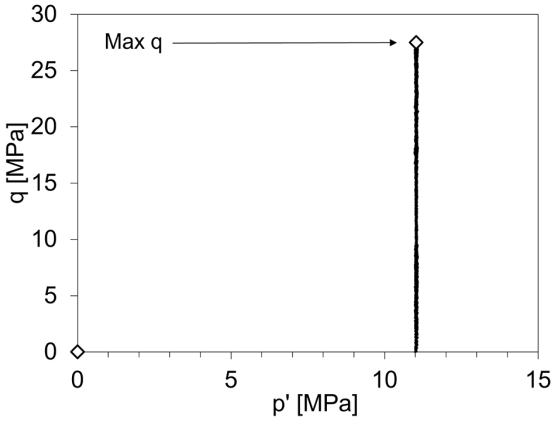

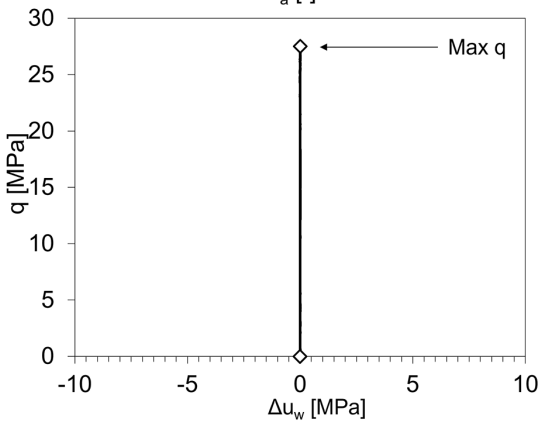

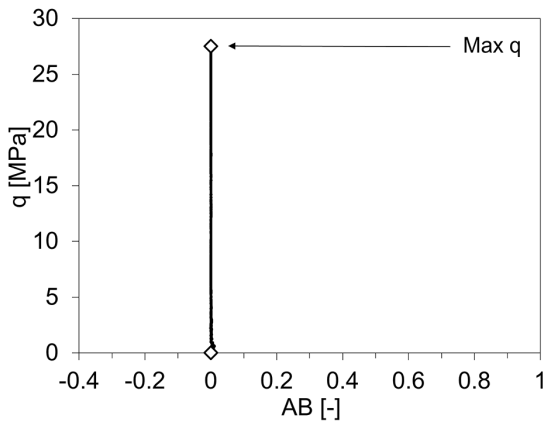

B2_STA3_1_857_02P7CTCU

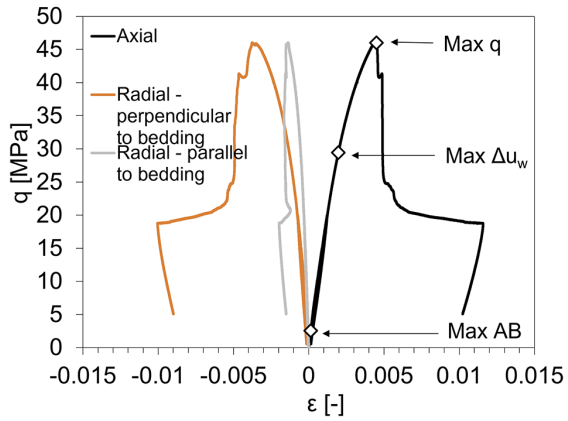

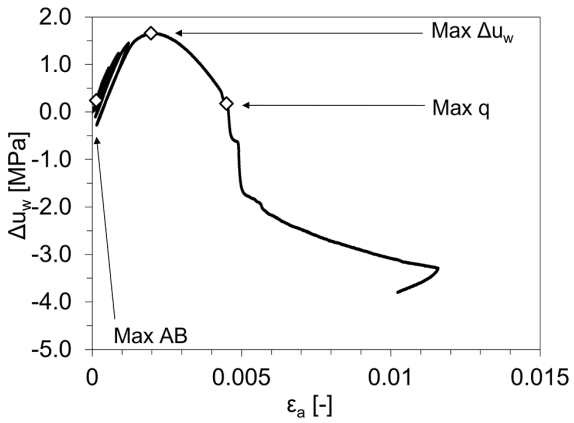

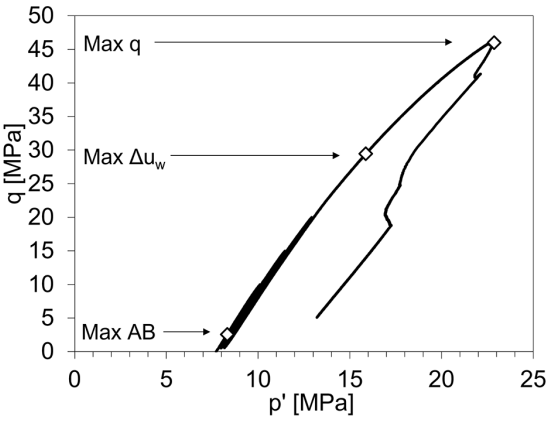

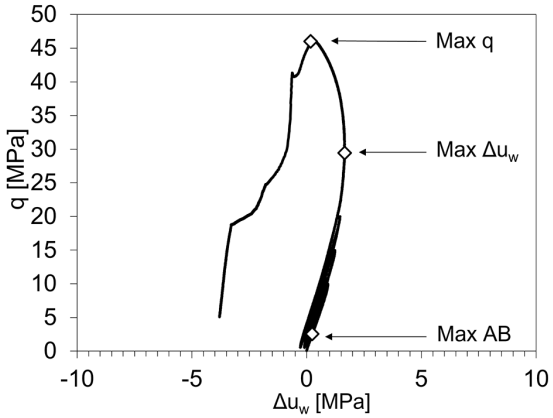

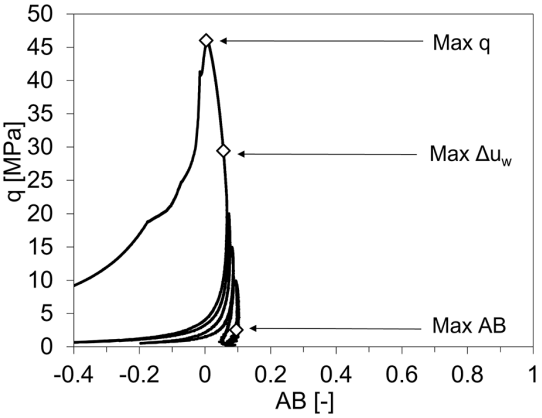

B7_STA3_1_857_07S13CTCU_DI

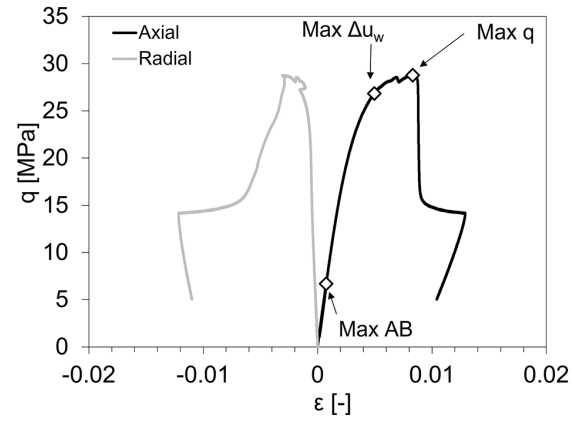

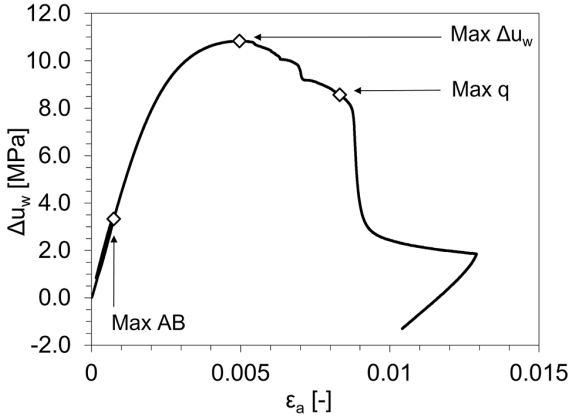

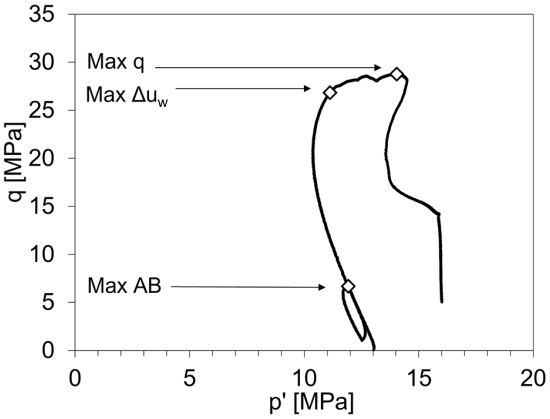

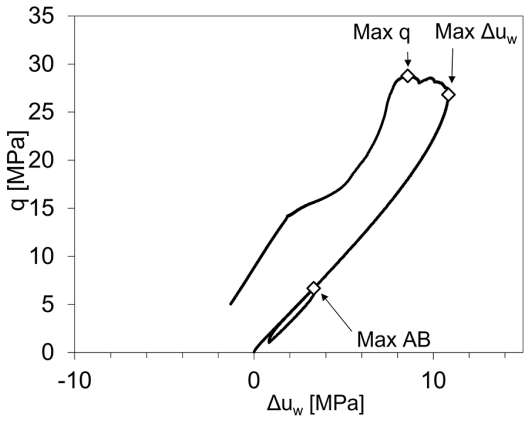

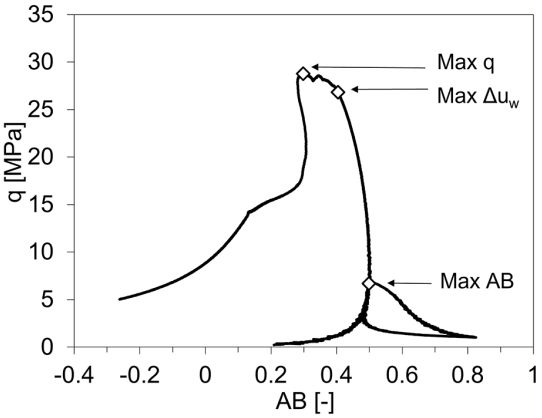

B5_STA3_1_857_07S7CTC

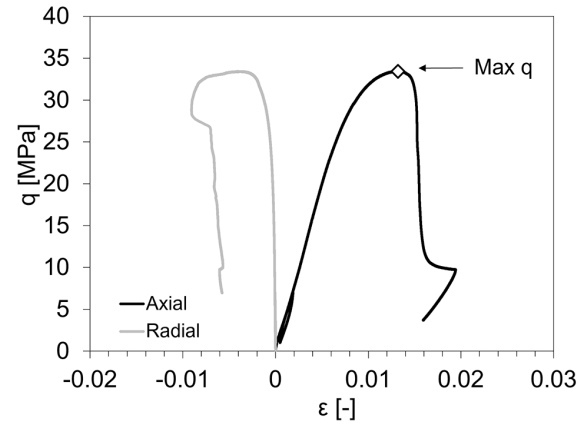

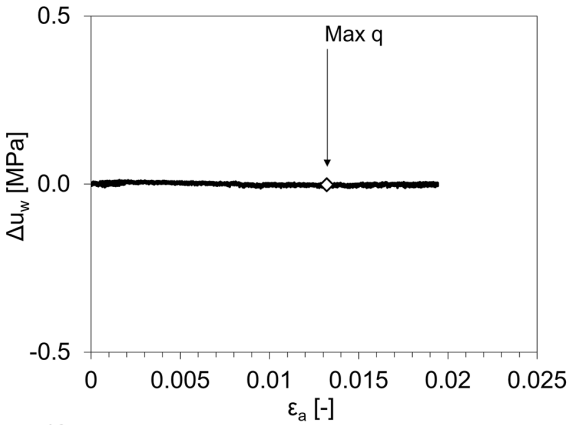

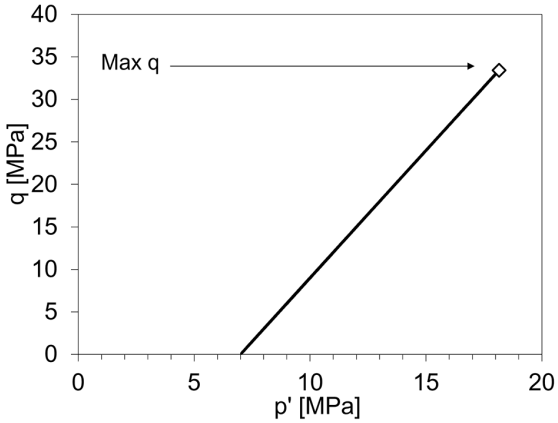

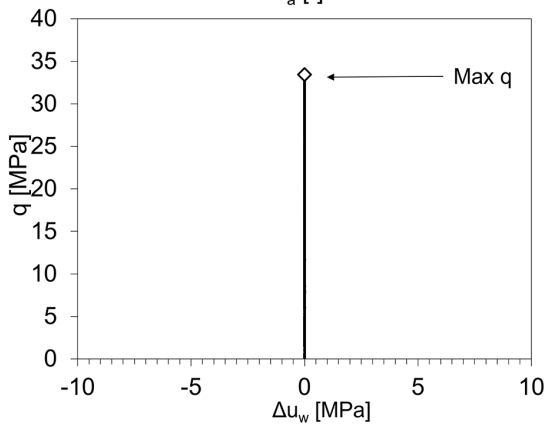

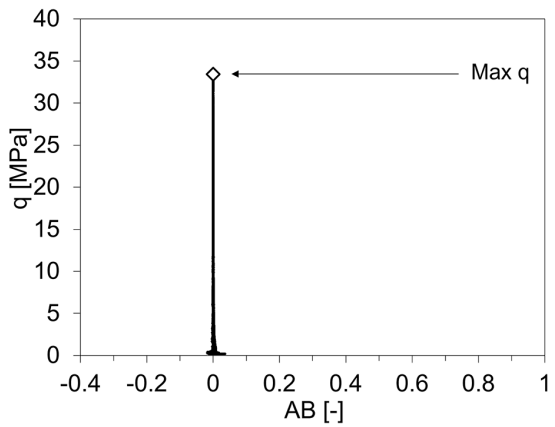

B4_STA3_1_857_07S20CTCU

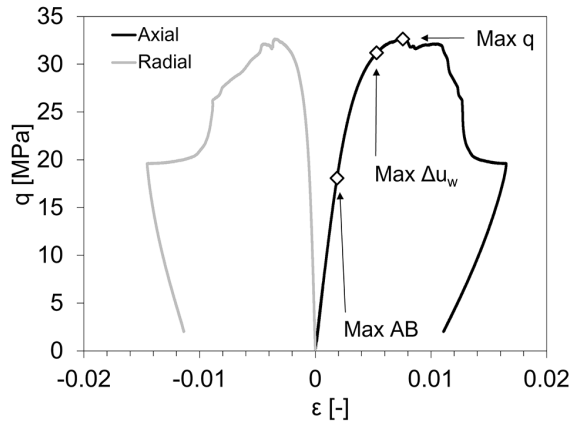

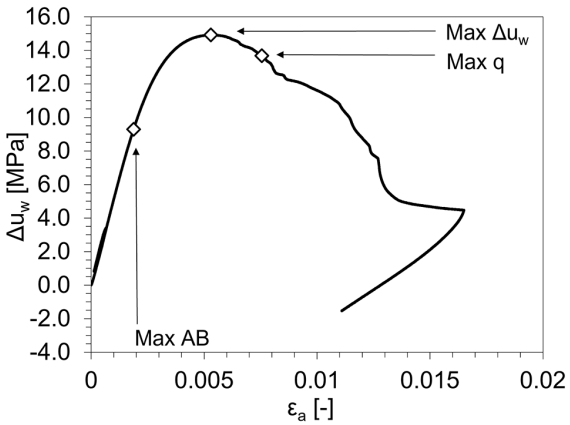

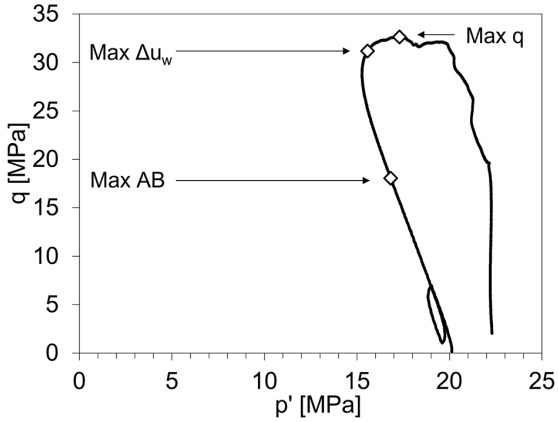

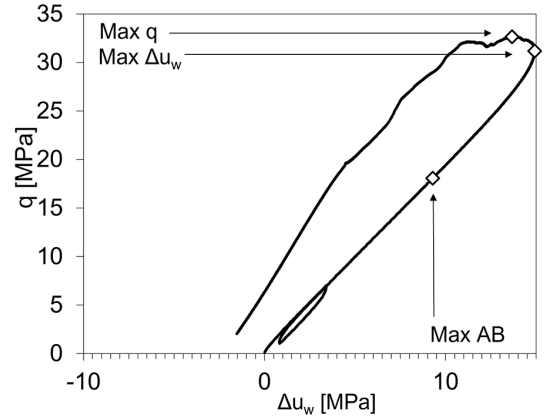

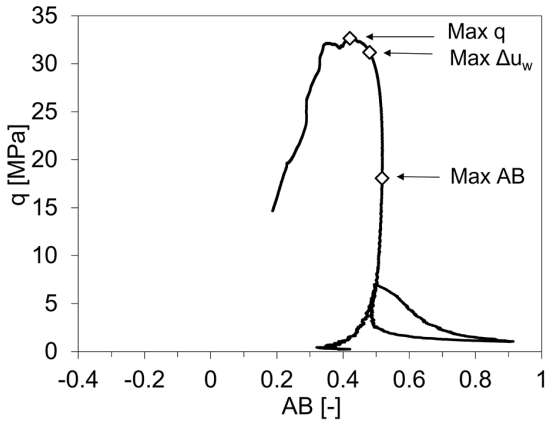

B3_STA3_1_857_07S13CTCU

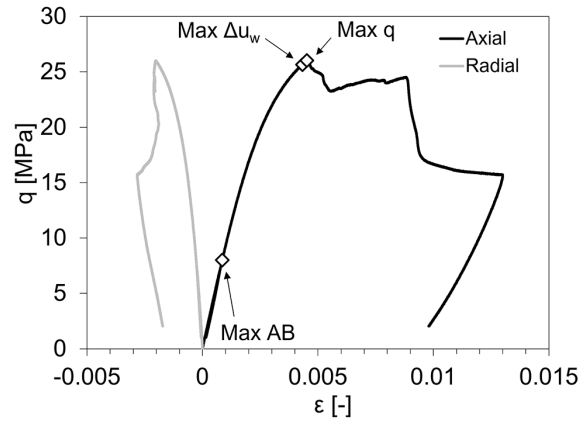

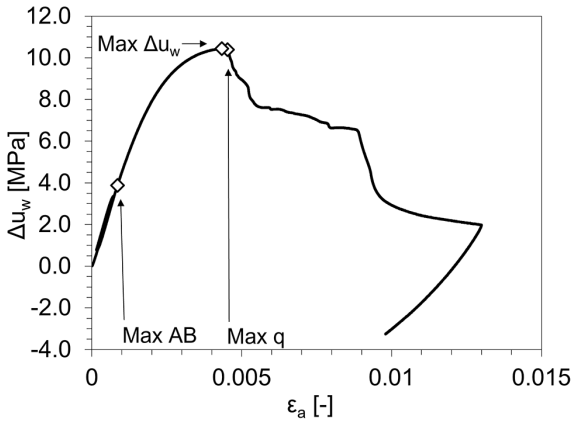

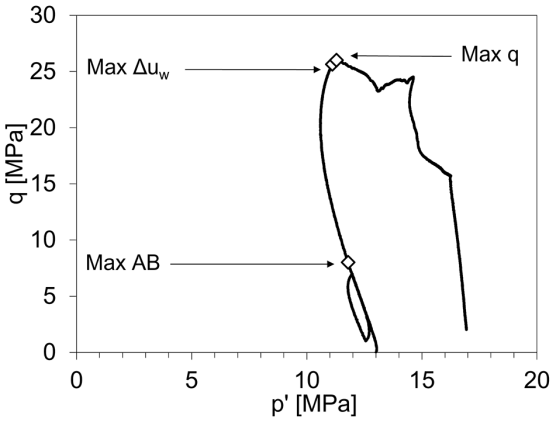

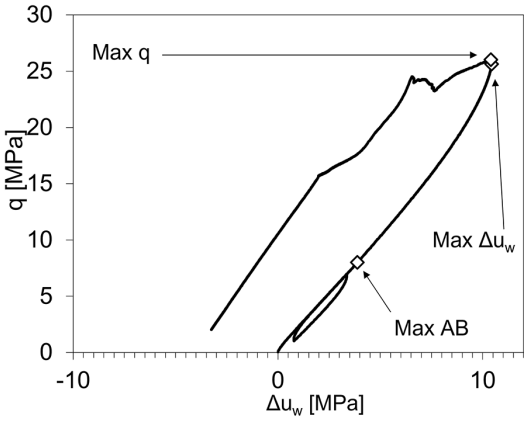

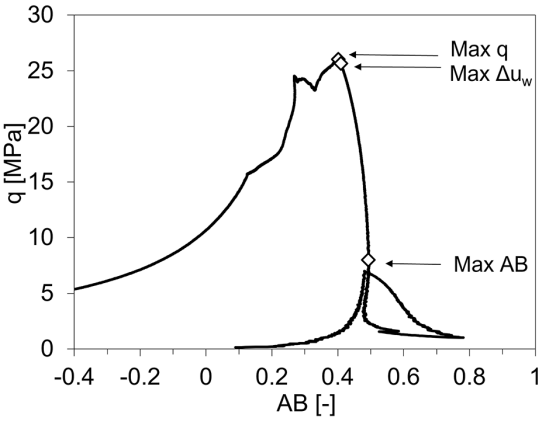

B1_STA3_1_857_07S7CTCU

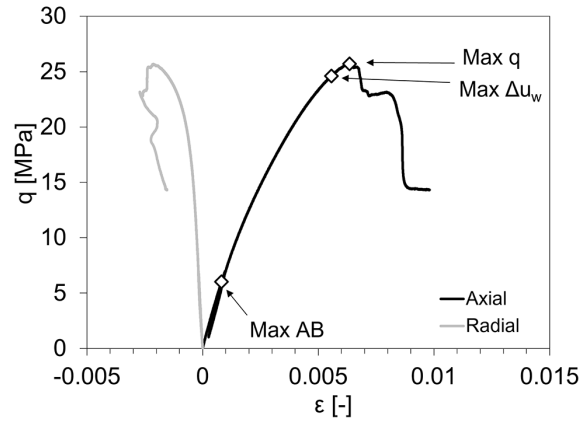

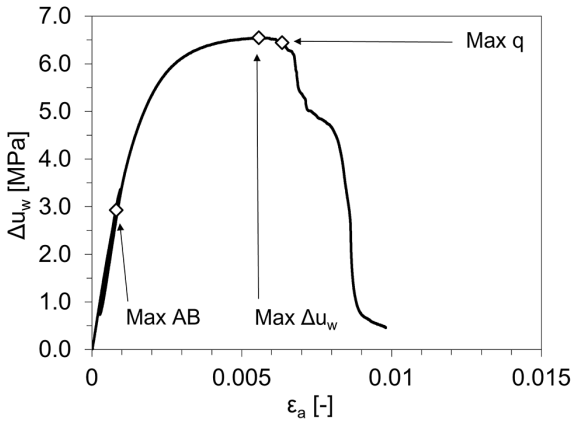

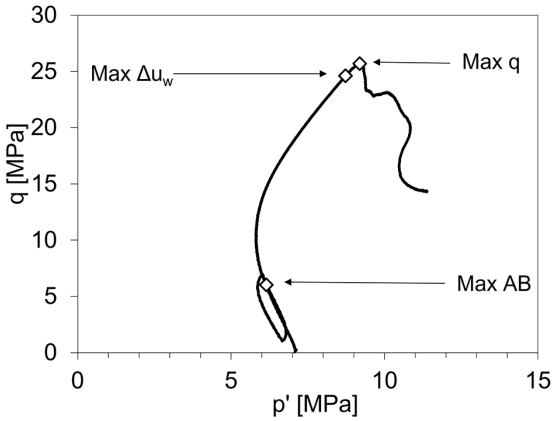

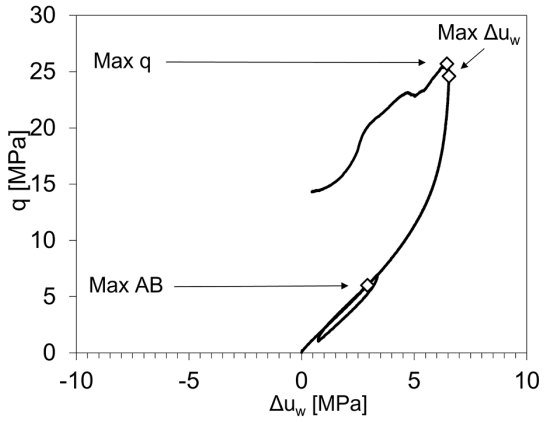

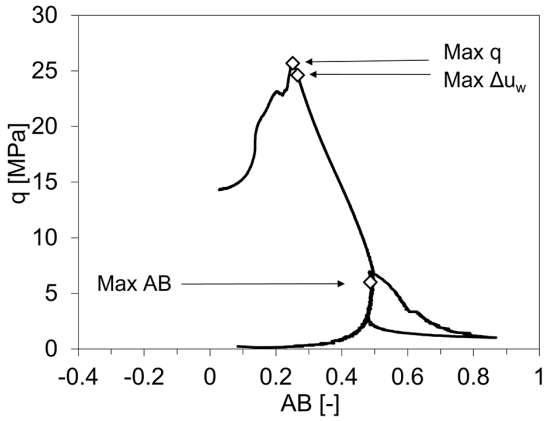

Appendix D Mineralogical analysis of the tested samples

Mineralogical analysis and grain density performed by the University of Bern on a series of specimens. Mineralogical analyses were performed on specimens that were not used in the mechanical programme, or negatives and chuncks from the specimen preparation. The ID of one of the specimens sourced from the same depth is reported. [a] Sample for mineralogy sourced below the mechanically tested sample in a section with high variability (see CT scan in Appendix B).

Specimen ID from same depth	**Depth** [m]	**S** [wt.-%]	**C(inorg)** [wt.-%]	**C(org)** [wt.-%]	**Quartz** [wt.-%]	**K-feldspar** [wt.-%]	**Plagioclase** [wt.-%]	**Calcite** [wt.-%]	**Dolomite/Ankerite [wt.-%]**	**Siderite** [wt.-%]	**Pyrite** [wt.-%]	**Clay minerals** [wt.-%]	**Grain density** [g/cm^3]	**Grain density STDEV** [10^{-4}/cm^3]
D1_OED_STA3_1	768.99	0.7	0.8	0.5	51.9	3.2	2.0	6.7			1.3	34.5		
A3_STA3_1_812_33S20CTCU	812.33	0.3	1.3	1.1	28.0	2.3	2.2	10.8			0.6	55.0	2.67	12
A5_STA3_1_812_44S13CTCU	812.45	<0.1	1.6	1.2	29.0	2.2	1.9	11.5		2.2	< 0.2	52.0		
A02_OS_STA3_1	812.49	0.1	1.0	1.2	22.2	2.2	1.9	5.8		2.6	0.1	63.9	2.67	7
A01_OED_STA3_1	812.58	0.2	1.8	0.9	31.9	2.5	3.1	13.2		2.1	0.4	45.9	2.69	9
A01_OS_STA3_1	812.61	0.4	1.7	0.8	31.6	2.4	2.4	11.6		3.0	0.7	47.6	2.69	7
B2_STA3_1_857_02P7CTCU	857.02	<0.1	1.3	1.1	18.1	2.2	2.1	5.8		5.9	< 0.2	64.9		
B1_STA3_1_857_07S7CTCU	857.07	<0.1	1.2	1.3	20.4	2.4	2.2	10.0			< 0.2	63.8	2.68	7

Appendix E Triaxial test results

Tab. E-1: Wave velocities recorded at the beginning of the shearing phase

Specimen ID, specimen geometry, mean effective and deviatoric stress (if applicable) at which the measurements were performed, P and S waves in the cylinder axis direction (*Vp*, *Vs*), P wave measured in the horizontal direction *Vph*. For specimen geometry see Fig. 4-1.

Specimen ID	**Specimen geometry**	*p'* [MPa]	*q* [MPa]	*Vp* [m/s]	*Vs* [m/s]	*Vph* [m/s]
A1_STA3_1_812_32_S7CTCU	S	7.0		3'435	1'413	
A2_STA3_1_812_32S13CTCU	S	13.0		3'439	1'463	
A3_STA3_1_812_33S20CTCU	S	20.0		3'323	1'604	
A4_STA3_1_812_33S5CTC	S	5.0		3'242	1'939	
A5_STA3_1_812_44S13CTCU	S	13.0				
A6_STA3_1_812_44S13CTCU	S	13.0		3'664	1'460	
B6_STA3_1_857_02P11TC	P	11.0		4'204	2'575	
B2_STA3_1_857_02P7CTCU	P	7.7		4'027	2'368	3'274
B7_STA3_1_857_07S13CTCU_DI	S	13.0		3'100	1'531	
B5_STA3_1_857_07S7CTC	S	7.0		3'064	1'794	
B4_STA3_1_857_07S20CTCU	S	20.1		3'145	1'843	
B3_STA3_1_857_07S13CTCU	S	13.0		3'104	1'518	
B1_STA3_1_857_07S7CTCU	S	7.1		3'039		

Specimen ID and corresponding initial characteristics are reported in Tab. 6-2, along with the results from the triaxial tests from the pre-shearing phases. Tab. E-2 includes:

- Specimen ID
- Core depth
- Formation
- Specimen geometry
- Bulk modulus ρ_{bulk} [g/cm^3]
- Initial void ratio, computed using a reference solid density of 2.70 g/cm^3
- Initial and final water content
- Measured values of the Skempton's B check, without correction (average B value over multiple determinations and corresponding mean effective stress)
- Swelling pressure obtained at the end of the saturation (radial and axial)
- Consolidation coefficient, obtained during the consolidation phase, and corresponding mean effective stress

Tab. E-3 presents the results from the shearing phases, including:

- Undrained elastic properties: Elastic modulus [GPa], Small Strain elastic modulus [GPa], Ratio of radial to axial strain [-], Ratio of radial (parallel to bedding) to axial strain [-] (only for P-samples), Mean effective stress at which the elastic properties were computed [MPa]
- Peak strength: Mean effective stress and deviatoric stress at peak
- Maximum *AB* value: Mean effective stress and deviatoric stress at the maximum *AB* value
- Maximum pore pressure: Mean effective stress and deviatoric stress attained at the maximum pore pressure
- Post peak strength: Mean effective stress and deviatoric stress

Tab. E-2: Triaxial test results (part 1)

For specimen geometry see Fig. 4-1.

Specimen ID	**Specimen geometry**	ρ_{bulk}	e_0	**Water content**		**B check**		**Swelling pressure**		**Consolidation phase**		**Strain rate**	**Stress path**
				Initial	Final	p'	B	Axial	Radial	p'	c_v	$\dot{\varepsilon}$	
		[g/cm^3]	[-]	[%]	[%]	[MPa]	[-]	[MPa]	[MPa]	[MPa]	[mm^2/s]	[s^{-1}]	
A1_STA3_1_812_32_S7CTCU	S	2.499	0.128	4.41	4.95	23	0.72	22.4	9.0	7	1.1E-03	1E-07	CTCU
A2_STA3_1_812_32S13CTCU	S	2.520	0.115	4.10	4.68	21	0.72	20.7	3.2	13	1.1E-03	1E-07	CTCU
A3_STA3_1_812_33S20CTCU	S	2.506	0.122	4.11	5.28	18	0.82	18.0	2.6	20	8.9E-04	1E-07	CTCU
A4_STA3_1_812_33S5CTC	S	2.534	0.104	3.58	4.29	23	0.76	22.6	3.2	5	4.9E-04	2E-08	CTC
A5_STA3_1_812_44S13CTCU	S	2.526	0.110	3.84	4.28	12	0.75			17	7.3E-04	1E-07	CTCU
A6_STA3_1_812_44S13CTCU	S	2.535	0.104	3.65	4.44	12	0.79			13	8.2E-04	2E-08	CTCU
B6_STA3_1_857_02P11TC	P	2.533	0.118	4.89	5.59	28	0.81	28.0	28.0	11	6.8E-04	1E-08	TC
B2_STA3_1_857_02P7CTCU	P	2.535	0.115	4.73	5.37	25	0.77	24.7	24.7	7	7.5E-04	7E-08	CTCU
B7_STA3_1_857_07S13CTCU_DI	S	2.516	0.130	5.27	5.59	20	0.85			13	8.8E-04	9E-08	CTCU
B5_STA3_1_857_07S7CTC	S	2.517	0.121	4.49	5.41	23	0.78	28.9	23.4	7	1.4E-03	2E-08	CTC
B4_STA3_1_857_07S20CTCU	S	2.516	0.129	5.23	5.30	24.4	0.77	31.0	24.5	20	1.1E-03	9E-08	CTCU
B3_STA3_1_857_07S13CTCU	S	2.520	0.126	5.03	5.36	27.5	0.83	27.7	21.0	13	1.2E-03	9E-08	CTCU
B1_STA3_1_857_07S7CTCU	S	2.516	0.130	5.30	5.54	26.4	0.83	26.1	20.7	4	9.1E-04	9E-08	CTCU

Tab. E-3: Triaxial test results (part 2)

Specimen ID	**Undrained elastic properties**					**Drained elastic properties**			**Peak strength** [MPa]		**Max. *AB* value** [MPa]		**Max. pore pressure** [MPa]		**Post peak strength** [MPa]		**Post peak elastic properties**	
	p' [MPa]	**Elastic modulus** [GPa]	**Small Strain modulus** [GPa]	**Ratio radial to axial strain** [-]	**Ratio radial** (parallel to bedding) **to axial strain** [-]	p' [MPa]	**E** [GPa]	$\nu_{\perp}$ [-]	q [MPa]	p' [MPa]	q [MPa]	p' [MPa]	q [MPa]	p' [(MPa]	q [MPa]	p' [MPa]	p' [MPa]	E [GPa]
A1_STA3_1_812_32_S7CTCU	6.7	9.10	11.4	0.345					23.0	10.7	5.7	6.6	20.4	8.0	16.3	13.2	13.8	6.0
A2_STA3_1_812_32S13CTCU	13.2	10.90	13.2	0.41					30.3	15.7	9.4	12.9	26.9	13.5	23.0	18.3	18.9	6.7
A3_STA3_1_812_33S20CTCU	19.9	9.80	12.6	0.38					34.2	21.3	17.4	18.7	31.1	18.7	23.5	23.9	24.0	5.5
A4_STA3_1_812_33S5CTC						6.0	4.0		30.1	15.0					11.8	8.9	8.6	2.8
A5_STA3_1_812_44S13CTCU	12.7	9.5	11.8	0.35					30.7	16.7	14.9	12.3	25.7	13.1	21.2	19.6	20.2	3.9
A6_STA3_1_812_44S13CTCU	12.8	9.9	11.4	0.275					29.5	16.3	6.1	12.7	25.3	13.8	19.0	18.7	19.1	6.6
B6_STA3_1_857_02P11TC									27.5	11.0					17.5	11.0		
B2_STA3_1_857_02P7CTCU	10.1	17.7	20.0	0.48	0.24				46.0	22.9	2.6	8.3	29.5	15.9	19.5	17.1	17.3	11.0
B7_STA3_1_857_07S13CTCU_DI	11.9	9.13	10.9	0.28					28.8	14.0	6.7	11.9	26.8	11.1	14.2	15.8	15.9	4.4
B5_STA3_1_857_07S7CTC						9.3	4.7	0.15	33.4	18.1					9.9	10.3	10.2	2.3
B4_STA3_1_857_07S20CTCU	19.0	10.7	12.3	0.24					32.6	17.3	18.1	16.8	31.2	15.6	21.1	21.7	22.1	4.8
B3_STA3_1_857_07S13CTCU	11.9	9.9	11.3	0.29					26.0	11.3	8.0	11.8	25.6	11.1	17.5	15.0	16.3	5.5
B1_STA3_1_857_07S7CTCU	6.0	8.2	10.2	0.29					25.7	9.2	6.0	6.1	24.6	8.7	14.5	11.0		

Appendix F Test results in oedometric conditions

Results of the oedometric test results are here reported in terms of oedometric curves (void ratio at the end of the primary consolidation) obtained for each test. In each graph the void ratio (e) versus the vertical effective stress (σ'_v) are reported. In each graph, it is highlighted the initial void ratio, the swelling pressure attained at the end of the resaturation phase (S_p) and the unloading (C_s) indexes.

D1_OED_STA3_1

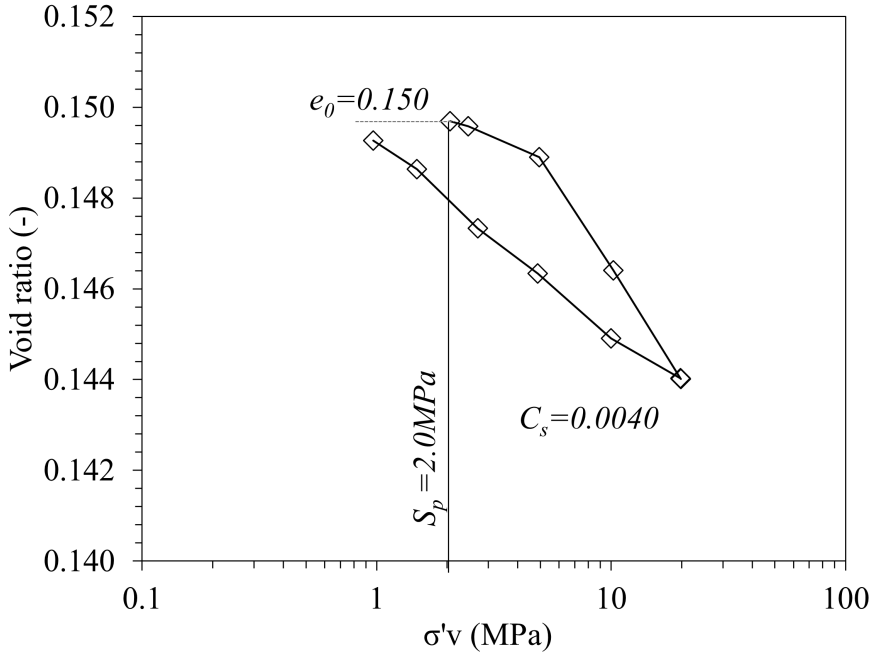

A01_OED_STA3_1

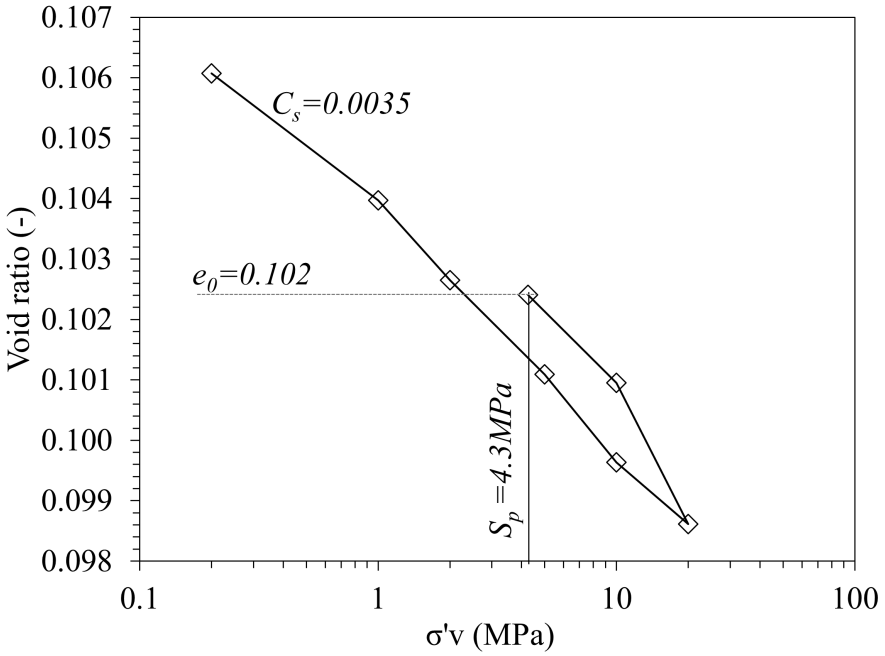

A02_OED_STA3_1

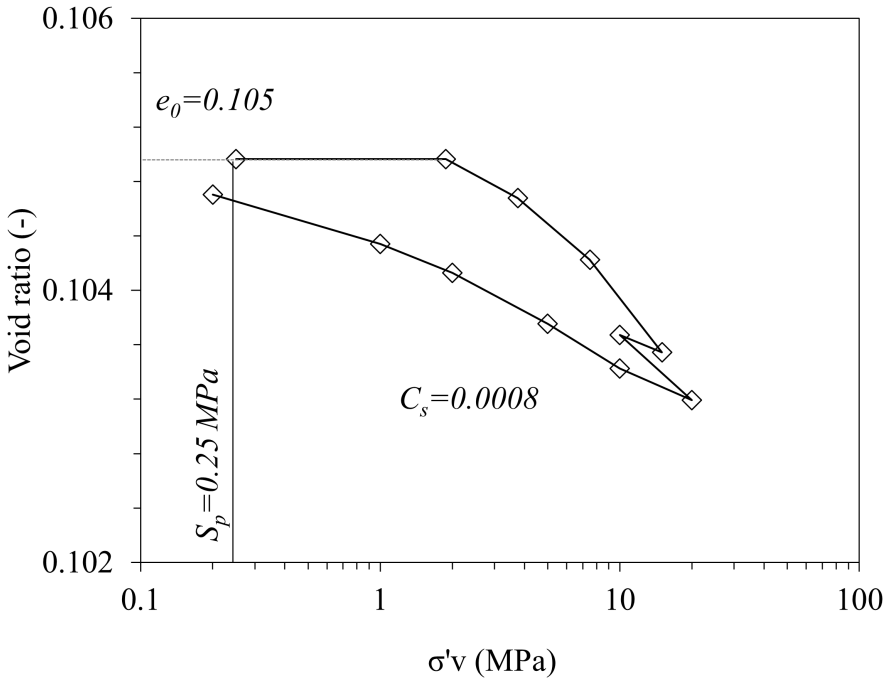

A01_OS_STA3_1

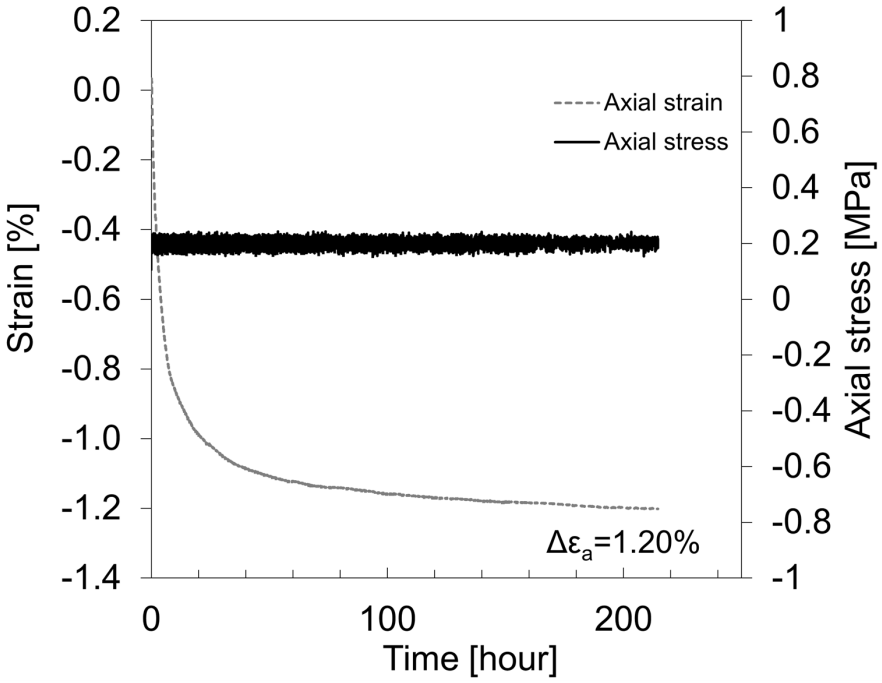

A02_OS_STA3_1